ÇUKUROVA UNIVERSITY
INSTITUTE OF NATURAL AND APPLIED SCIENCES

PhD THESIS

Ayşe Nur ACAR

INVESTIGATION OF PHYSICAL AND MECHANICAL PROPERTIES OF 316L AND 410 STAINLESS STEELS MANUFACTURED BY POWDER METALLURGY METHOD

DEPARTMENT OF MECHANICAL ENGINEERING

ADANA, 2019

ÇUKUROVA UNIVERSITY
INSTITUTE OF NATURAL AND APPLIED SCIENCES

INVESTIGATION OF PHYSICAL AND MECHANICAL PROPERTIES OF 316L AND 410 STAINLESS STEELS MANUFACTURED BY POWDER METALLURGY METHOD

Ayşe Nur ACAR

PhD THESIS

DEPARTMENT OF MECHANICAL ENGINEERING

We certify that the thesis titled above was reviewed and approved for the award of degree of the Doctora of Philosophy by the board of jury on 01/11/2019.

……..	……..	……..
Prof. Dr. Abdul Kadir EKŞİ	Prof. Dr. Faruk KARADAĞ	Prof. Dr. Erdem KOÇ
Supervısor	Member	Member
……..	……..	
Prof. Dr. Mustafa KURT	Assist. Prof. Dr. Durmuş Ali BİRCAN	
Member	Member	

This Phd Thesis is written at the Department of Institute of Natural And Applied Sciences of Çukurova University.
Registration Number:

Prof. Dr. Mustafa GÖK
Director
Institute of Natural and Applied Sciences

This project is supported by Cukurova University Research Project Units.
Proje Number: FBA-2018-11074

Not: The usage of the presented specific declerations, tables, figures, and photographs either in this thesis or in any other reference without citiation is subject to "The law of Arts and Intellectual Products" number of 5846 of Turkish Republic

ABSTRACT

PhD THESIS

INVESTIGATION OF PHYSICAL AND MECHANICAL PROPERTIES OF 316L AND 410 STAINLESS STEELS MANUFACTURED BY POWDER METALLURGY METHOD

Ayşe Nur ACAR

ÇUKUROVA UNIVERSITY
INSTITUTE OF NATURAL AND APPLIED SCIENCES
DEPARTMENT OF MECHANICAL ENGINEERING

Supervisor	:	Prof. Dr. Abdul Kadir EKŞİ
Co-Supervisor	:	Assoc. Prof. Dr. Ahmet EKİCİBİL
		Year:2019, Page: 139
Jury	:	Prof. Dr. Abdul Kadir EKŞİ
	:	Prof Dr. Faruk KARADAĞ
	:	Prof. Dr. Erdem KOÇ
	:	Prof Dr. Mustafa KURT
	:	Assist. Prof. Dr. Durmuş Ali BİRCAN

Stainless steels that have wide utilization areas in industry include of iron, chromium, nickel, carbon and other alloying elements and classified with four main branches as austenitic, ferritic, martensitic, and dublex stainless steels. In this thesis study, physical and electrochemical properties of austenitic and martensitic stainless steel prepared using powder metallurgy method using traditional pressing technique and heat treatment process were investigated. Experimental results showed that martensitic stainless steel samples have good physical properties such as high hardness, density, magnetization, specific heat capacity and enthalpy and high corrosion resistance as electrochemical behavior according to austenitic stainless steel samples. Both austenitic and martensitic stainless show phase transformations. On the austenitic stainless steel; α-martensite transformation happened from γ austenite whereas on the martensitic stainless steel; from martensite to reversed austenite transformation occurred.

Key Words: Austenitic stainless steel, martensitic stainless steel, powder metallurgy, physical and mechanical properties, corrosion resistance, thermophysical properties and surface characterization

ÖZ

DOKTORA TEZİ

TOZ METALURJİSİ YÖNTEMİYLE ÜRETİLEN 316L VE 410 PASLANMAZ ÇELİKLERİN FİZİKSEL VE MEKANİKSEL ÖZELLİKLERİNİN ARAŞTIRLMASI

Ayşe Nur ACAR

ÇUKUROVA UNİVERSITESİ
FEN BİLİMLERİ ENSTİTÜSÜ
MAKİNE MÜHENDİSLİĞİ ANABİLİM DALI

Danışman	:	Prof. Dr. Abdul Kadir EKŞİ
İkinci Danışman	:	Doç.Dr.Ahmet EKİCİBİL
		Yıl:2019, Sayfa : 139
Jüri	:	Prof. Dr. Abdul Kadir EKŞİ
	:	Prof Dr. Faruk KARADAĞ
	:	Prof. Dr. Erdem KOÇ
	:	Prof Dr. Mustafa KURT
	:	Dr. Öğr.Üyesi. Durmuş Ali BİRCAN

Endüstride geniş kullanım alanına sahip paslanmaz çelikler demir, krom, nikel ve diğer alaşım elementlerinden oluşur ve östenitik, ferritik, martenzitik ve çift fazlı paslanmaz çelikler olmak üzere 4 ana dal olarak sınıflandırılmaktadır. Bu tez çalışmasında; geleneksel pres tekniği ve ısıl işlem prosesi kullanılarak toz metallurjisi yöntemiyle üretilen 316L östenitik ve 410 martenzitik paslanmaz çeliklerin fiziksel ve elektrokimyasal özellikler inccelenmiştir. Deneysel sonuçlar; martenzitik paslanmaz çelik numuneler östenitik paslanmaz çelik numunelere göre, yüksek sertlik, yoğunluk ve çentik darbe dayanımına, yüksek manyetizasyona, özgül ısıl kapasitesine ve entalpisi gibi fiziksel özelliklere ve elektrokimyasal açıdan yüksek korozyona direncine sahip olduğunu göstermiştir. Hem östenitik hem martenzitik paslanmaz çelikler faz dönüşümüne sahip olduklarını göstermiştir. Martenzitik paslanmaz çelik te martensit fazdan ters fazlı östenite yapıya dönüşüm gerçekleşirken östenitik paslanmaz çelikte γ- östenit fazdan α-martenzit faz dönüşümü gerçekleşmiştir.

Anahtar Kelimeler: Östenitik paslanmaz çelik, martenzitik paslanmaz çelik, toz metalürjisi, fiziksel ve mekaniksel özellikler, korozyon direnci, termofiziksel özellikler ve yüzey karekterizasyonu

EXTENDED ABSTRACT

Stainless steels that have wide utilization areas in industry include of iron, chromium, nickel, carbon and other alloying elements. Stainless steels classified with as four fundamental branches as austenitic, ferritic, martensitic and duplex stainless steels; according to their microstructures. Austenitic stainless steel has FCC (Face Centered Cubic) crystal structure and shows good chemical and physical properties such as high electrochemical feature and impact strength and but non-magnetic property. Martensitic stainless steel has BCT (Body Centered Cubic) crystal structure and show good corrosion resistance and magnetic behavior. Austenitic and martensitic stainless steel have wide industrial areas such as structural, , automotive, medical, and also food industry.

For researchers; powder metallurgy method is attracted interesting due to obtain net and near net shaped material, good material utilization, very economical at large run sizes and approve serial product and high dimensionally products. Powder metallurgy method consits of three fundamental stages involving of powder and powder mixture preparation, shaping of prepared powder and densifying of shaped green products. Shaping of prepared powder is occurred by various methods such as compacting methods. Densifying of shaped /compacted products is meant to heat treatment process. Heat treated products have more densely more strengthening structure due to closed porosity and formation of grain bonding in the material structure.

In this thesis study, mechanical, magnetic, electrochemical, thermophysical properties and surface characterizations of 316L austenitic and 410 martensitic stainless steels manufactured using powder metallurgy method have been investigated. These stainless steels pressed under the 400 and 600 MPa pressures and compacted samples sintered at 1200 °C for a hour under inert gas atmosphere. In order to investigate these properties and surface characterizations of both austenitic and martensitic stainless steel samples; as hardness, density and Charpy

impact test as mechanical properties; corrosion resistace test as electrochemical test, magnetization moment behaviours against temperature and on the field as magnetic behaviours specific heat capacity and enthalpy behaviours of thermophysical properties have been performed. Corrosion resistances of these stainless steel have been performed on the alkali medium. These experimental results supported by SEM (Scanning Electron Microscopy) images , EDS (Energy Dispersive Spectroscopy) spectrums. Cystal structure of these austenitic and martensitic stainless steel were recorded by XRD (X-ray Diffraction) patterns . For experimental results; it is showed that martensitic stainless steel samples have high hardness, density and high Charpy-impact strength as mechanical property, high magnetization and corrosion resistance and high thermophysical greatness such as specific heat capacity and enthalpy according to austenitic stainless steel samples. Both of austenitic and martensitic stainless steels show phase transformations. On the austenitic stainless steel; α-martensite transformation occurred from γ austenite whereas on the martensitic stainless steel; from martensite to reversed austenite transformation occurred.

On the martensitic stainless steel samples, it interestingly realized that 410 martensitic stainless steel prepared on the low pressure has higher corrosion resistance than other martensitic stainless steel samples while expecting on the lower values and these experimental results related to decreasing carbide precipitations and reversed austenite phase transformation on the microstructure of martensitic stainless steel samples.

GENİŞLETİLMİŞ ÖZET

Endüstride geniş kullanım alanına sahip paslanmaz çelikler demir, krom, nikel ve diğer alaşım elementlerinden oluşur. Paslanmaz çelikler mikroyapılarına göre östenitik, ferritik, martenzitik, ve çift fazlı paslanmaz çelikler olmak üzere 4 ana dal olarak sınıflandırılmaktadır. Östenitik paslanmaz çelik YMK (Yüzey Merkezli Kübik) kristal yapısına sahiptir ve yüksek korozyon dayanımı ve çentik darbe dayanımı gibi iyi kimyasal ve fiziksel özellik gösterir, fakat manyetik özelliğe de sahip değildir. Martenzitik paslanmaz çelikler HMT (Hacim Merkezli Tetragonal) kristal yapısına sahiptir ve iyi korozyon direnci gösterir ve magnetic özelliğe de sahiptir. Östenitik ve martenzitik paslanmaz çelikler mimari ve inşaat, otomotiv ve taşımacılık, tıp, enerji ve ağır sanayiler ve gıda endüstrisi gibi geniş sanayi alanlarına sahiptir.

Toz metalurjisi yöntemi benzer veya benzer yakın şekilli malzeme edilmesi, iyi malzeme kullanımı, seri üretime izin vermesi ve yüksek hassasiyette ürünlerin üretilmesi bakımından araştımacılar için, ilgi çekici olmuştur. Toz metalurjisi yöntemi toz yada toz karışımı hazırlama, hazırlanan tozun şekillendirilmesi, ve şekillenen ham ürünleri yoğunlaştırılması olmak üzere 3 temel aşamadan oluşur. Hazırlanan tozun şekilledirrilmesi presleme yöntemleri gibi çeşiti yöntemlerle gerçekleşir. Şekilenen/preslenen ürünlerin yoğunlaştırılması, ısıl işlem sureci demektir. Isıl işlem uygulanmış ürünler malzeme yapısındaki kapanan gözeneklilik ve tane bağlanması oluşumundan dolayı daha yoğun, daha dayanıklı yapıya sahip olurlar.

Bu tezde; toz metallurjisi yöntemiyle üretilen 316L östenitik ve 410 martenzitik paslanmaz çeliklerin mekanik, manyetik, elektrokimyasal, termofiziksel özellikler ve yüzey karekterizasyonu incelenmiştir. Paslanmaz çelikler 400 ve 600 MPa basınçlarında preslenmiş ve preslenen numuneler inert gaz atmosferinde 1200°C ‘de 1 saat sinterlenmişlerdir. Östenitik ve martenzitik paslanmaz çeliklerin fiziksel ve kimyasal özelliklerini ve yüzey karekterizasyonunu

incelemek için, mekanik testler için sertlik, yoğunluk, ve Charpy darbe dayanımına, electrokimyasal davranışı için korozyon direncine, manyetik özelliği için hem sıcaklığa karşı hem alana karşı manyetik momentlerine ve ayrıca termofiziksel özellikleri için özgül ısı kapasiteleri ve entalpilerine incelenmiştir. Bu deneysel sonuçlar SEM (Taramalı Electron Mikroskopu) fotoğraflarıyla, EDS (Enerji Dağılım Spektroskopisi) spektrumlarıyla desteklenmiştir. Malzemelerin kimyasal yapıları XRD (X-Işınımı Kırınımı)desenleriyle kaydedilmiştir. Deneysel sonuçlar; martenzitik paslanmaz çelik numuneler östenitik paslanmaz çelik numunelere göre mekaniksel özellikler olarak iyi sertliğe, yoğunluğa ve çentik darbe dayanımına , yüksek manyetizasyona ve korozyon direncine ve ayrıca özgül ısı kapasitesi ve entalpi gibi yüksek termofiziksel özelliklere sahip olduklarını göstermişlerdir. Hem östenitik hem martenzitik paslanmaz çelikler faz dönüşüme sahip olduklarını gösteermiştir. Martenzitik paslanmaz çelik te martenzit fazdan ters fazlı östenite yapıya dönüşüm gerçekleşirken östenitik paslanmaz çelikte γ-östenit fazdan α-martenzit faz dönüşümü gerçekleşmiştir.

Martenzitik paslanmaz çelik numunelerde; düşük basınçta preslenen martenzitik paslanmaz çelik numunesi diğer martenzitik paslanmaz çelik numuneye göre düşük seyretmesi beklenirken, daha yüksek korozyon direncine sahip olduğunu göstermesi; ilgi çekici bir şekilde farkedilmiştir ve bu deneysel sonucun marenzitik paslanmaz çeliklerin mikroyapısında prese ve ısıl işleme bağlı azalan karbid çökeltilerine ve ters fazlı östenite faz dönüşümüne bağlanmaktadır.

ACKNOWLEDGEMENTS

Firstly, my thanks go to my supervisor, Prof. Dr. Abdul Kadir EKŞİ for his great guidance, support and encouragement. He has been a great source of motivation, both personal and technical.

I would like to thank my co-supervisor Assoc. Dr. Ahmet EKİCİBİL for their continues support, help and encouragements. Knowing and feeling his support during my PhD thesis helped me a lot.

I would like to thank Prof Dr. Birgul YAZICI for their continues support, help and encouragements to study electrochemical behaviour of my experiment samples and other materials and also her endless interest.

I am so grateful to my thesis monitoring committee and thesis jury of Prof Dr. Faruk KARADAĞ, Prof. Dr. Erdem KOÇ, Prof Dr. Mustafa KURT and Assist. Prof. Dr. Durmuş Ali BİRCAN for their endless interests and supports to all my thesis studies

I would like to thank Prof Dr. İsmail Hakkı ÇAĞATAY who is head of Civil Engineering Department and Res. Assist Ahmet AKKAYA for opening Civil Engineering laboratories and, helping and supporting to press my samples for my thesis study.

Also, I would like to thank Lecturer Dr. Selda KILIÇ ÇETİN, Lecturer Dr. Kadir Deniz TAKÇI, Lecturer Uğur ÇALYAN and also all personnel of Central Research Laboratory at Cukurova University in Adana, Turkey for opening, helping and supporting to my experiments for my thesis study.

I would like to thank my uncle Chemical Engineer Sabıt ACAR for continuous moral support, helping in my profession and private life. When i was a child, i did small pottery toys with my elbows from mud, soil and some water, in order words i played with mud :). Pottery toys were always cracked. I considered

when were they cracked, in my own way, i looked for solutions. I didn't know that my profession would be the same as my uncle's job and would be progessed accordingly. My uncle, i have taken you as a role model in my profession and private life and I will always take you a role model. So glad i have you.

I would like to thank Metallurgical and Materials Engineer Elif (KIYAK) KORKUT for helping and supporting to obtain particle size distributions of my experimental powders and also, her excellent friendship and also Ceramic Engineer Seher ÇETİN in Dumlupınar University for helping on the acquiring Archimedes water dispacement test values of my experimental samples and also her excellent frienship.

I am so grateful to Mehmet Ali DEMİR and Halit YAŞAR who are retired service chiefs from Turkey's Electricity Agency for their helping and supporting to my thesis study.

I would like to thank Technician Sefa MERAL for helping to obtain small samples from my samples and all technical supporting, and also Technician Ömer KÜTÜK for helping to prepare and press my samples and all technical supporting.

My heartfelt thanks go to my home mate Leyla (GÜNBAY) UZUN and Dr. Rasiha Nefise MUTLU for their continuous moral supporting, helping and excellent friendships

Many thanks go to my friends Res. Asst. Mete Han BOZTEPE, Res. Asst. Mustafa DAĞDELEN, Res. Asst. Ahmet ÇETİN for their moral support, help and excellent friendship.

In addition, I would like to thank all the staff of Departments of Mechanical Engineering at Engineering Faculty and Ceyhan Engineering Faculty at Çukurova University, Adana, Turkey

Last but not least, I would like to thank my father Mehmet ACAR, my mother Fatma ACAR and my sister Ahsen ACAR for their patience,trust and supporting from beginning of thesis study. You have always been my supportings when i thought everything was over and you were always with me even in my slightest rejoicing. So glad i have you. I love you very much.

I wouldn’t have achieved my thesis study without your supports and incentives. Thank you..

LIST OF ABBREVIATIONS

BCT	:	Body Centered Tetragonal
FCC	:	Face Centered Cubic
BCC	:	Body Centered Cubic
c_p	:	Specific Heat Capacity
ΔH	:	Enthalpy
FH	:	Field of Heated
FC	:	Field of Cooled
M	:	Magnetization
H	:	Magnetic ield
Rp	:	Polarization Resistance
SSA	:	Scanned Surface Area
D	:	Diameter
HB	:	Brinell Hardness
MSS	:	Martensitic Stainless Steel
ASS	:	Austenitic Stainless Steel
SEM	:	Scanning Electron Microscopy
XRD	:	X-Ray Diffraction
DSC	:	Differential Scanning of Calorimetry
PPMS	:	Physical Property Measurement System
EDS	:	Energy Dispersive Spectrometry
R_s	:	Unbalanced Solution Resistance
R_{ct}	:	Charge Transfer Resistance
R_{pore}	:	Resistance of Pores in the Natural Oxide Film
Q_{dl}	:	Constant Phase Elements Showing the Double Layer
Q_{ox}	:	Constant Phase Elements Showing the Oxides
CPE	:	Constant Phase Elements
EIS	:	Electrochemical Impedance Spectroscopy

“T	:	Temperature
R^2	:	Nonlinear –Squares Regression Value
DSS	:	Duplex Stainless Steel
RT	:	Room Temperature

CONTENTS **PAGE**

ABSTRACT I
ÖZ II
EXTENDED ABSTRACT III
GENİŞLETİLMİŞ ÖZET V
ACKNOWLEDGEMENTS VII
LIST OF ABBREVIATIONS X
CONTENTS XII
LIST OF FIGURES XVI
TABLE OF CONTENTS XXII
1. INTRODUCTION 1
1.1. The Types of Stainless Steel 4
1.1.1.The Alloying Elements of Stainless steel 9
1.2. Powder Metallurgy-Steel (PM Steels) 11
1.2.1.The PM Process Stages 11
1.2.1.1. The Powder Preparation and Blending/Mixing of PM-Steel 11
1.2.1.2. Compaction of Powder Blending/Mixing of PM Steel 13
1.2.1.3. Sintering of Compacted Parts of PM Steel 15
1.2.1.3.1.Mechanisms of Sintering 17
1.2.1.3.2.The Role of Sintering on the Mechanical, Electrochemical and Magnetic Properties of Formed Products 20
2.LITERATURE SURVEY 23
2.1. The Literature Survey of the Mechanical Properties of Austenitic Stainless Steels 23

2.2 The Literature Survey of the Mechanical Properties of Martensitic Stainless Steels 29
2.3 The Literature Survey of the Magnetic Properties of Austenitic and Martensitic Stainless Steels..... 32
2.4. The Literature Survey of the Electrochemical and Thermophysical Properties of Austenitic and Martensitic Stainless Steels..... 36
3. MATERIAL AND METHOD..... 41
3.1. Material 41
3.2. Method 43
3.2.1. Preparation Method of Specimens 43
3.2.2. Characterization Methods of Powder and Sintered Martensitic and Austenitic Stainless Specimens..... 47
3.2.2.1. Measurement of Mechanical Properties of Austenitic and Martensitic Stainless Specimens..... 47
3.2.2.1.1 Density Measurements of Austenitic and Martensitic Stainless steel Specimens 47
3.2.2.1.2. The Brinell Hardness Test..... 48
3.2.2.1.3. The V-Notch Impact Experiment..... 49
3.2.2.2. Measurement of Electrochemical Properties of Austenitic and Martensitic Stainless Specimens 52
3.2.2.3. Measurement of Physical Properties of Austenitic and Martensitic Stainless Steel Samples Via the Physical Properties Measurement Systems (PPMS)..... 53
3.2.2.4. Measurement of Thermophysical Properties of Austenitic and Martensitic Stainless Steel Samples Via the Differential Scanning Analysis(DSC) 55

3.2.2.5. Surface Characterization Methods of Powder and Sintered Martensitic and Austenitic Stainless Specimens 56
3.2.2.5.1. Particle Size Measurement of Powder of Martensitic and Austenitic Stainless Specimens 56
3.2.2.5.2. Scanning Electron Microscope (SEM) Characterization Methods 56
3.2.2.5.3. X-ray Diffraction (XRD) Characterization Method 58
4. RESULTS AND DISCUSSIONS 59
4.1 The Microstructural Analysis of Austenitic and Martensitic Stainless Steel Powders 59
4.2 The Density and Hardness Measurements of Austenitic and Martensitic Stainless Steels 63
4.3 The Charpy-V Impact Strengths of Austenitic and Martensitic Stainless Steels 66
4.4 The Surface Characterization of Fractured Surfaces of Austenitic and Martensitic Stainless Steels 67
4.5 The Electrochemical Behaviours of Austenitic and Martensitic Stainless Steels 75
4.6 The Surface Characterisation of Austenitic and Martensitic Stainless Steels 85
4.7 The Magnetic Measurements and Surface Characterization of Austenitic Stainless Steels 88
4.8 The Magnetic Measurements and Surface Characterization of Martensitic Stainless Steels 96

4.9 The Thermophysical Properties Measurements of Austenitic and Martensitic Stainless Steels 103
5. CONCLUSION 117
REFERENCES 121
CIRRICULUM VITAE 139

LIST OF FIGURES **PAGE**

Figure 1.1. Stainless Steel Family. 2

Figure 1.2. Schaeffler-Delong Diagram, A,M and F are defined as austenite, martensite, ferrite, respectively 4

Figure 1.3. The crystal structures of stainless steel (url 1) 5

Figure 1.4. The Pressing/Compacting Stages of P/M Steel 14

Figure 1.5. The density of PM steel with pressure. 15

Figure 1.6. The schema of stages of sintering 16

Figure 1.7. The Mechanisms of Sintering of Parts 18

Figure 1.8. The Sintering Sequence 20

Figure 2.1. Scanning electron micrographs of water-atomized (WA) and gas-atomized (GA) powders (Kyogoku *et al.*, 2003) 23

Figure 2.2. Influence of density on the impact value of sintered compacts 24

Figure 2.3. Effect of sintering atmosphere on microhardness of sintered 316L stainless steel compacted at 800 MPa 26

Figure 2.4. Charpy impact energy of the samples at room temperature 27

Figure 2.5. Schematic representation of Javanbakht *et al.* work 28

Figure 2.6. Relative density (measured by the Archimedes method) and porosity content (calculated by the image analyzer software) of the samples sintered at the different temperatures (experimental error < 1%) 28

Figure 2.7. Macrohardness values of the sintered samples (experimental error < 3%) 29

Figure 2.8. Comparison of the hardness of various wt.% NbC added 440C by the different sintering temperatures 31

Figure 2.9. The SEM images of the optimal N5, N10 and N15 specimens (sintered at 1270 °C for 1 h) after heat treatment (a) N5+HT,

(b) N10 + HT, (c) N15 + HT, and (d) EDS analysis location of the N10 + HT specimen 31
Figure 2.10. The *M–H* isotherms of Chi phase at different temperatures..... 33
Figure 2.11. The temperature dependence of magnetization of Chi phase at low-field 100 Oe. Samples cooled under zero-field (ZFC) and with applied field (FC) respectively. 33
Figure 2.12. Magnetisation vs.field dependence recorded at room temperature for as-sintered 304LN and 316LN and for aged 304LN at 875 1C for 8h 34
Figure 2.13. SEM micrographs of (a) as-sintered 304LN and (b) 316LN,(c) aged (875 1C and 48h) 304LN and (d) 316LN (Vilella etching)..... 34
Figure 3.1. The powders of 316L austenitic and 410 martensitic stainless steels 41
Figure 3.2. The mold used on this thesis study (a) assembled with stable and (b)female component of mold 43
Figure 3.3. (a) The mold is filling with powder (b) pressed to powder filled mold (c) sample extracted with applying reversible pressing (d) pressed sample..... 44
Figure 3.4. The technical drawing of compacted austenitic and martensitic stainless steel samples. 45
Figure 3.5. The atmosphere controlled furnace used on this study 46
Figure 3.6. The sintering cycle applied on this thesis study 46
Figure 3.7. Hardness Test Machine used for hardness measurements 49
Figure 3.8. The impact test schematic appearance of impact testing device (a) (Zhang, 2016; Yasuhisa *et al*.,2009) and the technical drawing appearance of austenitic and martensitic samples (b) (Ç.Ü. Ceyhan Mühendislik Fakültesi Deney Föyü) 51

Figure 3.9. (a) The samples prepared for impact testing experiment (b) The impact testing device 52
Figure 3.10. The Quantum Design-Dynacool-9 machine used for physical measurements 54
Figure 3.11. Mettler Toledo DSC3+ used on this study 55
Figure 3.12. The FEI -Quanta 650 Field Emission SEM machine used on this study 57
Figure 3.13. The PANanalytical-Empyrean XRD device used on this study 58
Figure 4.1. The SEM images and cumulative particle size distributions of 316L austenitic ((a) and b)) and 410 martensitic (410) stainless steel powders ((c and d)) (black line and blue line are referred as differential particle size and cumulative particle size distributions, respectively. 61
Figure 4.2. The XRD patterns of 316L austenitic (a) and 410 martensitic (b) stainless steels powder 63
Figure 4.3. The Charpy –V notch impact strength- hardness relationship of 316L austenitic and 410 Martensitic stainless steels prepared on the 400 and 600 MPa pressures 67
Figure 4.4. The SEM images of fracture surfaces of 316L austenitic (a,c,e,g) ve 410 martensitic (b,d,f,h) stainless steel samples prepared on 400 and 600 MPa pressures after impact experiment 70
Figure 4.5. The XRD patterns of 316L austenitic (a) and 410 martensitic (b) stainless steel samples prepared on 400 and 600 MPa pressures 73
Figure 4.6. Obtained the open pore potential-time curves of 316L austenitic and 410 martensitic stainless steel samples

prepared on 400 and 600 MPa pressures in 3.5% NaCl for 96 h of immersion time 75
Figure 4.7. The EIS Measurement of 316L austenitic and 410 martensitic stainless steel prepared on the 400 and 600MPa pressures at 30 min (top figures) and 96h (bottom figures) in 3.5% NaCl solution; Nyquist curve (left sides), Bode curve (right sides)) 80
Figure 4.8. The schema of equivalent circuit of EIS measurements 81
Figure 4.9. The Current – Potential curve of 316L Austenitic and 316L Martensitic Stainless steel Prepared on 400 and 600MPa pressures in 3.5% NaCl for 96 h of immersion time 82
Figure 4.10. The SEM images of 316L austenitic prepared on 400 before (a) and after (b); austenitic stainless steel prepared on the 600 MPa before (c) and after (d) and 410 martensitic stainless steel prepared on the 400 MPa before (e) and after (f) ; martensitic stainless steel on the 600 MPa before (g) and after (h) corrosion test. 87
Figure 4.11. The magnetization as a function of temperature [M(T)] curves of press-sintered 316L austenitic stainless steel on the a) 400 MPa and b) 600MPa pressures 88
Figure 4.12. The magnetization as a function of magnetic Field M(H) curves of press-sintered 316L austenitic stainless steel on the a) 400 and b) 600 MPa pressures 90
Figure 4.13. The SEM images of 316L austenitic stainless steel prepared on the 400 MPa (a and c) and 600MPa (b and d) pressures (a and b, 5,000x; c and d, 20,000x) 92
Figure 4.14. The separated regions with EDS spectrums of press-sintered austenitic stainless steel (316L) prepared on the 400 and 600MPa pressure 93

Figure 4.15. The magnetization as a function of Temperature [M(T)] curves of 410 martensitic stainless steel samples press-sintered on the a) 400 MPa and b) 600MPa pressures 96
Figure 4.16. The Magnetization as a function of Magnetic Field [M(H)] curves of 410 martensitic stainless steel samples prepared on the a) 400MPa and b) 600MPa pressures..... 98
Figure 4.17. The SEM images of 410 martensitic stainless steel prepared on 400 (a and c) and 600MPa pressures (b and d) 102
Figure 4.18. The EDS spectrums of 410 martensitic stainless steel prepared on 400 and 600MPa pressures..... 103
Figure 4.19. The specific heat capacity v.s temperature (above) and entalpy v.s. temperature (below) of 316L austenitic and 410 martensitic stainless steel samples prepared on 400 and 600 MPa pressures. 106

TABLE OF CONTENTS **PAGE**

Table 1.1. Use of stainless steel in the industry included of different product forms and application areas (Leffler) (%) 3

Table 1.2. Concentration of alloy elements in common stainless steel allotropes (Davis, J. R.; A.I.H. Committee, 1994) (wt%) 9

Table 1.3. Alloying elements and effects in steels 10

Table 1.4. The stages of sintering..... 17

Table 1.5. Process variables of sintering and their effects 19

Table 2.1. Effect of sintering temperature on the densification response and mechanical behavior of 316L stainless steel conventionally sintered at 1200, 1300 and 1400 °C, respectively (Pandhya *et al.,* 2012) 25

Table 3.1 Typical chemical compositions (wt%) of 316L austenitic and 410 martensitic stainless steel powders..... 42

Table 3.2. Typical particle size distributions of 316L austenitic and 410 martensitic stainless steel powders..... 43

Table 4.1. The particle size distributions of 316L austenitic and 410 martensitic stainless steel powders..... 62

Table 4.2. The Density and Percentage Water Adsorption Values of 316L austenitic and 410 martensitic stainless steel samples prepared on 400 and 600 MPa pressures..... 64

Table 4.3. The Brinell hardness values of 316L austenitic and 410 martensitic stainless steel samples prepared on 400 and 600 MPa pressures..... 64

Table 4.4. The Charpy-V notch impact strengths of 316L austenitic and 410 martensitic stainless steel samples prepared on 400 and 600 MPa pressures..... 66

Table 4.5. EDS spectrums of cracked surfaces of 316L austenitic ve 410 martensitic stainless steel samples prepared on 400 and 600 MPa pressures after impact experiment 71

Table 4.6. Fitted EIS measurements of 316L Austenitic and 410 Martensitic Stainless steel samples for 30min -96 h of immersion time 81
Table 4.7. The EDS spectrums of press-sintered 316L austenitic and 410 martensitic stainless steel prepared on the 400 and 600MPa pressures before and after corrosion test. 88
Table 4.8. The specific heat capacity v.s. temperature values of 316L austenitic stainless steel samples prepared on the 400 and 600 MPa Pressures 107
Table 4.9. The enthalpy v.s. temperature values of 316L austenitic stainless steel samples prepared on the 400 and 600 MPa Pressures..... 109
Table 4.10. The specific heat capacity v.s. temperature values of 410 martensitic stainless steel (410) samples prepared on 400 and 600 MPa pressures..... 110
Table 4.11. The enthalpy v.s. temperature values of 410 martensitic stainless Steel (410) Samples prepared on 400 and 600 MPa pressures. 113
Table 4.12. The fit coefficients and nonlinear–squares regression values of specific heat capacity behaviour of 316L austenitic and 410 martensitic stainless steel samples prepared on the 400 and 600 MPa pressures..... 115
Table 4.13. The fit coefficients and nonlinear –squares regression values of enthalpy behaviour of 316L austenitic and 410 martensitic stainless steel samples prepared on the 400 and 600 MPa pressures. 115

1. INTRODUCTION

In engineering applications, stainless steels have wide utilization areas such as automotive, medical etc. They are commonly defined as chemical composition that formed of iron, carbon and other elements. Carbon is basal element on heat treatable steels; therefore, steel can called as alloy that composed of iron, small amounts of carbon and other elements (Atrayago *et al.,* 2015).

Stainlessness property is occurred on the microstructure of steel, if at least about 11wt% chromium element must be added to steels. In relatively non-aggressive environments; at this Cr amount, it is occurred self-improved structure on the steel surface, in addition to this, in the hostile environments such as moist atmosphere, higher Cr amounts must be added because of protecting surfaces of steels from pitting (Lo *et al.,* 2009). Figure 1.1, give a small brief of the stainless steel family with alloying elements and effects on the physical and chemical properties of steels (ASM Alloy Digest Sourcebook: Stainless Steels, 2000).

The base of stainless steel is occurred both of Fe-Cr system and other alloying elements whose providing specific properties. As a shown in Figure 1.1.; for example; Mo is added improving resistance to pitting for 316 and 317 austenitic stainless steels, to decrease sensitization; Ti,Nb and Ta must be added for obtaining 321 and 347 stainless steel. Ni is austenite-forming elements, on the martensitic structures Ni element is not find. If Cr and Ni are added on existing amounts to alloy, the obtaining alloy is referred with heat-resisting alloy.

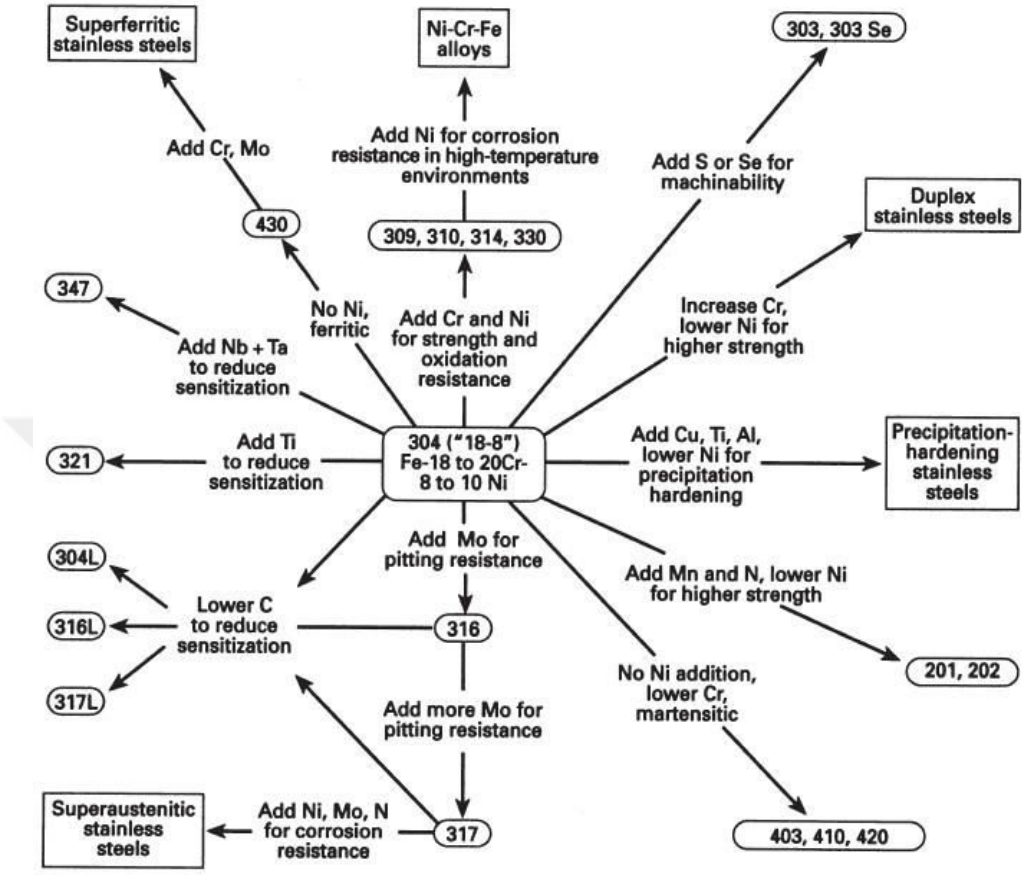


Figure 1.1. Stainless Steel Family (ASM Alloy Digest Sourcebook: Stainless Steels,2000).

In the below Table 1.1; it is observed the dominant item is cold rolled sheet (60%) as product form, application areas divided the main categories as consumer and industrial items; as application productions of the stainless steel, it has wide usage area in the food and chemical industry.

Table 1.1. Use of stainless steel in the industry included of different product forms and application areas (Leffler) (%)

Product Forms		**Application Areas**	
Cold rolled sheet	60	**Consumer items**	26
Bar and wire	20	Washing machines and dishes	8
Hot rolled plate	10	Pans, cutlery etc.	9
Tube	6	Sinks and kitchen equipment	4
Casting and other	4	Other	5
		Industrial equipment	74
		Food industry and breweries	25
		Chemical, oil and gas industry	20
		Transpot	8
		Energy production	7
		Pulp and paper, textile industry	6
		Building and general construction	5
		Other	5

At room temperature, the austenitic matrix can be stabilized using adding alloying elements like nickel, chromium or molybdenum. ‘‘Schaeffler-Delong Diagram’’ presents the conditions under which austenite is stable. This case shows the importance of diagram see in Figure 1.2. This diagram indicates the disposition for occurring of structures of austenitic, martensitic, ferritic and their’s mixtures as a function of both of chromium and nickel equivalents(Hoffelner, 2013).

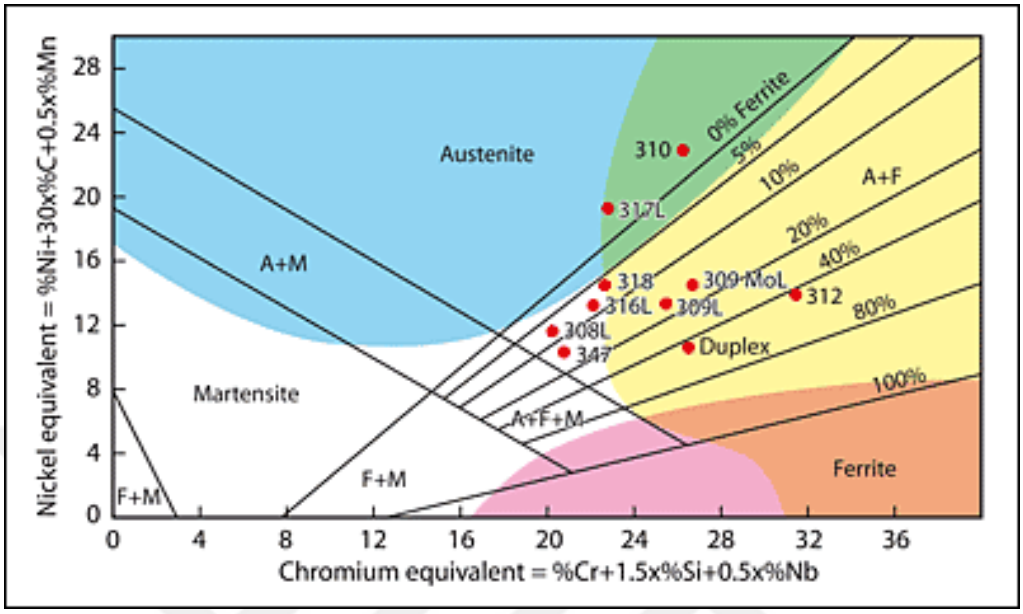


Figure 1.2. Schaeffler-Delong Diagram, A,M and F are defined as austenite, martensite, ferrite, respectively (Fortan *et al.*, 2017)

Schaeffler-Delong Diagram is a diagram that is applying to help determining the phases in the material according to the alloy elements concentrations in the materials and microstructural changes after heat treatment and hardening processes. According to this diagram; Cr and Ni equivalents are found by as a following equations (1.1) and (1.2);

$$Ni_{eq}\,(\%)=Ni+30\cdot C+0.5\cdot Mn \quad (1.1)$$

$$Cr_{eq}\,(\%)=Cr+Mo+1.5\cdot Si+0.5\cdot Nb \quad (1.2)$$

1.1. The Types of Stainless Steel

The types of stainless steel are classified with the crystal structure depended on the chemical composition. The main crystal structures of these steel is austenite (austenitic), martensite (martensitic) and ferrite (ferritic) structures as shown in Figure 1.3.

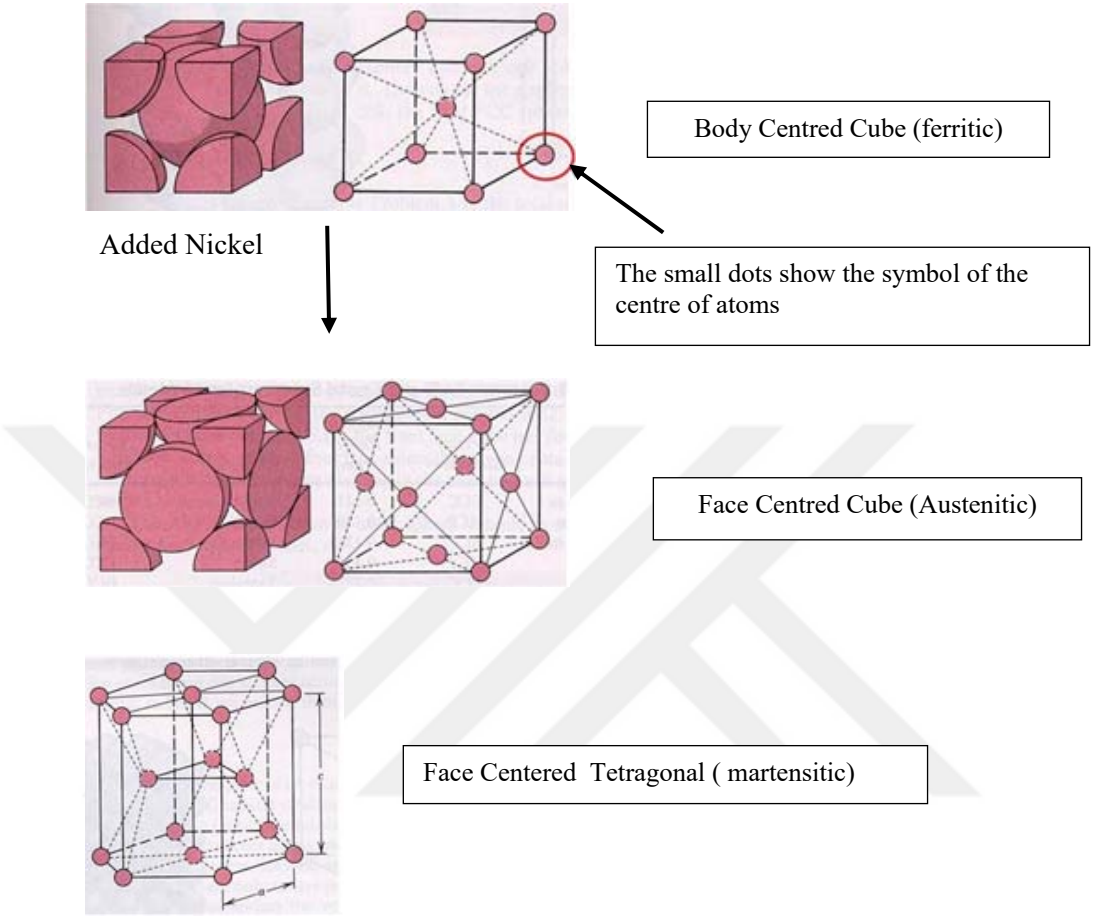


Figure 1.3. The crystal structures of stainless steel (url 1)

At medium temperature, ferritic structure has the body-centered cubic (bcc) as base crystal structure of iron or low carbon alloy steel. In order to explain this structure; it must be visualized the cube having an atom at each of eight corners and in the geometric centre of cube. This structure is repeated regularly in three-dimensional space at the grain. Into the grain, this structure repeated at different orientation contact and these contact areas is called grain boundaries. Grain boundaries consist of interface defects, grains etc., and play a significant role on the providing of characteristic properties of materials. Austenitic structure has face

centered cubic (FCC) form of unalloyed iron in the grains and occurred at higher temperature (>800°C). This structure is different from ferritic structure because of the atomic location. In this structure, each of atom is found each of eight corners and in the centre of the six faces of cube. When an atom that is placed to centre between atoms on the corners of surfaces is added to BCC crystal structure, this structure changes to FCC crystal structure. At room temperature, if this structure arrays, this structure has stable. The obtained alloy is called austenitic stainless steel. At ambient temperature, martensitic structure is more similar to the ferritic structure has body-centred cubic structure but different from at one direction. To form tetragonal structure, one axis of cube is elongated. To this structure is also called hexagonal closed packaged crystal structure. This structure is produced by various methods such as heat treatment, mechanical stress. Martensite structure is less workable due to have hardest, strongest structure. (Covert and Tuthill, 2000)

According to the this structures, the main types of stainless steel are categorized as ferritic stainless steel austenitic stainless steel and martensitic stainless steel In addition to the main types of stainless steel; duplex (dual) stainless steel, precipitation hardening stainless steel can be added (Lo *et al.*2009).

Ferritic Stainless Steels: Ferritic stainless steel are iron and chromium alloys consists of 11-30%chromium, very little or often no Nickel content at all this stainless steel and small amounts of ferrite stabilizers as Mo,Si,Al,Ti,Nb,Se and at low amount of C (0.03-0.20%) and have body-centered cubic structure. They have good ductility, magnetic property, good strength, but low hardness and show moderate or higher corrosion resistant related to the chromium content and because of carbide formation in this microstructure, also present low high-temperature corrosion resistance. They are non-hardenable and can not be strengthened via heat treatment. Formability of these steel are related to alloying elements into the constituent of these steels. In the automotive industry. Ferritic stainless steels are commonly utilized (Ozcan ,2012, Herdström, 2007, Cain, 2005).

Austenitic Stainless Steels: Austenitic stainless steels form the widest stainless steel family in terms of alloys and their usages and possess 0.03-0.05%C, basal alloying elements are Cr(17-24%) which stabilizes the face-centered cubic (fcc) austenite structure at room temperature, Ni(8-25%), Mo(2-4%) in order to occur carbide precipitation, Ti and Mo are added. To some extent by other austenite stabilizing elements such as manganese, nickel element is replaced. The properties of these steels explain in following:1) not heat treatable 2) nonmagnetic structure 3) rapid cooling results in the production of their softest conditions,4) high ductility, 5) high corrosion resistant and resistant to oxidizing acidic, alkali mediums, 6) very good forming properties, 7) easy to work and machine, 8) moderate strength, 9) excellent high temperature properties, 10) affected by cold working (ASM, Alloy Digest Sourcebook: Stainless Steels,2000; Weidmann et al.,). Applications are medical industry such as screws, implants, and low temperature applications, vessels and pipes in the chemical, pharmaceutical and food industries, kitchen utensils (Ozcan ,2012, Herdström, 2007, Cain, 2005; Weidmann *et al.,* URL1).

Martensitic Stainless Steels: The compositions are similar to the ferritic steels but, to allow hardening by heat treatment, the compositions have higher C and lower Cr and other elements as molybdenum, niobium, silicon, wolfram, vanadium,. Namely these steels are heat treatable alloys which had medium carbon content(up to 1.2 %.), 12-18%Cr, 2-4%Ni (Cunat ,2004; Hoffelner, 2013; Weidmann et al.). Martensite is produced by rapid cooling and features can then be optimized by subsequent temperature treatment. The alloys are magnetic. The microstructure can range from pure martensitic structure to fine tempered martensitic, due to thermal processing. (Weidmann et al). Properties of these steels are also high temperature and creep resistance, extremely strong and highly machineable, high strength and hardness factor, good wear resistance. The applications are; scalpels, knives, hooks and tweezers in medical applications, drive systems and high performance parts for airplanes (Weidmann *et al*).

Duplex(Dual) Stainless Steels: Duplex stainless steels are iron/chromium/nickel alloys and have mixed microstructure of both at equal amount of austenite and ferrite (approximately 50%austenite and 50% ferrite). This stainless steel involve Cr (20-30%), Ni (5-8%), Mo (up to4%), C (mostly 0.03%) and in addition to copper, nitrogen, tungsten. Some of the more highly alloyed, expecially corrosion-resistant grades are called as superduplex stainless steels. Compared to other stainless steel, they have unique properties due to have dual phase of austenite and ferrite. They show higher strength and electrochemical to austenitic stainless steel and higher ductility to ferritic stainless steel. They shows brittle fracture at elevated temperature because of Ferritic phase in the microstructures of stainless steel. They are used for load-bearing applications in corrosive atmospheres, e.g. in the off-shore industry (Ozcan ,2012; Herdström, 2007; Cain, 2005; Lo *et al.*,2009).

Precipitation Hardenable Stainless Steels: Precipitation Hardenable Stainless Steels are iron-chromium-nickel steels, which can be hardened through a solution and thermal processing, and contain alloying elements such as aluminium, copper or titanium some of which form precipitates and the other ones function as stabilizers, in addition to chromium, nickel, iron and carbon. They have three phase distribution as martensitic, austenitic and semi austenitic. These steel are used in required areas consisting specialized applications in high echnologies industry (Ozcan, 2012; Herdström, 2007; Cain, 2005; Lo *et al.*,2009).

In the following Table 1.2., it is given stainless steel types and concentration of alloying elements of their stainless steels.

Table 1.2. Concentration of alloy elements in common stainless steel allotropes (Davis, J. R.; A.I.H. Committee, 1994) (wt%)

	Alloying Stainless steel Types			
Alloying Elements	**Austenitic**	**Martensitic**	**Ferritic**	**Duplex**
C	0.03 – 0.15	0.10 - 1.10	0.08 – 0.20	0.03 – 0.20
Mn	2.0 – 19.0	1.0 – 1.25	1.00 – 2.50	1.00 – 2.00
Si	1.00 – 4.50	0.50 – 1.00	1.00	0.60 – 1.00
P	0.06 – 0.20	0.04 – 0.06	0.04 – 0.06	0.03 – 0.04
Cr	16.0 – 21.0	11.0 – 18.0	10.5 – 27.0	21.0 – 29.0
Ni	3.50-38.0	0.00 – 2.50	0.00 – 1.00	4.50 – 6.50
Mo	0.00 – 4.00	0.00 – 0.75	0.00 – 2.50	1.00 – 4.00
Others	Cu, N, Nb, S, Ti	Cu, N, S, V	Cu, N	Al, B, Cu, N, V, W

1.1.1.The Alloying Elements of Stainless steel

As a known and expressed at below, several stainless steels are composed of more than 30% chromium or less than 50% iron, because of their chromium rich compositions, they improve their stainless properties. Also, other elements such as nickel, manganese, molybdenum, copper, titanium, are added to achieve prominent characteristics. The alloying elements added to stainless steel gives the specifical properties to these steels. Therefore, the alloying elements and effects of these elements to stainless steels are briefly given in Table 1.2. From Table 1.2, it is also observed the alloying elements are added to which kinds of stainless steel besides gained properties of stainless steels. As negotiated from Table 1.2., some alloying elements such as Cr,Ni,Mo etc. are added to all types of stainless steel, other alloying elements such as Nb, P, O etc. are added specified stainless steel in following.

Table 1.3. Alloying elements and effects in steels(Davis, J. R.; A.I.H. Committee, 1994.)

Element	**Steel type no.**	**Effect**
Carbon	All types	Increases the strength, Supports development of precipitants which reduce corrosion resistance, rising C content decreases critical cooling speed
Chromium	All types	Works as ferrite developer, rises oxidation- and corrosion-resistance
Nickel	All types	Works as austenite developer, Increases toughness at low temperature, grain-refining
Oxygen	Special types	Works as strong austenite developer (20 to 30 times stronger than Nickel)
Niobium	1.4550, 1.4511, , 1.4580	Bonds carbon reduces tendency to intergranular corrosion
Manganese	All types	Rises austenite stabilization, Reduces hot crack tendency by formation of manganese sulphide
Molybdenum	1.4404, 1.4435, 1.4401, and others	Enhances creep- and corrosion resistance to reducing media, moves as ferrite developer
Phosphorus, selenium, or sulphur	1.4104, 1.4305, 1.4005, ,	Enhances machinability, Lower weldability, reduces slightly corrosion resistance
Silicon	All types	Enhances scale resistance, moves as ferrite developer, All types are alloyed with small contents for desoxidation
Titanium	1.4541, 1.4571,1.4510, , and others	Bonds carbon, reduce disposition to intergranular corrosion, Acts as a grain refiner and as ferrite developer
Aluminum	Type 17-7 PH	Works as strong ferrite developer, mainly used as heat ageing additive
Copper	Type 17-7 PH, 1.4506, 1.4505	Developes corrosion resistance against certain media, reduces disposition to stress corrosion cracking,developes ageing

1.2. Powder Metallurgy-Steel (PM Steels)

In the manufacturing of steel components having wide application areas such as automotive, medical and aerospace industry and other areas; powder metallurgy (PM) method ensures to obtain small components with a complex shape and net-shape or near-net shape of components. Powder metallurgy methods is also provide good mechanical and physical properties such as high surface finish, high stregth/toughness.

PM steels can be categoized as iron-carbon steels (with and without copper and/or nickel addition), low-alloy steel and stainless steel. PM stainless steels have different machinablity features compared to plain-carbon steel and low-alloy steel. Because, throughout machining pocess, stainless steels show agglutinant and work harden, otherwise they consist of high alloy with non-carbon addition, therefore machinability of stainless steel is harder (Roland *et al.*, 2013).

The PM process consists of powder preparation and mixing with and without lubricants, additives etc., formation of shape (i.e. compacting, pressing) from powder mixing, consolidation/densification of forming shapes with sintering stage and finally sizing operations to the efface the undesired regions of steel components.

1.2.1.The PM Process Stages

1.2.1.1. The Powder Preparation and Blending/Mixing of PM-Steel

According to the German, powder production method determines dimension, shape, purity, microstructure, cost and other properties of produced powders. Selecting a powder manufacturing method to the other methods is important for practicability, economically of method and obtained powder features and application areas (German, 2007). The powder production methods are categorized on the following techniques;

-Mechanical Powder production methods such as metal cutting, grinding, mechanical alloying

- Electrolyzing powder production methods

-Chemical powder production methods such as precipitation from liquids/gases,

-Atomization techniques such as water and gas atomization

-Evaporation methods

-Submicron and nano-dimensioning powder production methods

-Special powder production methods (German, 2007).

In mechanical powder production methods, there is production methods as impact , abrasively grinding, cutting and compressing. It is occurred together with impact, abrasively grinding, cutting and compressing. With impact, materials cut off small particles, abrasively grinding is provide minimizing of powder dimensioning due to friction of dusts together, by cutting methods, the obtained powder is large scale and with compressing, a material become powder when applied power to fracture point. On the electrolyzing powder production methods, obtained powder has dendritic and spongelike shape, and dimension and shape of powders can significantly be controllable (German, 2007).

In the chemical powder production methods, powder production is occurred from the change metal to metal powder from ore oxides, and also acquires at the temperature below melting point. In this method, dimension and shape of powders are arranged by controllable variations of reactions in the powders. Atomization technique is melted metal and separating particles of melted metals and this technique is applied to metals, polimers, ceramics, alloys and in this technique with good process control, better quality powder is obtained. Atomization techniques are categorized as gas atomization, liquid/water atomization, centrifugal atomization and plasma. With evaporation technique, high purity and small-sized powder is acquired (German, 2007).

In order to gain successful results in compaction and sintering; the starting powders must be blended and mixed. As if blending and mixing processes are

seem to be have the same meaning, actually the processes are applied to the different properties of powders. On blending, powders have same chemistry, but conceivable different particle size. With mixing, powders having different chemistry are mixed. On the blending and mixing, lubricants, binders, sintering aids etc. can be added besides alloy powders. Lubricants and flocculants are added because of ensuring the powders' characteristic and easily separating from mold or holding to die, binders are waxes, dekstrins and additives due to gaining the green density, sintering aids are also added owing to accelerate densification on the heat treatment stage. A successfully powder blending or mix has capability of meeting the desired properties of a specific alloy and requires to enable working (German, 2007).

1.2.1.2. Compaction of Powder Blending/Mixing of PM Steel

To obtain desired compact shape, powder blending/mixing must be compacted with applying elevated pressure. One of the compaction methods is the pressing method widey used in the application areas. The schema of pressing method is given on the following with stages. Firstly (1) powder blending/mixing is filled to die cavity (2) and (3) through compacting/ pressing process stage, powder blending/mixing are pressed by the aid of upper and lower punches (4) the pressed/compacted part is ejected from mold (see in Figure 1.4) (v, F symbols specified in Figure 1.4 are referred pressing rate and pressing load , respectively).

At the following Figure 1.5., the representative appearances and density of the powder blending/mixing with the applied pressure.

(1) powders filling to die have small density.
(2) as the pressure increased, density of part is increased.
(3) the same condition as on the (2) stage is occurred.

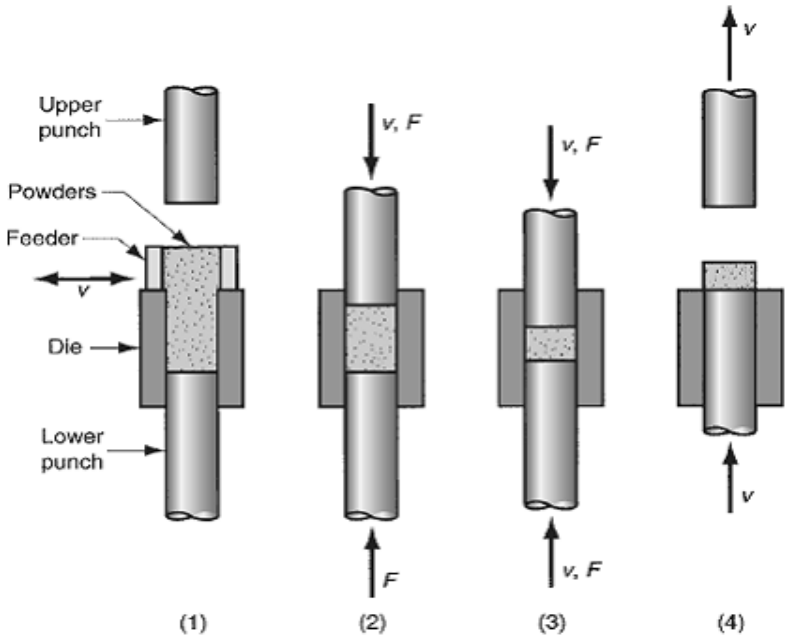


Figure 1.4. The Pressing/Compacting Stages of P/M Steel (German, 2007)

When the final green density is reached, as the pressure are increased, the density of parts is not increased. Because the bonding of grains and densification is occurred, and the resistance to more bonding of grains will be become. Therefore the final green density is not fully occurred.

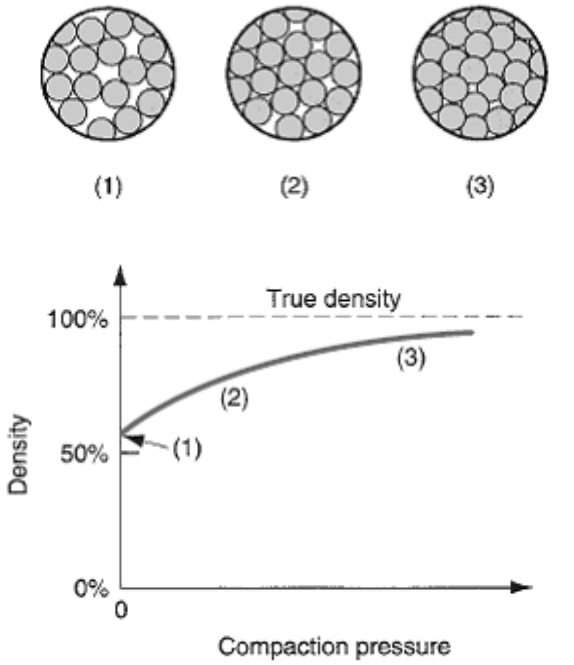


Figure 1.5. The density of PM steel with pressure (German,2007).

1.2.1.3. Sintering of Compacted Parts of PM Steel

Sintering is heating process improving strengthening microstructure and providing desired properties to compacted/formed and green densely materials with increasing grain boundary. This stage is performed on the above of melting point and at high temperatures, atomic diffusion and surface energies of small particles are accelerated, and so sintering is come true. Throughout powder preparation process, surface area/energy of material is increased with absorbed material energy, this energy is eliminated by sintering stage. Particle size inversely proportional to surface energy per volume at following formulas (1.3) and (1.4).

As assumed particle shape is spherical;

$$V = \frac{\pi}{6} D^3 \quad (1.3)$$

$$A = \pi D^2 \quad (1.4)$$

Arccording to these equations (1.3) and (1.4) ; small sized particles have high surface energy, therefore this particles are rapidly sintered (German, 2007).

Sintering is occurred from the heat treatment stages and this sintering stages are showed at Figure 1.10 and explained briefly at Table 1.4.

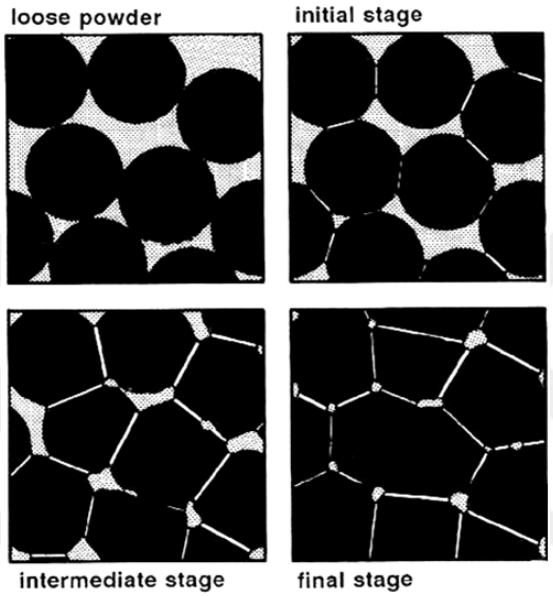


Figure 1.6. The schema of stages of sintering (German,2007).

At the Table 1.4. and Figure 1.6., first stage of sintering is consisting of loose particles in contact with each other and this loose particles as the same time have open pore structure and high porosity. Continuing of sintering, at the intermediate stage, neck growth, grain growth and pore reduction are occurred. As the pore rounding, separate grains are less appearent. Finaly at the final stage; porosity reduced, closed and circular pores occurred, grains grow and coarsen.

Table 1.4. The stages of sintering(German, 2007)

Stage	**Process**	**Loss surface Area**	**Condensation**	**Coarsening**
Adhering	Surface contact formation	Minimum surface area without compression at high pressures	Nothing	Nothing
Early stage	Neck growth	Importantly, loss of 50%	Occurred small at first.	Minimum
Intermediate stage	Pore rounding and elongation	Total loss of open porosity	Significant	Increase on the size of grain and porosity
Final stage	Closing of porosity and final condensation	Umimportant, more loss	Slowly and relatively less	Growing of big grain and porosity

During sintering, until it is reach final shape, grain growing/shape and porosity material is affected from sintering process effects and the variations are briefly explained at Table 1.5.

1.2.1.3.1.Mechanisms of Sintering

At Figure 1.7.; the mechanisms of sintering occurred on the grains are schematised.

The sintering process can be explained with mass transport mechanism. The mechanism can be categorized as densifying and non-densifying mechanisms. Grain boundary diffusion and lattice diffusion to the pore from the grain boundary

are the densifying mechanisms, surface diffusion, lattice diffusion throughout the volume of grain boundary and vapor transport(evaporation densification) are non-densifying mechanisms and non-densifying mechanisms cause to neck growth without densification. Plastic flow commonly occurred sintering in the metallic powders is dislocation motion and resulted with neck growth and densification. Non- densifying mechanisms affect also the rate of densification, When the mechanism occur, they decrease the curvature of neck surface and also reduce rate of densification. (Rahaman 2000).

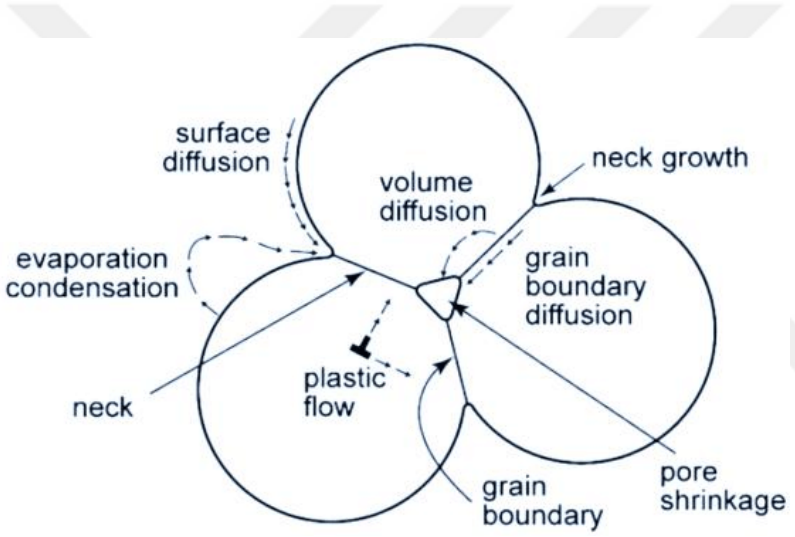


Figure 1.7. The Mechanisms of Sintering of Parts (Rahaman, 2000)

In sintering process; furnace medium is controlled because of protecting from oxidation, minimizing probable chemical reactions in the compacted green body, removing of impurities which can exist in the oxide film, supporting in removing of lubricants and binders used to in the compacting process in order to give the shape to powders(i.e. pressing) Sintering atmospheres are inert gas (i.e. Ar, He), nitrogen-derivated, hydrogen, and vacuum atmosphere etc. (Rahaman,2000, German,2007).

Table 1.5. Process variables of sintering and their effects (German , 2007 and 2014)

Sintering Process Variables	**Effects**
Reducing of grain size	Rapid sintering More cost High impurity Increasing hazards
Increasing of duration	More cost Grain growing and coarsening Reducing efficiency Increasing tensile ratios Grain growth
Increasing of temperature	More cost Low sensibility High quality properties Furnace limitations Porosity coarsening
Increasing of density	Less tensile ratios Less pores High final density Homogen measurements Density gradients High strength
Alloying increasing /Additives	Homogenization problems Sintering at high temperatures Faster sintering Lower sintering temperatures
Using of sintering aids	Embrittlement Distortion Grain growth control

Sintering sequence is occurred at three zone as pre-heat, hot and cooling zones. On the pre-heat zone, lubricants used in the forming of shapes are melted, spread to surface of parts or evaporated. On the pyrolyzing lubricant decomposition products oxidizing atmosphere are required and gas flow is

adjusted. The hot zone has low dew point and oxygen content. On the this hot zone, insufficient de-lubricating is cause to the boasting on the surface of materials and swelling, and also oxides are decreased, diffusion of alloy additions are replaced. On the final zone, cooling zone is unheated region at the end of hot zone. Water veiled cooling zone decrease the part temperature before charge, protecting of air intake and oxidation of parts is provided with atmosphere in cooling zone (Figure 1.8) (Rahaman,2000).

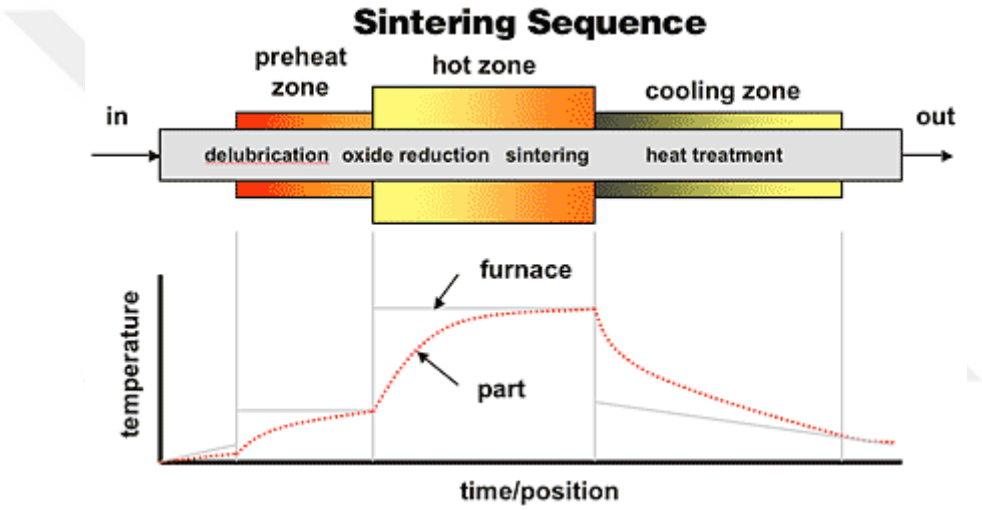


Figure 1.8. The Sintering Sequence (Rahaman,2000)

1.2.1.3.2.The Role of Sintering on the Mechanical, Electrochemical and Magnetic Properties of Formed Products

By sintering, the physical and mechanical properties such as porosity, specific surface area, density, strength improve. At high sintering temperature; pores closed, porosity reduces grain grow and coarsen. Density of parts increases, grain size improved and the microstructure of steels has more durable structure..Removing of pores is important for high strength and mechanical properties. Pores decreases influential cross-sectional area and therefore negatively

affects strength. For this reason, pores occurred in the parts must be removed, grains grow and density of parts will be increased, the strength of parts will be increased and other mechanical properties such as density, hardness. The permeability (μ_i) of parts are increased while coercive (H_c) and remanence decreased.

Powder metallurgy method that is one of the preparing of stainless steels, provides high quality product and accurately low cost. The usable of stainless steels produced by powder metallurgy method is restricted because of their low density. Therefore; corrosion resistance of these materials are deteriorated due to their higher porosity (Cabral- Miramontes *et al.,* 2013, Carcia *et al.*, 2007). Electrochemical features of sintered steels is lower due to happening of intermetallic compounds, high content of interstitial elements and also high porosity permiting the penetration of electrolyte via open pores throughout sintering process (Cabral- Miramontes *et al.,* 2013).

2.LITERATURE SURVEY

2.1. The Literature Survey of the Mechanical Properties of Austenitic Stainless Steels

Kyogoku *et al.,* (2003) compared the mechanical and structural properties of sintered compacts of water –atomized and gas atomized austenitic stainless steel powders. They appeared the values of tensile stregths of both stainless steel powder is similar to but the elongation of water-atomised powder compact is lower than that of gas-atomized powder compact and they showed the increasing in the impact energy with increasing decreasing density; but on the water atomized powder compact ; with increasing of debinding temperature; impact energy is decreased, on the other gas –atomized powder compact as debinding temperature ; impact energy is increased. They observed water atomized powder compact having small sized porosity and Si oxide embedded in the small pores and gas atomized powder compact having bigger porosity (Kyogoku *et al.,* 2003)(see in Figures 2.1-.2.2)

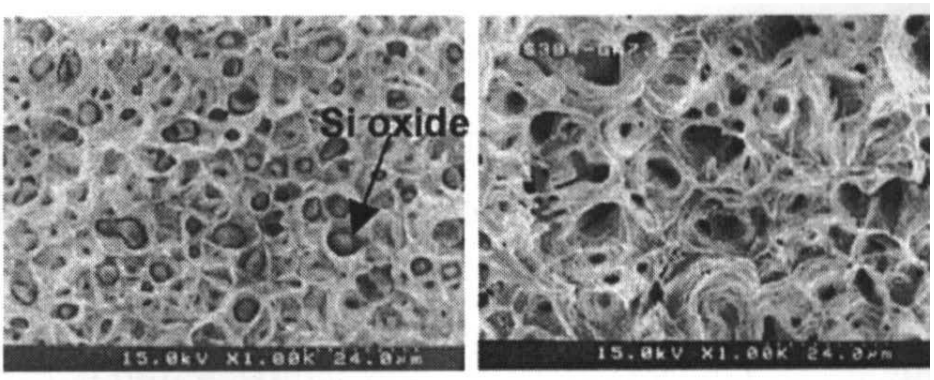


Figure 2.1. Scanning electron micrographs of water-atomized (WA) and gas-atomized (GA) powders (Kyogoku *et al.,* 2003)

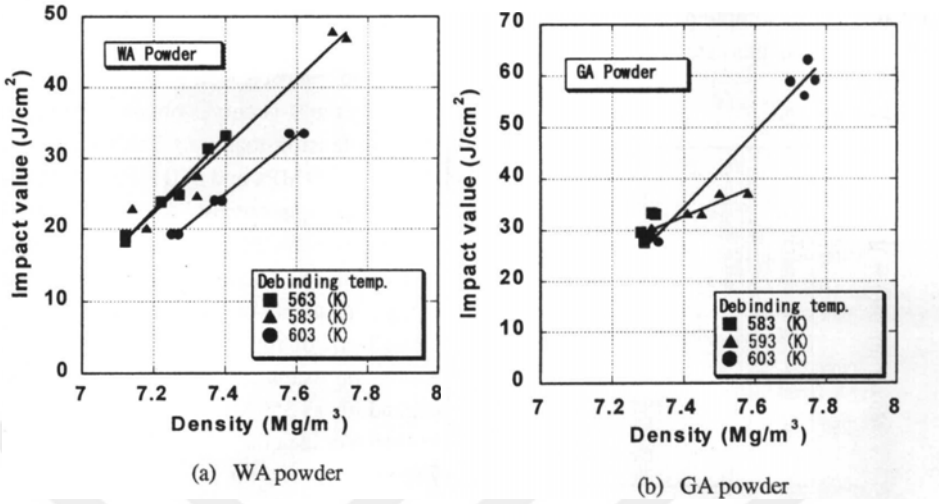


Figure 2.2. Influence of density on the impact value of sintered compacts (Kyogoku *et al.,* 2003)

Ghosh *et al.*(2012) investigated the influence of cold deformation on the strain induced α'martensite transformation and mechanical properties of austenitic stainless steel 30% and 40% cold rolled and observed 24% and 31.5 % martensite formation on the both structures, respectively. Authors recorded improving mechanical properties such as hardness related to the increasing deformation (Ghosh *et al.,*2012).

Pandhya *et al.* (2012) examined the mechanical properties consisting of density, hardness, strength and elongation of traditional solid state sintered (1200° and 1300°C) and supersolidus state sintered (1400°C) AISI316L austenitic stainless steels. They acquired the highest mechanical properties including sintered density of 7.168 g/cm^3 (with 89.60%Th), bulk hardness of ~126~HV_5, and recorded the obtained result similar to the wrought 316L values. Authors examined the highest values at the high temperature with uniformly distributed regular sized such as cups and cones as the particles adequately sintered; but, at the other sintered temperatures insufficient bonding between grains already dominated (Pandhya *et al.,* 2012) (see in Table 2.1).

Table 2.1. Effect of sintering temperature on the densification response and mechanical behavior of 316L stainless steel conventionally sintered at 1200, 1300 and 1400 °C, respectively (Pandhya *et al.*, 2012)

	Sintering Temperature (°C)			
	1200	1300	1400	Wrought 316L[1]
Sintered density (g/cm^3) (%Th)	6.641 83.01	6.845 85.56	7.168 89.60	-
Bulk Hardness (HV_5)	9.7±2.6	109±3.8	126±1.8	220 max

[1] ASTM A479 (Specification for annealed bar), A167-A240 (Specification for annealed Plate).

Kurgan (2013) worked the influence of sintering atmospheres on the mechanical properties consisting of sintered density, hardness and structural properties including grain boundary of 316L austenitic stainless steels. Author used argon and nitrogen as sintering atmospheres. He obtained the maximum hardness of 355,2 $HV_{0,1}$ on the nitrogen atmosphere sintered austenitic stainless steel, on the other atmosphere sintered austenitic stainless steel hardness values is lower. The elongation is acquired on the argon sintered 316L austenitic stainless steel (Kurgan, 2013) (see in Figure 2.3.).

Kan *et al.* (2014) examined the improving effect of micropores occurred on the 316 Laustenitic stainless steel prepared by powder metallurgy method applied hot forging and then heat treatment processes. They appeared the enhancing both the pore size homogeneity and relative material density on the various forging temperatures by hot forging methods and also showed, at high temperatures,

spheroidized the irregular pores and transforming to stable inner grain pores based on the deformation and diffusion bonding (Kan *et al.*, 2014).

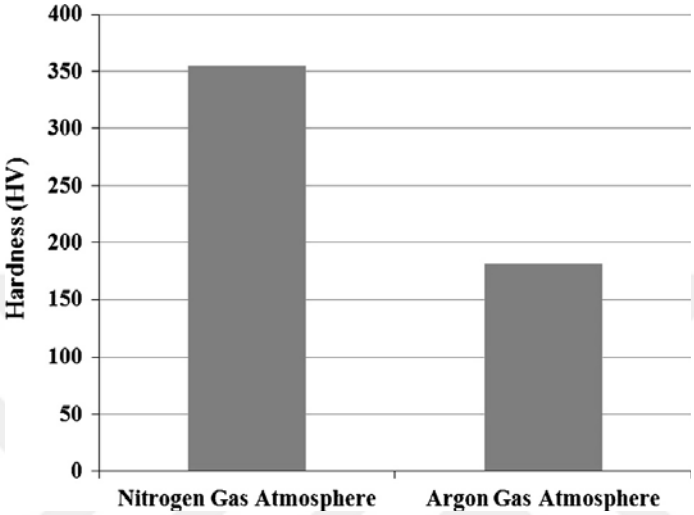


Figure 2.3. Effect of sintering atmosphere on microhardness of sintered 316L stainless steel compacted at 800 MPa (Kurgan, 2013).

Shashanka and Chaira (2014) compared the phase transformation and microstructure of ferritic and nano structured-austenitic stainless steels manufactured using planetary milling method and heat treated under nitrogen and argon atmosphere ın the 750°C for 1 hour. Authors observed the powder particles having micron range and indiscriminate size before milling and as-milling and as milling time continued, particles had strain hardening and spherical shape and also milling time continued for a while about 10 h, observed the crystallite size decreasing to 9-11nm in the both stainless steels. They recorded the transformation from ferritic to austenite supporting on both atmosphere but, the favourite atmosphere of nitrogen due to greater extent of austenitic transformation according to argon atmosphere (Shashanka and Chaira, 2014).

As seen in Figure 2.4; Javanbakht *et al.,* (2015) examined the effect of Ni amount (0-6wt%) on the mechanical properties of nanocrystalline medical-grade

stainless steels manufactured by powder metallurgy. They observed the increasing in and impact energy from 1 to 1.6 J) as increasing of additive content % to stainless steel (Javanbakht *et al.*,2015).

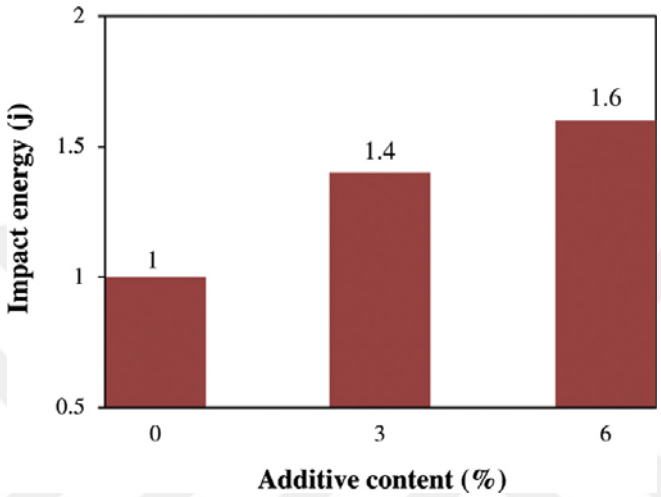


Figure 2.4. Charpy impact energy of the samples at room temperature (Javanbakht *et al.*,2015)

Javanbakht *et al.* (2016) studied the mechanical and structural properties of nano-structured ASTM F2581 austenitic stainless steel used medical area. Authors liquid phase sintered this austenitic stainless steel with 6 wt.% Mn–Si additive at various temperatures range 1000-1300°C. They observed the increasing of relative density, related to, decreasing of the porosity at different sintering temperatures and recorded the maximum relative density of 95% and in correspondence with the lowest porosity level having 6.8%. Authors obtained the optimum mechanical properties consisting of hardness(38HRC) and 95% relative density on the sintered austenitic stainless steel at 1150°C for 1 h and examined increasing of the mechanical properties related to the relative density increase and decrease of porosity amount (Javanbakht *et al.*, 2016) (see in Figure 2.5-2.7).

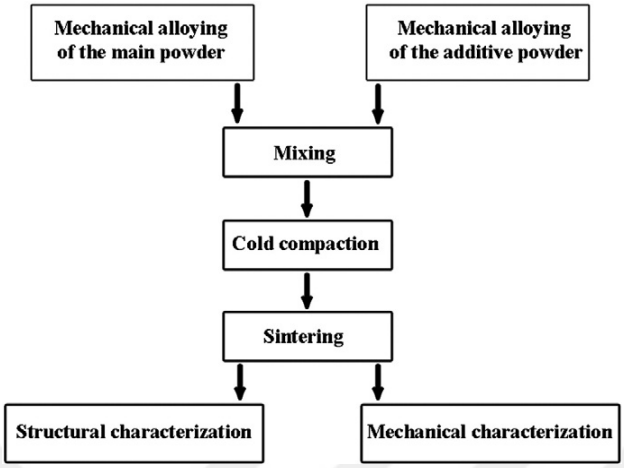


Figure 2.5. Schematic representation of Javanbakht *et al.* work (Javanbakht *et al.*, 2016)

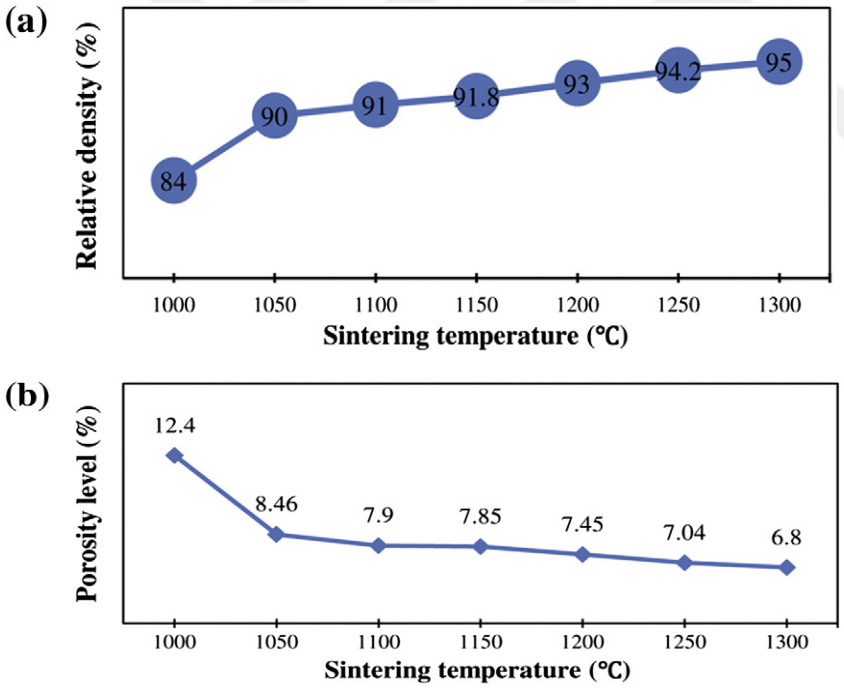


Figure 2.6. Relative density (measured by the Archimedes method) and porosity content (calculated by the image analyzer software) of the samples sintered at the different temperatures (experimental error < 1%) (Javanbakht *et al.*, 2016)

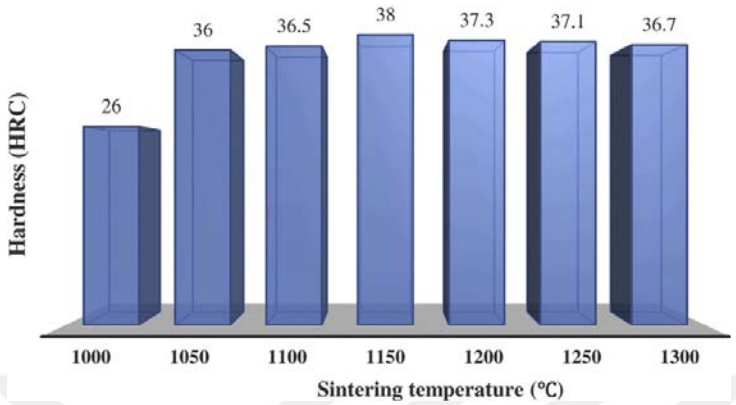


Figure 2.7. Macrohardness values of the sintered samples (experimental error < 3%)(Javanbakht *et al.*, 2016)

Yoon *et al.* (2016) examined the microstructural behaviour and mechanical property including relative density of sintered Fe-12wt.%Mn-0.2wt.% C alloy steel. They recorded relative density linearly increasing with increasing of volume fraction of ferrite and cementite, in response this, decreasing of austenite phase (to approximately 1.0%) with decreasing temperature and also examined the decreasing of austenite phase related to the initial relative density of sintered sample (Yoon *et al.,* 2016).

2.2 The Literature Survey of the Mechanical Properties of Martensitic Stainless Steels

Forghani *et al.*(2014) investigated the microstructural variations of yitrium (on the 0.05% and 0.8% ratios) bearing Fe-10Ni-7Mn martensitic steels and found the occurring of (Fe, Ni, Mn)17Y2 precipitates with hexagonal structure in a Fe-10Ni-7Mn-0.8Y (wt.%) alloy. Authors supported occuration of Y2O3 sub micron particles in the yitrium based bearing steels with their obtained results and also examined the influence of this particles on the austenite grain structure and

determined to the playing efficiently a role on the controlling the prior austenite grain structure (Forghani *et al.*,2014).

Wiessner *et al.* (2017) studied the transformation of reversed austenite form from martensite and the effect of this transformation on the tensile and impact strengths of the tempered martensitic stainless steel. They observed the decreasing the tensile strength with increasing tempered temperature but at approximately 600°C starting to the increase and on the impact strength, decreasing to the approximately 400°C, then from this temperature increase on the impact strength is occurred and then also approximately 600°C, impact strength is restart to the decreasing. Authors determined the decreasing and increasing of tensile and impact strengths reversibly. Maximum and minimum impact strengths were 130J (at 600°C) and 98J (at 410°C) and explained the reason of maximum impact strength is the highest value of the mass fraction of austenite occurring at intermediate tempering temperatures and also the mean dislocation density in martensite increasing and increasing fraction of newly transformed martensite caused to lower impact strength values (Wiessner *et al.,* 2017).

Huang *et al.* (2017) examined the mechanical and structural properties of 440Cstainless steel blended with niobium carbide powder with 5,10 and 15wt% amounts and sintered at various temperatures (1260, 1270, 1280 and 1290°C) for 1 h respectively They appeared that as increasing sintering temperatures having effects such as the increasing in the volume shrinkage ratio and hardness values while the decreasing of porosity and also observed the firstly increasing then decreasing in the transverse rupture strength values with increasing sintering temperatures (Huang *et al.*,2017). In Figure 2.8, increasing hardness values of these materials with increasing temperature observed and also in Figure 9; the SEM images of the optimal N5, N10 and N15 specimens (sintered at 1270 °C for 1 h) after heat treatment are appeared.

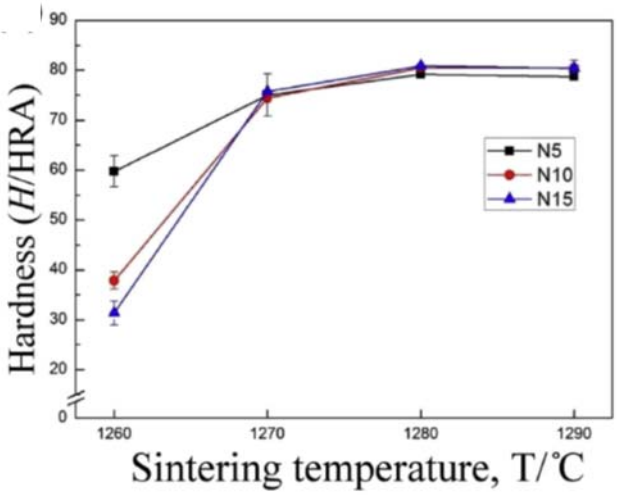


Figure 2.8. Comparison of the hardness of various wt.% NbC added 440C by the different sintering temperatures (Huang *et al.*,2017)

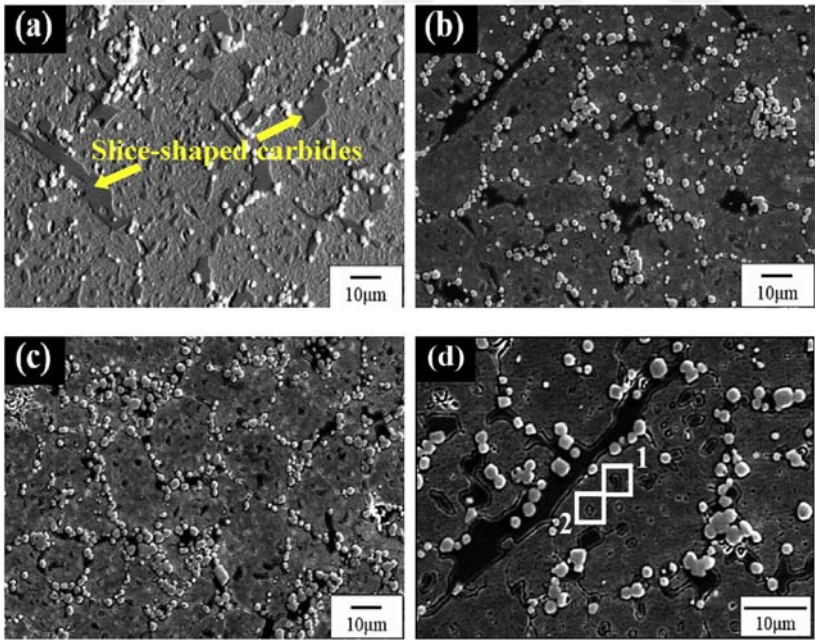


Figure 2.9. The SEM images of the optimal N5, N10 and N15 specimens (sintered at 1270 °C for 1 h) after heat treatment (a) N5+HT, (b) N10 + HT, (c) N15 + HT, and (d) EDS analysis location of the N10 + HT specimen (Huang *et al.*,2017)

2.3 The Literature Survey of the Magnetic Properties of Austenitic and Martensitic Stainless Steels

Tavares *et al*. (2002) examined the ferromagnetic properties of the 304 austenitic stainless steel related to applied deformation (Tavares *et al*., 2002). Mumtaz *et al.* (2003-2004) correlated between the martensitic transformation and magnetic features of 304 austenitic stainless steel under compressively deformation conditions. They stated that as basing on the volume percentage of α' martensitic transformation related to the temperature and plastic strain the saturation magnetization increased (Mumtaz *et al.* 2003 and Mumtaz *et al.,* 2004). Also, they (2004) showed the effect of the reverse martensitic transformation on the magnetism of the 304 austenitic stainless steel cold rolled besides direct martensitic transformation. authors revealed the decreasing of coercive force at temperatures 400-500°C due to increasing of α'martensite phase content, further decreasing of coercive force is owing to the moping out of some dislocations from α'martensite phase and also followed sharp increasing of coercive force is resulted from anisotropic magnetic effect (Mumtaz *et al.,*2004) Lai *et al.* (2004) worked the electrotically extracted precipitates and magnetic properties of thermal aged 316L austenitic stainless steel in the range of 5-375K with a up to 70 kOe magnetic field and the magnetic transitions related to the zero field-colled and field-cooled. Authors stated the existence of Chi phase and the effect of chi phase on the magnetization of the austenitic stainless steel and also magnetization against magnetic field at 200K had higher values for chi phase. They recorded the Neel points for chi and sigma phase of 100 and 75K, respectively and observed the magnetic transition relating to zero field-cooled increases with temperature, reach to maximum magnetization value at 50K, after then, magnetization was sharply decreased (Lai *et al.,* 2004) (Figure 2.10-2.11).

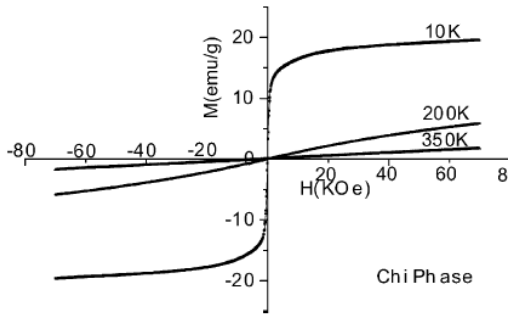


Figure 2.10. The *M–H* isotherms of Chi phase at different temperatures (Lai *et al.*, 2004)

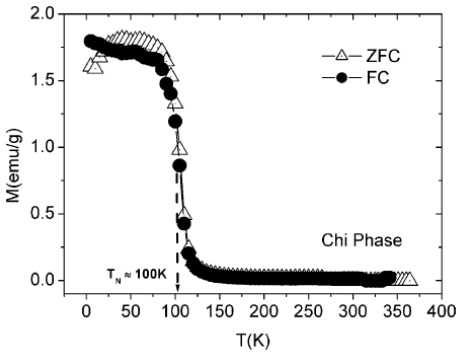


Figure 2.11. The temperature dependence of magnetization of Chi phase at low-field 100 Oe. Samples cooled under zero-field (ZFC) and with applied field (FC) respectively. (Lai *et al.*, 2004)

García *et al.* (2009) studied the structural and magnetic properties of AISI304 and AISI316L manufactured by powder metallurgy method and sintered under nitrogen atmosphere. They stated the AISI316L sintered under the nitrogen medium showed the paramagnetic feature, whereas the other stainless steel treated the ferromagnetic behaviour, and also stated the both the stainless steels had paramagnetic behaviour after solution annealing. Authors observed the base microstructural behaviour possessed the lamellar constituent occurred via nitride precipitates and austenite and/or ferrite interlamellar matrix and expressed the abnormal magnetic response was resulted from the these structures (as seen in Figure 2.12 and 2.13) (García *et al.* 2009).

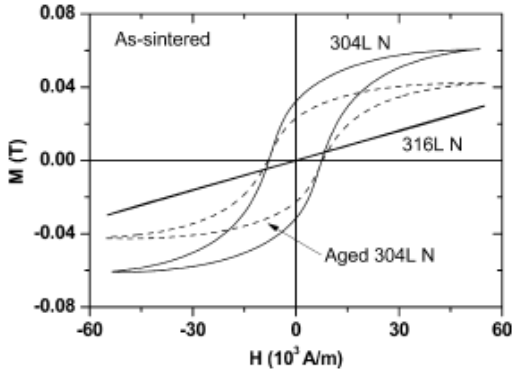


Figure 2.12. Magnetisation vs.field dependence recorded at room temperature for as-sintered 304LN and 316LN and for aged 304LN at 875 1C for 8h (García *et al.* 2009).

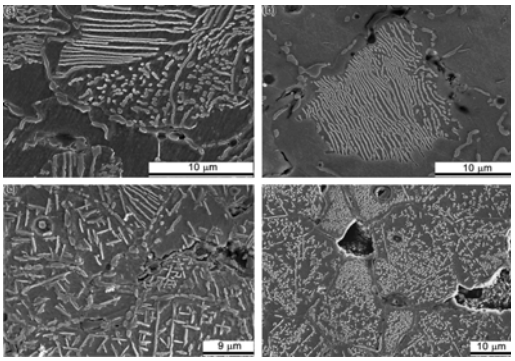


Figure 2.13. SEM micrographs of (a) as-sintered 304LN and (b) 316LN,(c) aged (875 1C and 48h) 304LN and (d) 316LN (Vilella etching) (García *et al.* 2009).

Yang *et al.* (2012) investigated the presence and developing of magnetic phase on the cold-drawn AISI 316L austenitic stainless steel fiber consisting of 18.5%strain-induced martensite. They expressed that the existence of strain induced martensite increased the magnetic behaviour of the 316Laustenitic stainless steel in heating TMA curves in the range of 460-470 °C and throughout cooling period , the increasing of magnetization but showed not to significant phase transformation (Yang *et al.*, 2012). Choi *et al*. (2013) also worked the effect of magnetic field on the isothermal martensitic transformation of the sensitized 304 austenitic stainless steel (Choi *et al.*,2013).

Mondal *et al.* (2012 and 2015) investigated the effect of Cu content on the magnetization of the 316L austenitic stainless steel produced by powder metallurgy method applied ball milling and annealing. On the effect of Cu content (25wt%); powder mixtures ball milled resulted to the austenite stabilizer Ni in the 316L austenitic stainless steel to Cu element; this case was caused to the bcc structure transformation of 316L austenitic stainless steel from the FCC structure of

austenitic stainless steel and authors stated that this bcc structure is led to treat the ferromagnetic behaviour of stainless steel on the annealing at the higher temperatures. On the effect of Cu content (75wt%); aftter milling at 40h, the bcc Fe is nearly dissolved in Cu element, but after milling during 70h; it does not come to any changes on the structure. Stimulating of soft ferromagnetic behaviour of austenitic stainless steel is resulted from bcc Fe precipitates in Cu element (Mondal *et al.,* 2012 and Mondal *et al.,* 2015).

Yetim *et al.* (2014) and Yazıcı *et al.* (2014) worked the influence of temperature of plasma nitriding on the magnetic and apprasive properties of plasma nitride 316L austenitic stainless steel and expressed that owing to the S-phase in the modified layer and increasing of the plastic deformation resistance; it was caused to the wear and magnetic properties of 316L austenitic stainless steel plasma nitrided enhanced with rising treating temperature (Yetim *et al.* 2014 and Yazıcı *et al,* 2014).

Das (2014) investigated the effect of low cycle fatigue deformation on the magnetization of nuclear grade AISI304LN austenitic stainless steel and observed the ferromagnetic α' bct martensite transformation from local stress/strain induced phase transformed paramagnetic behaviour γ-austenite phase. Author expressed the with the increasing strain amplitude resulted to the rise the magnetization and decreasing the coercivity (Das, 2014).

Watanabe *et al.,* (2015) worked the relationship among the structural and magnetical properties the electrochemically nitride 316Laustenitic stainless steel in molten LiF KF salt involving from Li3N at 873K and observed the changing of the crystal structure to bct structure from fcc and varieting of the magnetic behaviours from non magnetic to ferromagnetic due to nitriding process. Authors recorded the magnetization value of 81 emu/g and saturated magnetic moment at the 20 kOe magnetic field (Watanabe *et al.*,2015). Brink *et al.,* (2016) also investigated the structural propeties and magnetical properties of 316L austenitic stainless steel low temperature nitrided thin foils (Brink *et al.,* 2016)

Souza Filho *et al.*(2016) worked the relationship between the strain-induced martensite and magnetization of a cold-rolled AISI201 austenitic stainless steel and showed the deformation twin and shear bands with the increasing of the strain and also increasing of saturation magnetization on the existence of strain-induced martensite (Souza Filho *et al.,* 2016) (see in Figure 2.4-2.6).

In literature survey; there are at least work on the magnetic properties of martensitic stainless steels prepared by powder metallurgy method. Tavares *et al.* (2000) investigated magnetic behaviours of AISI420 steel at different heat treatment conditions (quenching and tempering).This study showed that this steel has magnetically softer in annealing and after oil quenchıng condıtıons and increasing coercive force , resıdual ınductıon, decrease of saturatıon (Tavares *et al.,* 2000). Oxley *et al.*(2009) studied the magnetic properties of ten different types of The magnetic properties ferritic and martensitic stainless steels at RT and at 77 K. and observed that RT measureements show the harder magnetic behaviour and steel which have low carbon has higher permeability and lower coercivity. Cooling to 77K, measurements show the harder magnetic behaviour.(Oxley *et al.,* 2009)

2.4. The Literature Survey of the Electrochemical and Thermophysical Properties of Austenitic and Martensitic Stainless Steels

Fossati *et al.*(2006) worked electrochemical feature of AISI 316L austenitic stainless steels that glow-discharge nitrided at temperature range from 673 to 773K at applying pressure of 10mbar for 5h. Untreated and glow discharge treated samples were experimented in 5% NaCl aerated solution at RT. Crevice corrosion experiments of these samples were experimented in 10% NaCl solution at fixed temperature of 328K for 60 days. Authors observed that untreated 316L austenitic stainless steels has low pitting and crevice corrosion resistance in NaCl solution medium. Glow discharged 316L austenitic stainless steel at low

temperature has increased corrosion resistance of crevice and pitting and surface hardness (Fossati *et al.*, 2006).

Li and Bell (2006) worked electrochemical behaviours of AISI410 martensitic stainless steel samples which are plasma nitride at temperatures of 420, 460 or 500°C temperatures for 20 h on the 500 Pa of chamber pressure under 25% N_2 + 75% H_2 atmosphere. Electrochemical behaviours of these samples performed in 3.5%NaCl and 1wt%HCl solutions. Authors specified that plasma nitrided martensitic stainless steels have both of higher surface hardnesses, corrosion resistances and lower weight losses and corrosion rates than that of untreated samples (Li and Bell, 2006)

Łepicka and Grądzka-Dahlke (2013) investigated influence of plasma nitriding and thermal treatment on electrochemical behaviour of 440B martensitic stainless steel that traditional thermal treated (quenched at 250, 390 and 605°C temperatures) and plasma nitrided in (50.50, 35.65 and 20.80) N_2:H_2 ratios. corrosion resistance of these samples were performed in 0.9 wt% NaCl solution. Authors observed that martensitic stainless steel tempered at 250 or 390°C temperatures has similar corrosion resistance. It is not commented that effect of high tempering temperature on the intergranular corrosion of martensitic stainless steels (Łepicka and Grądzka-Dahlke, 2013).

Cabral-Miramontes *et al*. worked corrosion resistance of AISI 409Nb stainless steel prepared by PM (powder metallurgy) method in 0.5M H_2SO_4 and 0.5M NaCl. These stainless steels mixed with boron that changed from 0.8 to 1.2 (wt%) and boron mixed stainless steels pressed on the 700MPa pressure and after, pressed samples sintered at 1150°C temperature for an hour under hydrogen atmosphere. Authors observed that green and sintered stainless steel samples experimented in sulphuric acid solution have higher corrosion rates than that tested in NaCl solution. Also, authors determined that stainless steel containing 0(wt%) boron experimented in NaCl solution has the best corrosion resistance and commented that this situation resulted from lower carbon amounts that blocked the

carbide occurring, which moves as corrosion beginning areas. Boron additives are worsening effect on the corrosion resistance of AISI 409Nb stainless steels prepared by powder metallurgy method (Cabral-Miramontes *et al*.2013).

Vignal *et al.*, (2014) investigated microstructure and electrochemical behaviours of X4CrNiMo16.5.1 stainless steel. They observed that for pitting corrosion; precursor clusters accumulate in the martensite phase. And determined that cold-worked layer on the this material has a important role on the initiating of pit after polishig proces, while has no effect on propagating of pit (Vignal *et al.*,2014)

Olaseinde (2015) examined temperature effect on the electrochemical properties of 316 austenitic and 2205 duplex stainless steels (DSS) obtained as plates with thickness of 6 mm in 1M sulphuric acid and 1 %NaCl solution medium at 25, 40, 60 and 80° C temperatures. By potentiodynamic method; these properties of these materials were determined. Critical current density of 316 austenitic stainless steel has higher than that of other stainless steel and the passive range of 316 austenitic stainless steel has longer appearance than that of other stainless steel. Better corrosion resistance obtained on the 2205 DSS at 25°C temperature (Olaseinde, 2015).

In the literature; there are a little studies about thermophysical properties of stainless steel prepared by powder metallurgy method. Raju *et al.* (2010) prepared the 9.05 Cr, 1.0 W, 0.0036 Mo, 0.50 Si, 0.56 Mn, 0.09 C, 0.0206 N, 0.0036 Al, 0.0043 Co, 0.226 V, 0.005 Cu, 0.0024 Ti, 0.0039 Nb, 0.063 Ta; the remained ratio of Fe material using vacuum induction melting, then, vacuum arc refining method. The enthalpy of this material show non-linear increase with increasing temperature and this property varied with martensite transition at 793K (Raju *et al.,* 2010). According to article of Wiltham *et al.*, (2008) thermophysical properties such as specific heat capacity , enthalpy of DIN 1.4435 (X2CrNiMo18-14-3) material were determined at 500-2500K temperature range (Wittham *et al.*, 2008).

In this thesis study; the physical, mechanical, electrochemical, magnetic and thermophysical properties of 316L austenitic and 410 martensitic stainless steels prepared by powder metallurgy method were investigated. As seen in above literature studies; there are more studies about physical, mechanical and electrochemical properties of these stainless steels but there are at least work about magnetic and thermophysical properties of these stainless steels, especially martensitic stainless steels. The relationships between magnetic, thermphysical properties and other properties of these stainless steels were determined also effects of chemical compositions and particle size distributions of these sainless steel powders on these properties were specified.

3. MATERIAL AND METHOD

3.1. Material

In this thesis work, the materials used were 316L austenitic and 410 martensitic stainless steel powders, which were obtained from North American Höganas via importer company Sintek Toz Metalurjisi Industry and Trade Inc. Shi Jia Zhuang Daye Metal Powder Factory in China, respectively (see in Figure 3.1).



Figure 3.1. The powders of 316L austenitic and 410 martensitic stainless steels

In literature; 316L austenitic and 410 martensitic stainless steel powders are called as X2CrNiMo17-12-2 austenitic and X12Cr13 martensitic stainless steels, repectively. The chemical composition and particle size characteristics of 316L austenitic and 410 martensitic stainless steel powders utilized in this work are given in Table 3.1. and Table 3.2.

As seen in Table 3.1; the austenitic and martensitic stainless steels are based on additions of impending principal Chromium, nickel and iron elements; molybdenum, silicon, carbon, phosphorus, carbon and etc. On the martensitic stainless steels carbon content is higher and chromium content is lower.

Chromium, molybdenum, phosphorus and silicon are ferrite developer; nickel and manganese are austenite stabilization and also carbon in microstructure supports development of precipitations increasing of corrosion resistance.

Table 3.1 Typical chemical compositions (wt%) of 316L austenitic and 410 martensitic stainless steel powders

	316L austenitic stainless steel	410 martensitic stainless steel
Cr	16.41	13.3
Ni	13.18	-
Mo	2.17	-
Si	0.98	0.83
Mn	0.23	0.21
C	0.02	0.041
P	0.018	0.02
S	0.00	0.02
Fe	Balance	Balance
Binder	Acrawax(1.0%)	Lithium Stearate (0.7%) Micronized PE Waxes (0.3%)

Table 3.2. Typical particle size distributions of 316L austenitic and 410 martensitic stainless steel powders

	316L austenitic stainless steel	410 martensitic stainless steel
D10(µm)	1.789	0.971
D50(µm)	14.04	7.211
D90(µm)	56.39	28.78
Scattering Type	Mie	Mie
Dispersant Type	Water	Water

3.2. Method

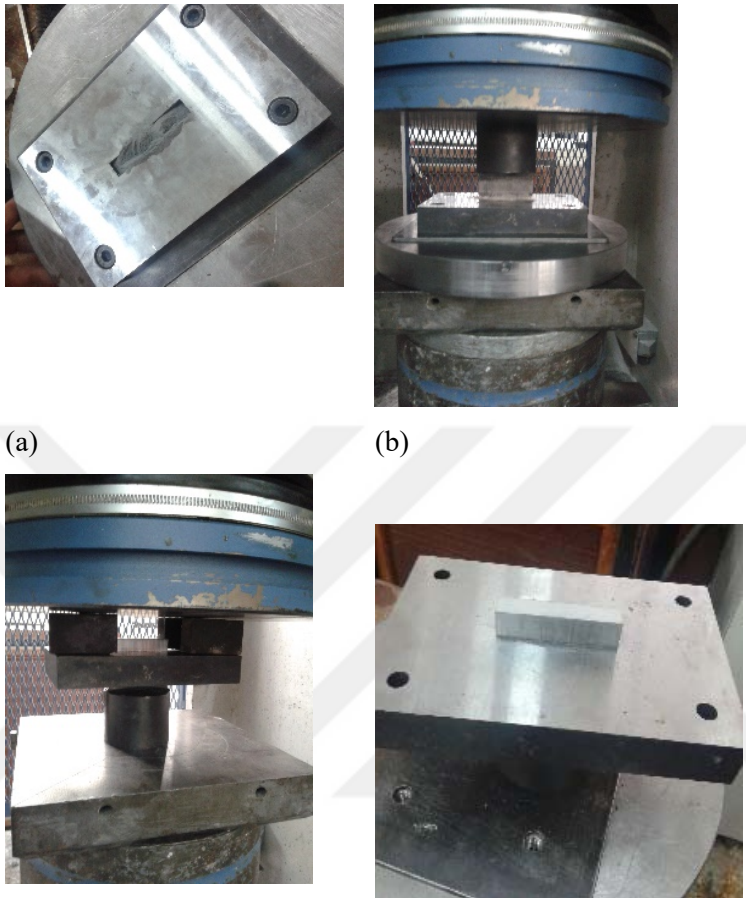
3.2.1. Preparation Method of Specimens

In this thesis work, the 316L austenitic and 410 martensitic stainless steel specimens, were previously prepared. The specimens were compacted in a prismatic mold of 10×10×55 mm which has almost 37 g in mass with an accuracy of 0.001 g for static features. They were pressed on the 400 and 600 MPa pressures at the 5.3m/s rate the press machine in the Civil Engineering in Cukurova University in Adana, Turkey (see in Figures 3.2- 3.4).



(a) (b)

Figure 3.2. The mold used on this thesis study (a) assembled with stable and (b)female component of mold



(a) (b)

(c) (d)

Figure 3.3. (a) The mold is filling with powder (b) pressed to powder filled mold (c) sample extracted with applying reversible pressing (d) pressed sample.

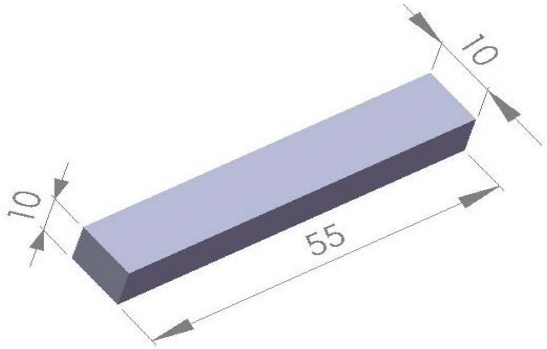


Figure 3.4. The technical drawing of compacted austenitic and martensitic stainless steel samples.

Pressed samples sintered in the atmosphere controlled furnace showed at the Figure 3.5 for specified sintering cycle as seen in Figure 3.6 under Ar atmosphere. Samples were waited on the 600 and 900°C temperatures for 30 min because of the delubricating or debinding between grains, removing of oxides, uniform temperature distribution during heat treatment process; and also waited on the 1200°C for 1 h for next sintering stage (Pandya *et al.*, 2012; Butković *et al.*, 2012; Butković , 2013). After then, the samples cooled to room temperature in the furnace medium. Heating and cooling rate was 5°C/min. Sintering stage was ocuurred at at Mechanical Engineering Laboratory in Engineering Faculty in Çukurova University in Adana,

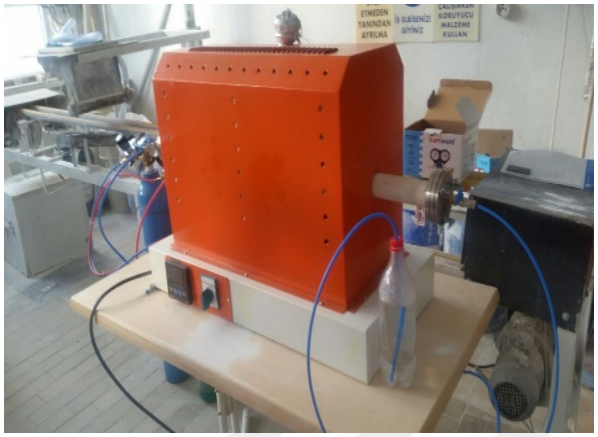


Figure 3.5. The atmosphere controlled furnace used on this study

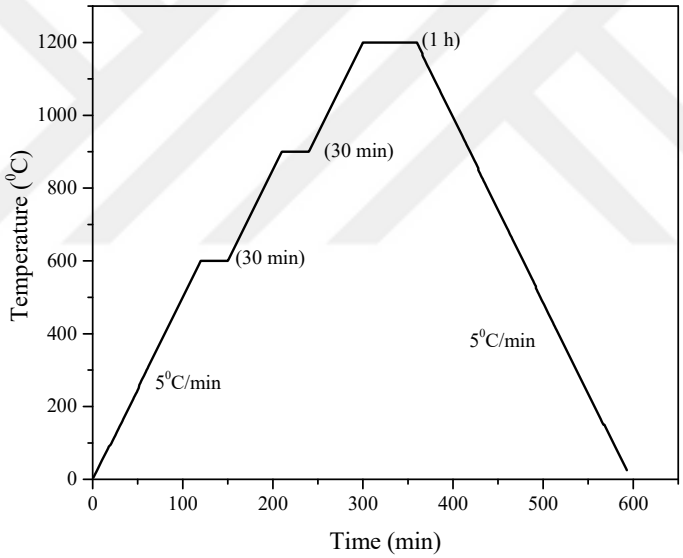


Figure 3.6. The sintering cycle applied on this thesis study

3.2.2. Characterization Methods of Powder and Sintered Martensitic and Austenitic Stainless Specimens

3.2.2.1. Measurement of Mechanical Properties of Austenitic and Martensitic Stainless Specimens

3.2.2.1.1 Density Measurements of Austenitic and Martensitic Stainless steel Specimens

In order to assess density and percentage of porosity measurements of sintered austenitic and martensitic stainless steel samples; Archimedes water displacement technique was used. This experiment was performed at Materials and Metallurgy Engineering Laboratory, in Materials and Metallurgy Engineering department, in Engineering Faculty in Dumlupınar University in Kütahya, Turkey. These experiments based on this technique were performed using Scaltec sec31 with precision of 0.0001g.

Firstly; 316L austenitic and 410 martensitic stainless steel samples cut to small prismatic specimens in order to take place chamber of assay balance; austenitic and martensitic stainless steel were weighted with scale, and sizes of samples measured with a micrometer. After, sampled were boiled to 100 °C in pure water, boiled samples in pure water waited for 4 hrs for homogeneously dispersing of water into the pores in the materials. After then, samples in the water cooled to room temperature and cooled samples dried with dishtowel. Dried samples were separately weighted in air and suspended in pure water. Density and porosity values of samples were calculated with obtained weighting values of samples. Equations (3.1-3.4) giving values of Density and porosity were given following;

Bulk Density (ρ_{bulk}) (g/cm^3) = $\frac{W_K}{W_D - W_A} \times \rho_{suyu}$ (3.1)

Apparent solid density ($\rho_{apparent}$) (g/cm^3) = $\frac{W_K}{W_K - W_A} \times \rho_{suyu}$ (3.2)

Apparent porosity (%) = $\frac{W_D - W_K}{W_D - W_A} \times 100$ (3.3)

Water adsorption (%) = $\frac{W_D - W_K}{W_K} \times 100$ (3.4)

From equations; W_K,W_A and W_D are referred as dried weight, suspended weight in pure water, weighted in air , respectively.

3.2.2.1.2. The Brinell Hardness Test

As a known hardness is defined the resistance of materials to the deformation. In this thesis study; to specify Brinell hardness values of austenitic and martensitic stainless steel specimens, The Brinell Hardness test method which is referred in ASTM10 has been applied using BMS Digirock Hardness Tester (see in Figure 3.7) at Mechanical Engineering Laboratory in Engineering Faculty in Çukurova University in Adana, Turkey. In this hardness test is applied examining of minimum three different indenter diameters resulted from pinning out 2.5 milimeter steel ball with 31.25 N force, by optical microscope helped and Brinell hardness values of samples are calculated in given following formula according to measured diameters of indenters. On the equation (3.5) P is called applying load in kilograms(kg) D, d are maximum indenter diameter and minimum indenter diameter (mm), respectively. The unit of Brinell hardness is given as N/mm^2.

$$HB = \frac{2P}{\pi D\left(D - \sqrt{D^2 - d^2}\right)} \quad (3.5)$$



Figure 3.7. Hardness Test Machine used for hardness measurements

3.2.2.1.3. The V-Notch Impact Experiment

Impact test of Notched bar metals gives information about defect under high velocity conditions causing to abrupt fracture. Absorbed energy called toughness relate to the area under stress-strain curve. Ductile materials have wide area, hence the toughness of ductile materials is high, absorbed energy of this materials is high and the appearance of this materials have hard and less crystalline. As ductility is decreased, the area under stress-strain curves and thereby absorbed energy and toughness of this materials are decreased. This materials is brittle materials. This materials have relatively smooth and more crystalline appearances. There are two standardized impact test as Charpy-v-notch,and izod impact test. In this thesis study; Charpy-v-notch impact test was used owing to commonly utilization of this test type on the steel materials.

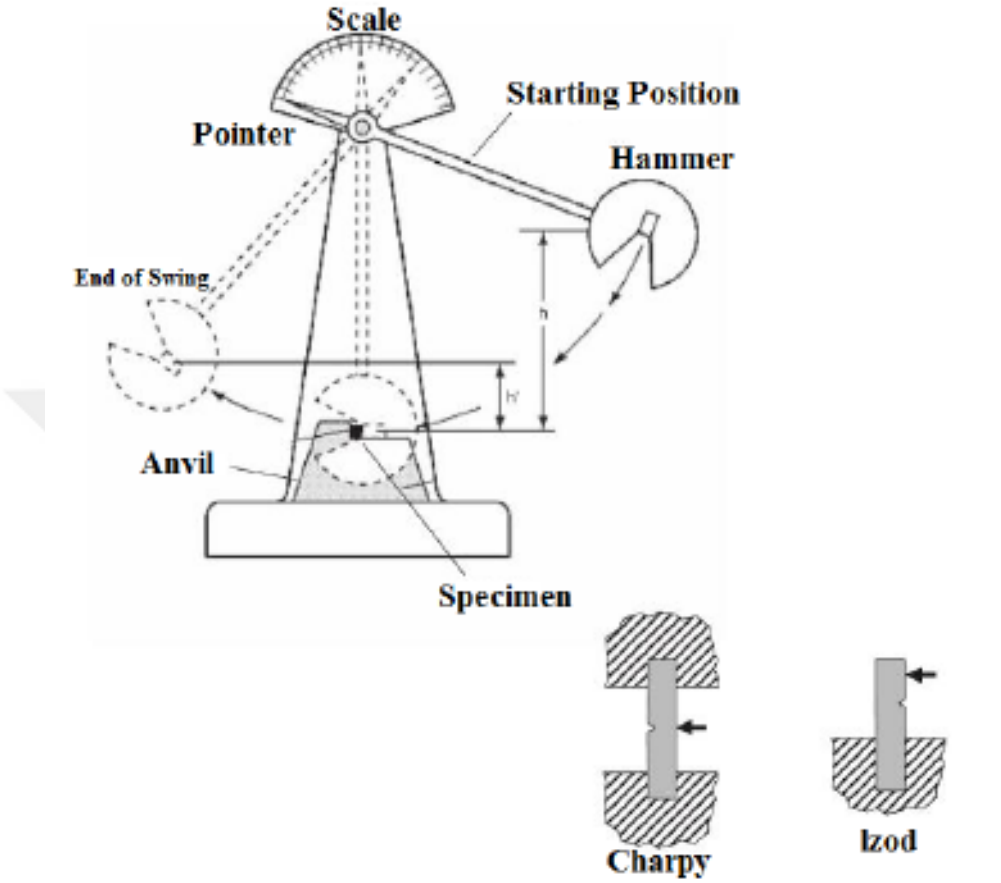
On the Charpy-v-notched impact test; with notching press, notchs on the medium of (10×10×55) austenitic and martensitic stainless steels were occurred as notch angle of 45° and notch type of 2 mm. then as shown in Figure 3.9. specimen is placed to instrument and this specimen is fractured. Absorbed energy (E,J), is calculated by given following formula.

$E_k = m.g.(h-h')$ (3.6)

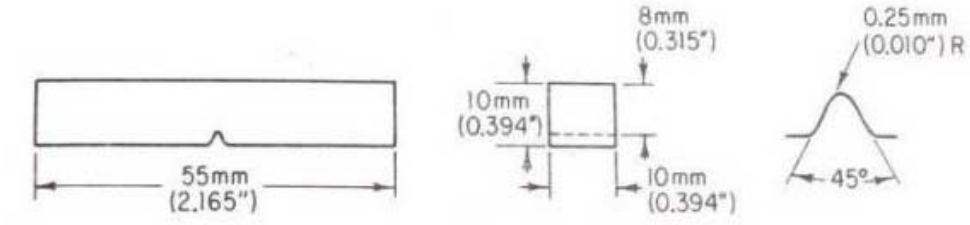
m is defined the pendelum mass g is also gravitional acceleration.

Charpy impact strength ($\sigma_ç$, J/mm^2) $= \frac{E_K}{A}$ (3.7)

On the equation; A is defined as cross sectional area (mm^2). Charpy impact strength is symbolized as $\sigma_Ç$ (J/mm^2).



(a)



(b)

Figure 3.8. The impact test schematic appearance of impact testing device (a) (Zhang, 2016; Yasuhisa *et al*.,2009) and the technical drawing appearance of austenitic and martensitic samples (b) (Ç.Ü. Ceyhan Mühendislik Fakültesi Deney Föyü)

In this study; Charpy-V-notched impact strenghts tests of materials have been evaluated according to the pressure differences and fractured surface of samples examined with the SEM machine. Charpy –V-Notched impact experiments have been performed at Mechanical Engineering Laboratory in Engineering Faculty in Çukurova University in Adana, Turkey



(a) (b)

Figure 3.9. (a) The samples prepared for impact testing experiment (b) The impact testing device

3.2.2.2. Measurement of Electrochemical Properties of Austenitic and Martensitic Stainless Specimens

The corrosion resistance of 316L austenitic and 410 martensitic stainless steel prepared on 400 and 600MPa pressures (on (10×15×70) mm prismatic mould) and heat treated as stated in Figure 3.6. were examined in Chemistry Laboratory in Chemistry Department in Sciences and Letters Faculty, in Çukurova University, in

Adana, Turkey. The samples were immersed in a 3.5%NaCl solid solution open to air with a thermostat (Nuve BS302 serial number 03-0033) set to 298K temperature (RT) during the immersion time from 30 min to 96 hrs and electrochemical measurements performed via CHI (604D) Electrochemical Analyser under computer controllable. Three electrode experimental set was applied and platinum layer with surface area of 2 cm^2 as referans electrode, and Ag/AgCl (3MKCl) electrod as auxiliary electrode was used. Electrochemical Impedance Spectroscopy (EIS) measurements were performed and obtained experimental results were fitted according to equivalent circuit drawing via ZView software program and these fitted EIS parameters were calculated. After immersion time of 96 hrs in test solution polarization curves were acquired with a scanning speed of 1 Mv/s

3.2.2.3. Measurement of Physical Properties of Austenitic and Martensitic Stainless Steel Samples Via the Physical Properties Measurement Systems (PPMS)

The PPMS manufactured by Quantum Design are different temperature field systems on the measuring physical behaviours such as magnetic, thermal and electrical properties of materials. In the thesis study; in order to measure the physical properties; the Quantum Design-Dynacool which a type of PPMS, has been utilized. In order to cool both sample chamber and superconducting magnet; this instrument provides a minimum amount of condensed liquid Helium-4 and works with an integrated cryopump. This cryopump is applied on pumping the specimen out to a vacuum of $<10^{-4}$ torr. On the controlling and stabilizing temperature, enhancing cooling power, novel gas flow regulation system on the Quantum Design- DynaCool is applied. At high temperatures (400K) required on the minimal cooled power and intermediate temperatures on the needed rapid twisting and large cooling and also smaller temperatures than 1.8K which stable operation near the basal temperature, this instrument provides impeccable transformations and cooling of the system is applied with the liquid helium and lso

acquired on the temperature changes from 300Kto 1.9K under 40 minutes. The puping of cryopump out is occurred to under 10^{-4}Torr in less than 10 minutes. The system is equipped with devices which will applied on the cooled superconductor magnetic, on the 9T or 14T conductors.

As PPMS measurements; the magnetization measurementts of sintered 316L austenitic and 410 martensitic stainless steel samples have been performed at CUMERLAB (Çukurova University Central Laboratory) in Çukurova University Adana, Turkey. Magnetization measurements of these sintered austenitic and matensitic stainless steel samples, against applied field (M-H measurements) were measured at 300, 350 and 400 K temperatures up to 4T magnetic field; for M-T measurements depended on Field –cooled (FC) and Field-heated (FH); these measurements were examined at the temperature range from 300 to 400K under 0,5 T magnetic field.

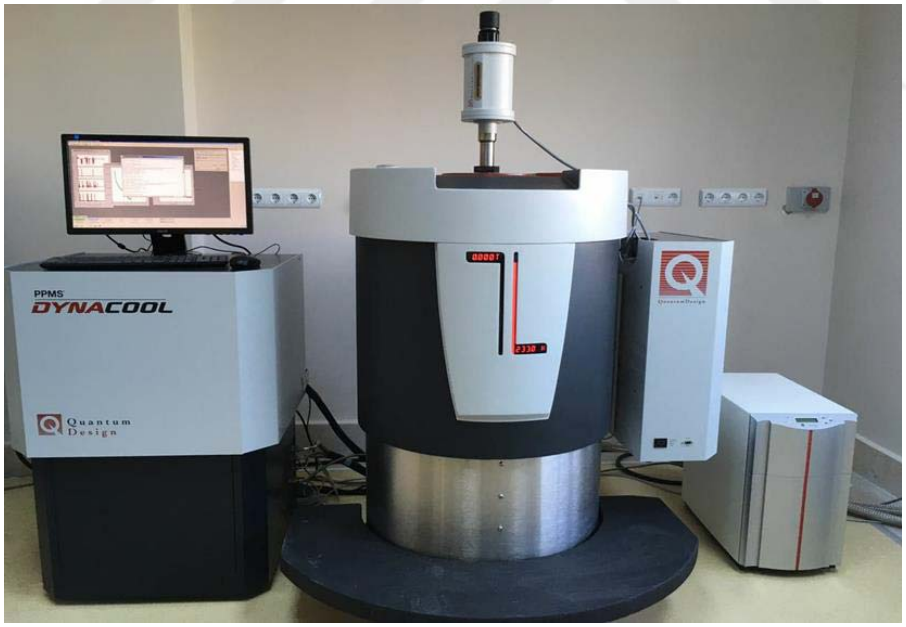


Figure 3.10. The Quantum Design-Dynacool-9 machine used for physical measurements

3.2.2.4. Measurement of Thermophysical Properties of Austenitic and Martensitic Stainless Steel Samples Via the Differential Scanning Analysis(DSC)

The DSC measures adsorbed and floated energy amount on the heating, cooling or waiting at isothermal constant temperature of material. Also, enthalpy of samples are measured due to related to thermal transitions and chemical reactions. This method is used to defined and qualify the materials.

In the thesis study; in order to evaluate the thermophysical properties of austenitic and martensitic stainless steel samples; Mettler Toledo DSC3+ used with technical properties as working temperature range up -170°C – 700, accuracy of temperature of ±0.2°C, resolution of temperature of ±0.02°C, rate of temperature of 0.02°C ile 300°C/min, measuring range up ± 350 mW, ceramic FRS5+, (56 thermocouple) as cencor and calorimeter sesnsitibility of 0.02 µW.



Figure 3.11. Mettler Toledo DSC3+ used on this study

In the thesis study; for thermophysical properties of 316L austenitic and 410 martensitic stainless steel, specific heat capacity and enthaply of samples were performed via this device with working temperature of RT to 600 °C, working

atmosphere of N_2 atmosphere, and gas flow of 20°C/min, at CUMERLAB (Çukurova University Central Laboratory) in Çukurova University Adana, Turkey.

3.2.2.5. Surface Characterization Methods of Powder and Sintered Martensitic and Austenitic Stainless Specimens

3.2.2.5.1. Particle Size Measurement of Powder of Martensitic and Austenitic Stainless Specimens

In the thesis study; before mechanical, physical, thermophysical and electrochemical properties of austenitic and martensitic stainless steel samples were performed, powders of stainless steel samples were investigated using BT-9300HT Laser particle Size Analyser with size range up 0.1-716µm, repeatability of < 1%(CRM D50) , accuracy of < 1%(CRM D50), measuring principle of Mie scaterring , laser of Import optical fiber semiconductor laser, operating system of Win XP/Win7, photodetector og 80pcs, ultrasonic power of 50w, tank capacity of 500mL, circulating flowrate: 1500 mL/min, small volume cell capacity of 20mL, small volume cell agitator speed of 120rpm, voltage of 220V, 50/60HZ. As medium; water was used. Particle size Distributions of 316L austenitic and 410 martensitic stainless steel powders have been examined at Reseacher and Development Laboratory in Ercan Cam Mozaik Çinikoop Co. in Kütahya, Turkey.

3.2.2.5.2. Scanning Electron Microscope (SEM) Characterization Methods

In examined the microstructures on the scanning electron microscope; sample preparation has great importance. The specimens are cut, moulded, grinded and finally polished the surface of specimens. These steps are occurred the main-branches of metallography science.

In the Scanning Electron Microscopy (SEM), as electrons bombarded on the structures of the samples and led to charge the structures, the examining of electrically isolated material happens. In this thesis study the SEM used for

examining microstructure of specimens is FEI -Quanta 650 Field Emission SEM. This machine have 12nm secondary electrode (SE) at 30kV, 2.3 and 3.0nm (SE without electron deceleration) at 1Kv for high vacumm medium, 2.0 nm(SE) AT 30kV for low vacuum medium,accelerating voltage of 100V-30kV,prob current of 100nA and also magnification of 6-1.000000x. SEM has also high vacuum SE and backscattered four segmented BSE detector, high vacuum BSEand SE detectors, energy distributed X-ray spectroscopy(EDXS), GSED detector (for ESEM mod), back-invitable STEM detector, BSE detector workable at the low vacuum medium.

The SEM images of powder and sintered austenitic and martensitic stainless steel samples were obtained using FEI Model: Quanta 650 Field Emission SEM with 20.00 kV EHT and high vacuum, at CUMERLAB (Çukurova University Central Laboratory) in Çukurova University Adana, Turkey.



Figure 3.12. The FEI -Quanta 650 Field Emission SEM machine used on this study

3.2.2.5.3. X-ray Diffraction (XRD) Characterization Method



Figure 3.13. The PANanalytical-Empyrean XRD device used on this study

The XRD characterization method bases on the basis of breaking of X-rays in their characteristics order related to intrinsic atomical packages of each of crystalline. In this thesis study; in order to examine the phases of austenitic and martensitic stainless steel, PANalytical-Empyrean XRD device has been used. This device has the features including of X-ray tube of Cu-Kα, working voltage range of 2-50kV, working current range of 5-60 mA, goniometer diameter of 480mm, minimum step size of 0.00010(θ/2θ), maximum usable measurement angles (2θ) varieting from -111° to 168° Pixel-based fast detector, minimum pixel area of (70×70)μm and Bragg-Brentano optical modul,

The XRD patterns of powder and sintered austenitic and martensitic stainless steel samples were recorded via PANalytical –Empyrean XRD with tube voltage of 45kV, tube current of 40 mA, scanning rate of 0.013 °/min, Cu-Kα radiation type, at CUMERLAB (Çukurova University Central Laboratory) in Çukurova University Adana, Turkey.

4. RESULTS AND DISCUSSIONS

4.1 The Microstructural Analysis of Austenitic and Martensitic Stainless Steel Powders

In the Figure 4.1., the SEM images and particle size distributions of 316L austenitic and 410 martensitic stainless steel powders shows. Firstly; according to the SEM images of both these powders, it is observed that both austenitic and martensitic stainless steel powders have irregular shaped particles, which is the typical property of water-atomised powder. This shaped particles are tended to easier and better pressurability because of consisting of filling gaps among the particles to the compactibility of circular shaped particles (Rudianto *et al*., 2015a, 2015b). As the examined the particle size distributions of these stainless steels powders; particle size distributions of both austenitic and martensitic stainless steel powders exhibit positively particle size distributions due to mostly fine particles in the stainless steel powders.

The Particle Size Distributions of 316L austenitic and 410 martensitic stainless steel powders are given on the Table 4.1. It is appeared D10, D25,D50, D75 and D90 values and D [3,2] and D[4,3] values of both these stainless steel powders. D10,D90 and D50 values are showed by fine, coarse and median particle size fractions, respectively, Median particle size diameter is also expressed with centre of the size distribution. D [3,2] and D[4,3] values are stated by Sauter and de Broucker mean diameters. Souter mean diameter is weighting avearge surface diameter supposing spherical particles of the same surface area of the real particles. De Broucker mean diameter is referred by weighted average volume diameter taking spherical particles of the same volume as the genuine particles into account (A Guidebook to Particle Size Analysis, Horiba Scientific, Dyankova *et al.*,2016). In other words, Sauter mean diameter is meant to surface area moment mean and de Brouckere man diameter is also called to volume or mass moment mean. In addition to; Sauter mean diameter is the most sensitive on the existence of fine

particles and de Broucker mean diameter is the most critical on the existence of big particles. Both these means are similar to inertia moments and show the frequency centre point around which the distribution would spin and actually meant to gravity centres of the separate distributions (A Guidebook to Particle Size Analysis, Horiba Scientific, Dyankova *et al.*,2016). On the Table 4.1; it is observed that; for austenitic stainless steel powder, D10, D90 and D50 values are 1,789, 56,39 and 14,04 μm, respectively, and also Sauter and de Brouckere mean diameters are 3,597 and 22,90μm , respectively; For martensitic stainless steels, D10, D90 and D50 values are 0,971, 28,78 and 7,211 μm, respectively, and also Sauter and de Brouckere mean diameters are 2,210 and 11,68 μm , respectively. Quartile ratio is defined by the distribution width obtained from cumulative distribution and calculated using the ratio of D75 and D25. Quartile ratios of austenitic and martensitic stainless steel powders in this thesis study are calculated as 5,930 and 5,830. To evaluate the width of the size distribution, SPAN value calculated using extracting from D90 to D10 values and relative SPAN value is acquired with dividing SPAN obtained to median mean dimeter (D50) and as it is seen, this relative SPAN value is dimensionless width measure. In the thesis study; SPAN values of both stainless steel are calculated as 54,601 μm for austenitic stainless steel powder and 27,809 μm for martensitic stainless steel powder, relative SPAN values of both these stainless steel powders are obtained as 3,888 for austenitic stainless steel and 3,856 for martensitic stainless steel. As it is seen; the quartile ratios and relative SPAN values of both austenitic and martensitic stainless steel powders are close to each other.

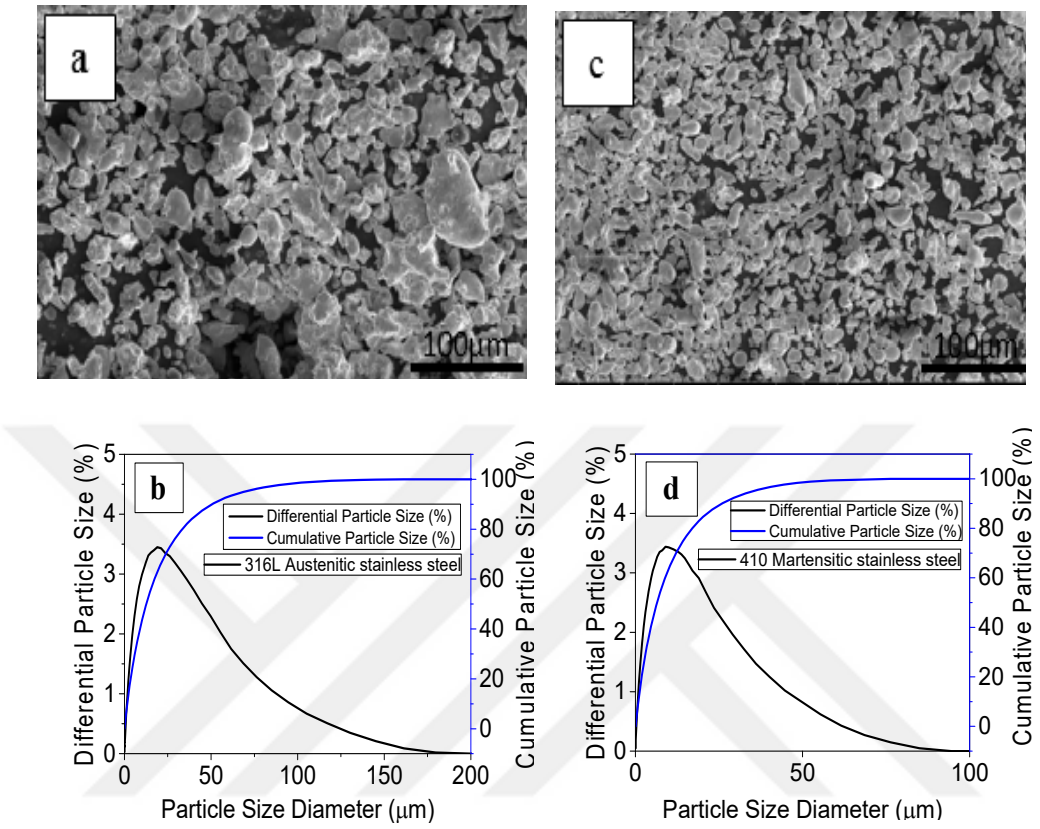


Figure 4.1. The SEM images and cumulative particle size distributions of 316L austenitic ((a) and b)) and 410 martensitic (410) stainless steel powders ((c and d)) (black line and blue line are referred as differential particle size and cumulative particle size distributions, respectively.

Table 4.1. The particle size distributions of 316L austenitic and 410 martensitic stainless steel powders

The Particle Distribution of 316L Austenitic Stainless Steel Powder							
D10	**D25**	**D50**	**D75**	**D90**	**D[3,2]**	**D[4,3]**	**SSA***
(µm)	(µm)	(µm)	(µm)	(µm)	(µm)	(µm)	m^2/kg
1,789	5,254	14,04	31,16	56,39	3,597	22,90	538,0
The Particle Distribution of 410 Martensitic Stainless Steel Powder							
D10	**D25**	**D50**	**D75**	**D90**	**D[3,2]**	**D[4,3]**	**SSA***
(µm)	(µm)	(µm)	(µm)	(µm)	(µm)	(µm)	m^2/kg
0,971	2,732	7,211	15,93	28,78	2,210	11,68	875,6

*SSA: Scanned surface area

The XRD patterns of 316L austenitic and 410 martensitic stainless steel powders are presented in Figure 4.2. It is showed that the microstructure of austenitic stainless steel powder has γ-Fe austenitic phase with α-FCC lattice structure and the γ-Fe austenitic phase peaks for 2θ angles of 43.671°, 50.827° and 74.684° for the austenitic stainless steel powder (Weng *et al*., 2019). For martensitic stainless steel powder; it is showed that the microstructure of this powder has the typical form of cubic structure of BCC- Fe, in example ferrite and also existence of tetragonal type of martensitic structure (BCT) is tenuously observed on the various diffraction angles. This α-Fe phase peaks for 2θ angles of 44.74°, 65.021°,82.261° for this martensitic stainless steel powder (Weng *et al.*, 2019).

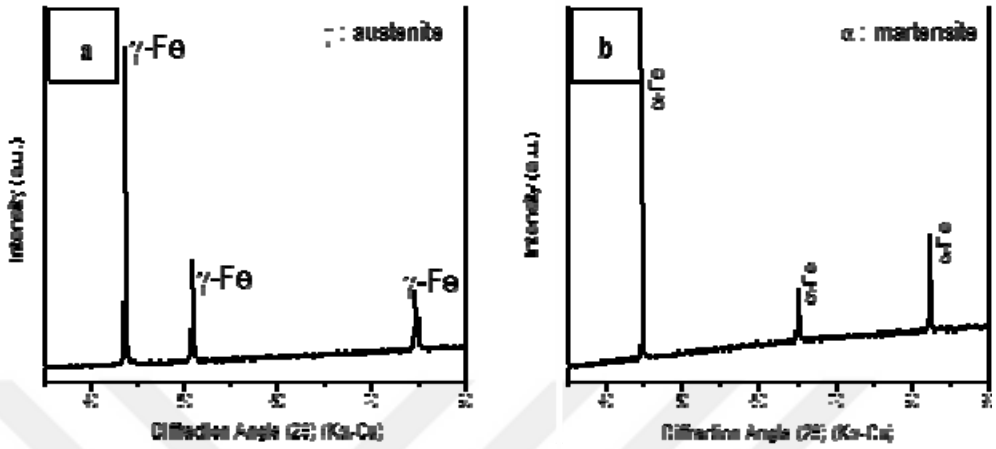


Figure 4.2. The XRD patterns of 316L austenitic (a) and 410 martensitic (b) stainless steels powder

4.2 The Density and Hardness Measurements of Austenitic and Martensitic Stainless Steels

As shown in Table 4.2; the bulk density (g/cm^3), apparent solid density (g/cm^3), apparent and total porosities (%) and also water adsorption (%) values of 316L austenitic and 410 martensitic stainless steels prepared on 400 and 600 MPa pressures were given. As pressure increased; bulk (g/cm^3) and apparent solid density (g/cm^3) values of stainless steels increased, whereas apparent porosity (%) and water adsorption (%) values of them decreased. The high bulk density values obtained as 6.9160 g/cm^3 for the austenitic stainless steel prepared on the high pressure and 6.1174 g/cm^3 , for the sintered martensitic stainless steel prepared on the high pressure. The high apparent solid density values obtained as 7.2238 g/cm^3 for the austenitic stainless steel prepared on the high pressure and 6.3941 g/cm^3 for the martensitic stainless steel prepared on the high pressure. The low apparent porosity values obtained as % 4.2615 g/cm^3 for the austenitic stainless steel prepared on the high pressure and % 3.3890 for the martensitic stainless steel

prepared on the high pressure. The low apparent porosity values obtained as 4.2615% for the austenitic stainless steel prepared on the high pressure and 3.3890 % for the martensitic stainless steel prepared on the high pressure. The low water adsorption values obtained as % 0.6162 g/cm^3 for the austenitic stainless steel prepared on the high pressure and % 0.5486 for the martensitic stainless steel prepared on the high pressure.

Table 4.2. The Density and Percentage Water Adsorption Values of 316L austenitic and 410 martensitic stainless steel samples prepared on 400 and 600 MPa pressures

	316L Austenitic Stainless Steel		**410 Martensitic Stainless Steel**	
	400 MPa	600 MPa	400 MPa	600 MPa
Bulk Density (g/cm^3)	6.5814	6.9160	5.8437	6.1174
Apparent Solid Density (g/cm^3)	7.1185	7.2238	6.3231	6.3941
Apparent Porosity (%)	7.5455	4.2615	7.5818	3.3890
Water adsorption (%)	1.1465	0.6162	1.2974	0.5486

Table 4.3. The Brinell hardness values of 316L austenitic and 410 martensitic stainless steel samples prepared on 400 and 600 MPa pressures

Brinell Hardness (HB;N/mm^2) values		
	400MPa	**600MPa**
316L	80.81	85.79
410	93.24	110.09

The hardness values of 316L austenitic and 410 martensitic stainless steel samples prepared on 400 and 600 MPa pressures observed in Table 4.3. The high hardness values acquired as 85.79 N/mm^2 for austenitic stainless steel prepared on the high pressure and 110.09 N/mm^2 for the martensitic stainless steel prepared on the high pressure

As pressure increases; grain bonding increases and porosity decreases. With heat treatment process including high sintering temperatures (~1200°C) after applied pressure; atomic vibrations within the grains of stainless steels increases, atomic diffusion occurs and then, more atoms move with atomic diffusions (Yao *et al.,* 2016). Due to motion of atoms with atomic diffusion; at the contact areas within the stainless steels binding surfaces among atoms occur. With extending of binding surfaces, sintering necks among atoms occur. As occurred sintering necks grows; structures of stainless steels become more strengthening structures (Yao *et al.,* 2016). Austenitic and martensitic stainless steel powder grains have fine particles as stated in a Table 4.1. Binding of more fine particles occurs more grain boundary; this case improves the hardness and density values of austenitic and martensitic stainless steels (Yıldızlı, 2015; Butković ,2013). Also, in Table 4.2; it is observed that bulk and apparent solid density values of austenitic stainless steel have higher according to that of martensitic stainless steels and we can be considered that the high-density values related to the Ni content within austenitic stainless steel. Because increased Ni content within the austenitic matrix activates and accelerates sintering and easier transfer of atoms into structures. With transferring of more atoms, structure become denser (Tosangthum *et al*., 2006).

4.3 The Charpy-V Impact Strengths of Austenitic and Martensitic Stainless Steels

Table 4.4. The Charpy-V notch impact strengths of 316L austenitic and 410 martensitic stainless steel samples prepared on 400 and 600 MPa pressures

Materials	Charpy Impact Strength (kJ/mm^2)
316L/400 MPa	13.941
316L/400 MPa	20.242
410/400 MPa	19.194
410/600 MPa	34.073

As given in Table 4.4; the Charpy-V notch impact strengths of 316L austenitic and 410 martensitic Stainless Steel Samples prepared on 400 and 600 MPa pressures were observed. As pressure increased the Charpy impact strength values of stainless steels increased. The high Charpy impact strengths obtained as 20.242 kJ/mm^2 for press-sintered austenitic stainless steel on the high pressure, and 34.073 kJ/mm^2 for press-sintered martensitic stainless steel on the high pressure. The high Charpy impact strength was acquired on the press-sintered martensitic stainless steel on the high pressure as the same hardness values in Table 4.3 (110,09 N/mm^2 for martensitic stainless steel prepared on the high pressure). Because increasing of austenitic phases in martensitic matrix phase, decreasing of carbide precipitations and homogeneous distribution of decreased carbide precipitations besides grain bonding, decreasing porosity with applying pressure and heat treatment process (Isfahany *et al.,* 2011; Hsu *et al.,* 2004)). It also considered that very small obtained impact strengths related to, insufficient pressing and thus insufficient grain bonding and also still open porosity into the structure if else applied pressure and heat treatment. In the Figure 4.3., The Charpy

–V notch impact strength- hardness relationship of 316L austenitic and 410 Martensitic stainless steels prepared on the 400 and 600 MPa pressures are given. Charpy –V-Notch strengths of samples were directly changed with hardness values of these samples.

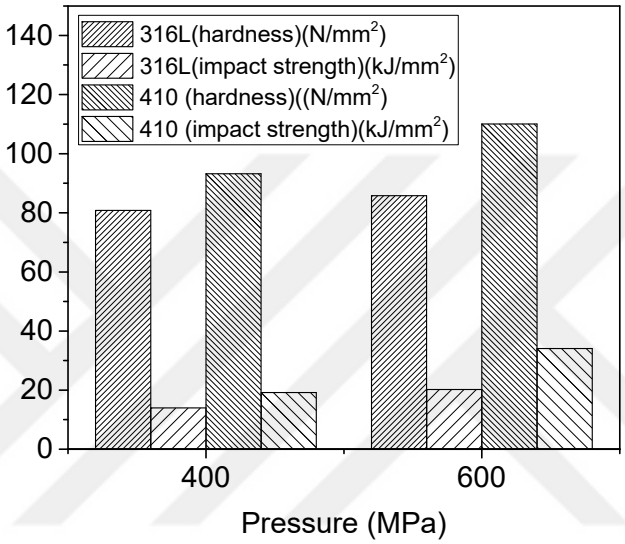


Figure 4.3. The Charpy –V notch impact strength- hardness relationship of 316L austenitic and 410 Martensitic stainless steels prepared on the 400 and 600 MPa pressures

4.4 The Surface Characterization of Fractured Surfaces of Austenitic and Martensitic Stainless Steels

In Figure 4.4; the SEM images of cracked surfaces of 316L austenitic and 410 martensitic stainless steel prepared on the 400 and 600MPa pressures. Small-scaled magnified (500X) SEM images of cracked surfaces of them; each stainless steels have salebrous surfaces due to brittle fracture. It observed that surfaces of sintered austenitic stainless steel samples have bigger than that of martensitic stainless steel samples. Sintered austenitic stainless steel has smaller particles than other austenitic stainless steel. This case is in sighted on the surfaces of sintered

martensitic stainless steel samples. Surface of sintered martensitic stainless steel on the high pressure has finer particles than other stainless steel samples. Finer particles occur more grain boundaries; these grain boundaries absorb impact effect. Therefore, this case increases the strengths of stainless steels. This situation clearly observed on values of Charpy –V impact strengths of austenitic and martensitic stainless steel samples in Table 4.4. On the SEM image of surface of sintered martensitic stainless steel (D1) on the 600 MPa pressure; it is also observed that this surface has quasicleavage fracture besides having finer particles.

On high-scaled magnified (5000X) SEM images of cracked surfaces of sintered 316L austenitic and 410 martensitic stainless steel samples; it is observed that surfaces of each austenitic stainless steels have porous sponge-like surfaces and these sponge-like surfaces and big vacancies partially decreases on the sintered austenitic stainless steel on the high pressure to other austenitic stainless steels. Comparing of surfaces of austenitic stainless steels, surfaces of martensitic stainless steel samples have different surfaces and shows partially ductile fractured-behaviours. Cracked surface of sintered martensitic stainless steel on the low pressure possesses tiny particles. These particles considered the carbide precipitations. During cooling stages after sintering, high amounts of carbides precipitates due to the high contents of carbon and chromium into the structure of stainless steel (Wang *et al.*2014). Sintered martensitic stainless steel on the low pressure having high sized carbide precipitates has low Charpy-V impact strength and also hardness value to other martensitic stainless steel. This case is supported with Charpy-V impact strength and hardness values on Table 4.3 and 4.4 and also in order to be seen Figure 4.4 (b) in terms of carbide precipitations. On the intently examining SEM image of sintered martensitic stainless steel on the high pressure; regions specified with dark circles has more prominently quasicleavage structures realizes (Wang *et al.*2014). As stated on the article of Wang *et al*. white-band like structures on the quasicleavage formations. These white-band like structures also resemble needlike structures and includes of thin-long internode

structures which is confined vacancies (Wang *et al*,2014*)* . Formation of quasicleavage formations gains ductile fractured-behaviour of stainless steels (Wang *et al*.2014).

It is observed that EDS spectrums of cracked surfaces of sintered austenitic and martensitic stainless steel samples on the Table 4.5. On the examining of EDS spectrums of sintered austenitic stainless steel samples; sintered austenitic stainless steel on the high pressures has higher Fe, Ni, Mo and Si and lower Cr and O contents to other austenitic stainless steel sample. Besides pressure effect, increasing Ni and Mo contents play role on the Charpy V impact strengths. Also examined EDS spectrums of sintered martensitic stainless steel samples; sintered martensitic stainless steel on the high pressure has higher Mn, Si, Fe and lower Cr and C contents to the other martensitic stainless steel sample. According to other stainless steel ; it can be considered to sintered martensitic stainless steel on the high pressure has high hardness and Charp-V impact strength values due to increasing Si, Mn, and Fe contents into the structures and it can also be recommended Si and Mn contents besides Fe content into structure of stainless steels play improving role on the physical properties of stainless steels.

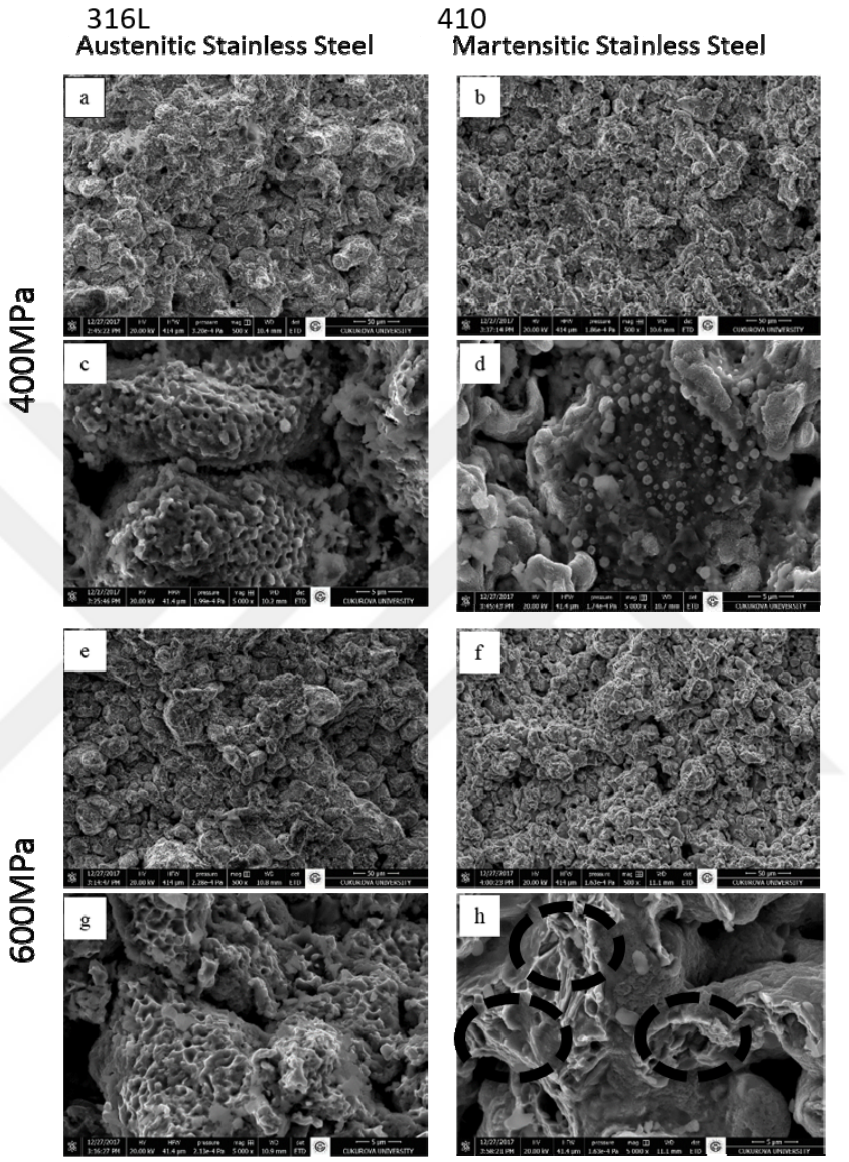


Figure 4.4. The SEM images of fracture surfaces of 316L austenitic (a,c,e,g) ve 410 martensitic (b,d,f,h) stainless steel samples prepared on 400 and 600 MPa pressures after impact experiment

Table 4.5. EDS spectrums of cracked surfaces of 316L austenitic ve 410 martensitic stainless steel samples prepared on 400 and 600 MPa pressures after impact experiment

		Fe	**Mn**	**Ni**	**Cr**	**Mo**	**Si**	**O**
316L	**400 MPa**	32.19	-	4.67	42.92	0.21	1.06	17.35
	600 MPa	39.15	-	6.06	34.79	0.28	2.02	16.32
410	**400 MPa**	51.73	0.86	-	25.03	-	1.90	20.47
	600 MPa	71.79	1.29	-	14.27	-	2.23	10.41

The XRD peaks of press-sintered austenitic and martensitic stainless steel on the 400 and 600MPa pressures are observed in Figure 4.5. In Figure 4.5 (a), on the structures both press-sintered austenitic stainless steel on the 400 and 600 MPa pressures; it was seen mostly γ-austenite, α-martensite phases and locally placed Cr- and Fe-oxides. γ-austenite phase was shown in peaks of 37.289°; 42.712°; 49.921°; 63.931°; 71.520°; 77.061°; 87.237° and 89.889° for 2θ angles for press-sintered austenitic stainless steel on the 400MPa pressure and 37.276°; 42.581°; 49.592°; 63.904°; 71.625°; 77.008°; 87.421° and 89.495° for 2θ angles for press-sintered austenitic stainless steel on the 600MPa pressure. α-martensite phase were seen in peaks of 43.553°, 64.049° and 77.258° for 2θ angles for press-sintered austenitic stainless steel on the 400 MPa pressure and 43.526°; 64.049° and 77.271° for 2θ angles for press-sintered austenitic stainless steel on the 600MPa pressure (García *et al.,* 2009a; 2009b*;* Martin *et al.,* 2015*;* Mumtaz *et al.* 2003, 2004*;* Zhao *et al.,* 2002, Ma *et al.,* 2016; Multigner *et al.,* 2009*;* Ozturk *et al;* 2009*;* Slotwinski *et al.* 2014*).* We can consider that the γ→α martensitic transformation on the structures of these austenitic stainless steels observed in same peaks of 40-45°; 60-65° for and 75-80° for 2θ angles. Also; it was concluded that γ→α martensitic transformation on the structures of these austenitic stainless steels has more severely intensity on the peak of 40-45° for 2θ angles according to the other peak degrees. α-martensite phase was shown more dominant intensity to

γ-austenite phase. On the structures of both these austenitic stainless steels locally Cr- and Fe- oxides were shown. Cr-oxides were shown in peaks of 28.243°; 32.864°; 41.189° and 48.030° for 2θ angles for press-sintered austenitic stainless steel on the 400MPa pressure and 28.256°; 41.084° and 48.109° for 2θ angles for press-sintered other austenitic stainless steel. Fe-oxides were seen in peaks of 53.991°; 61.725° ; 73.765°;74.698° and 81.407° for press-sintered austenitic stainless steel on the 400 MPa pressure and 73.358°; 74.337° and 81.341° for 2θ angles for press-sintered other austenitic stainless steel (García *et al.,* 2009a; 2009b*;* Martin *et al.,* 2015*;* Mumtaz *et al.* 2003, 2004*;* Zhao *et al.,* 2002, Ma *et al.,* 2016*;* Multigner *et al.,* 2009*;* Ozturk *et al*; 2009*;* Slotwinski *et al.* 2014*)* . For press-sintered austenitic stainless steel on the high pressure; formations of Cr-oxides were sparsely placed to Fe-oxides. According to press-sintered austenitic stainless steel on the 600MPa pressure; for press-sintered other austenitic stainless steel ; Cr-and Fe- oxides were more apparent and also shown in same diffraction degress with other austenitic stainless steel. Also on the structures of both these austenitic stainless steel ; there are trace amounts of carbide precipitations, phosphorus and sulphur formations but not showed on the peaks because of C,P and S amounts of relatively small quantities in chemical composition of austenitic stainless steel powder stated in Table 3.1.

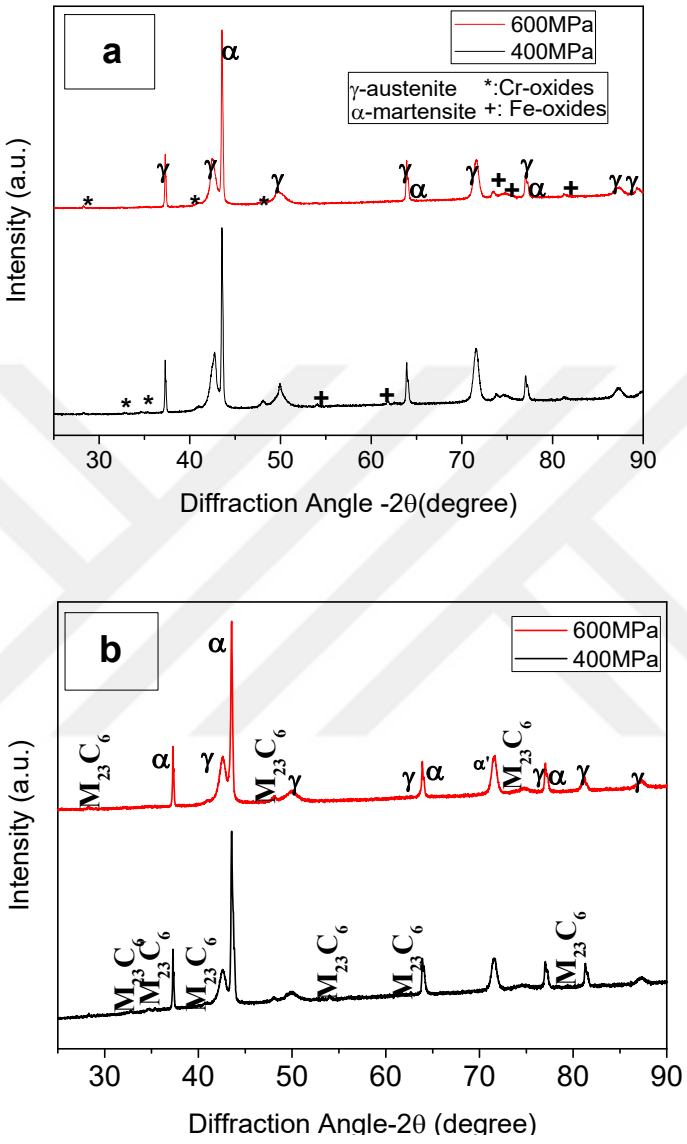


Figure 4.5. The XRD patterns of 316L austenitic (a) and 410 martensitic (b) stainless steel samples prepared on 400 and 600 MPa pressures

In Figure 4.5 (b), on the structures both martensitic stainless steel prepared on the 400 and 600 MPa pressures; it was seen mostly γ-austenite, α-martensite

phases and $M_{23}C_6$ carbide precipitations. γ-austenite phase was shown in peaks of 42.607°; 49.868°; 63.957°; 76.982°; 81.223° and 87.316° for 2θ angles for press-sintered martensitic stainless steel on the 400MPa pressure and 42.476°; 49.908°; 63.891°; 76.995°; 81.131°; and 87.132° for 2θ angles for press-sintered martensitic stainless steel on the 600MPa pressure. α-martensite phase were seen in peaks of 37.289°; 43.526°; 64.206°;71.573° and 77.310° for 2θ angles for press-sintered martensitic stainless steel on the 400MPa pressure and 37.303°; 43.539°;64.115°; 71.533° and 77.258° for 2θ angles for press-sintered martensitic stainless steel on the 600MPa pressure (Li and Bell, 2006; Xi *et al.*, 2008; Sabetghadam *et al.*, 2010, Espitia et al., 2015; Carraouge et al, 2004; Lin et al., 2010; Ferreira *et al.*, 2015, Anjos *et al.,* 2015; Pinedo and Monteiro ,2014; Wu *et al.,* 2010; Azevedo *et al.*, 2014; Li *et al.,* 2014; García de Andrés *et al.*, 1998; Tsuchiyama et al., 2012; Lee *et al*,2003-2015a-2015b; Borgioli *et al.,* 2002; Stagno *et al.,* 1997; Subramaniam *et al.,* 2015; Song *et al.,* 2010, Ma *et al.*, 2012; Kundalkar *et al.*, 2010; Kishor *et al*., 2014). We can consider that γ-Fe transformation from α-Fe phase on the structures of both of these martensitic stainless steel seen compared to XRD pattern of martensitic stainless steel powder as shown in Figure 4.1 and this transformation appeared in same peaks of 40-45°;50-52°;63-65°;76-78°;82-84° and 87-89° for 2θ angles. It was observed that and $M_{23}C_6$ carbide precipitations were appeared in peaks of 28.190°; 32.773°;35.359°;40.553°;53.899°;62.670°;74.553° and 79.648° for 2θ angles press-sintered martensitic stainless steel on the 400MPa pressure and 28.335°; 47.872° and 75.013° for 2θ angles press-sintered other martensitic stainless steel (Li and Bell, 2006; Xi *et al.*, 2008; Sabetghadam *et al.*, 2010, Espitia et al., 2015; Carraouge et al, 2004; Lin et al., 2010; Ferreira *et al.*, 2015, Anjos *et al.,* 2015; Pinedo and Monteiro ,2014; Wu *et al.,* 2010; Azevedo *et al.*, 2014; Li *et al.,* 2014; García de Andrés *et al.*, 1998; Tsuchiyama et al., 2012; Lee *et al*,2003-2015a-2015b; Borgioli *et al.,* 2002; Stagno *et al.,* 1997; Subramaniam *et al.,* 2015; Song *et al.,* 2010, Ma *et al.*, 2012; Kundalkar *et al.*, 2010; Kishor *et al*., 2014). It was

observed that $M_{23}C_6$ carbide precipitations on the press-sintered martensitic stainless steel on the high pressure has lower than that of press-sintered other martensitic stainless steel sample. It is also predicted that $M_{23}C_6$ carbide precipitations can be rich for $Cr_{23}C_6$ / $(Cr,Fe)_{23}C_6$ carbides (Yi *et al.*, 2017).

4.5 The Electrochemical Behaviours of Austenitic and Martensitic Stainless Steels

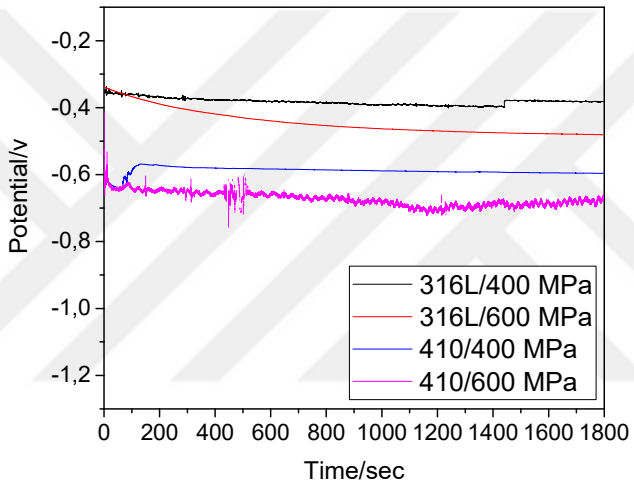


Figure 4.6. Obtained the open pore potential-time curves of 316L austenitic and 410 martensitic stainless steel samples prepared on 400 and 600 MPa pressures in 3.5% NaCl for 96 h of immersion time

In Figure 4.6.; open pore potential- time curves of 316L austenitic and 410 martensitic stainless steel samples prepared on the 400 and 600 MPa pressures were observed. These curves were obtained in 3.5%NaCl solution for 1800 seconds. Potential values of these stainless steels have been in balance over time and potential values of austenitic stainless steel have more positive values than that of other stainless steel. As the examining of potential values of austenitic stainless steel, potential value of austenitic stainless steel prepared on the low pressure has

in balance at 50sec and gives -0.38V potential value. It was also observed this -0.38V potential value increased to -0.35V potential value at about 1400sec. For austenitic stainless steel prepared on the high pressure; potential value decreases with increasing time and has in balance at approximately 1400 sec and give -0.4V potential value. According to article of Huttunen-Saarivirta *et al.,* we can also be recommended that decreasing of potential values resulted from degradation of the air-formed passive layer owing to the Cl^- adsorption and movements of Cl^- ions (Huttunen-Saarivirta *et al.,* 2016). Potential values of martensitic stainless steel prepared on the 400 MPa pressure have been in balance at 200 sec and give -0.6V potential value. For other martensitic stainless steel sample; potential values of this stainless steel have been in balance at 150 sec and give -0.62 V potential value. According to these results, Potential values of martensitic stainless steel on the low pressure have more positive values than that of other martensitic stainless steel. It was also observed that on the potential values of martensitic stainless steel prepared on the high pressure; frustating occurs at the range 150-200sec and it can be considered that pit nucleation and passivation on the surface of stainless steel lead to sharp decrease and increase of potential values (Pahlavan *et al.,* 2016), then, again potential values of this stainless steel have in balance over time. It can also considered that low frequency time related to slower processes occuring in the oxide layer while high frequency based on the faster charging/discharging processes occurred at the electrode/electrolyte interface (Huttunen-Saarivirta *et al.,* 2016).

In Figure 4.7, it was appeared that EIS measurements of sintered 316L austenitic and 410 martensitic stainless steels were obtained in 3.5%NaCl solution after 30 min and 96h immersion time and the whole Bode curves of stainless steels are analysed. One of two loops of Nyquist curves is involved of high frequency capacitive loop, other loop of Nyquist curve is included of low frequency capacitive loop.

The frequency semicircle parts of 316L austenitic and 410 martensitic stainless steel prepared on the 400 and 600MPa pressures were acquired as fitting equivalent circuit seen in Figure 4.7. In Table 4.6, it was seen the fitting results of sintered austenitic and martensitic stainless steels obtained in 3.5%NaCl solution after 30 min and 96 h immersion time. From Table 4.6; R_s, R_{ct}, R_{pore} , Q_{dl} and Q_{ox} are referred as unbalanced solution resistance, charge transfer resistance, resistance of pores in the natural oxide film, constant phase elements (CPE) showing the double layer and oxide capacitances, respectively. R_p is also defined as polarization resistance and proportional to the sum of the R_{ct}, R_{pore} resistances.

From Table 4.6.; for 30 min of immersion time; polarization resistance of sintered austenitic stainless steel decreases with increasing pressure while polarization resistance of sintered martensitic stainless steels increases as pressure increases. Polarization resistances of sintered austenitic stainless steels are acquired as 1744.3 (for pressed on the 400MPa) and 1215.3 Ω cm^{-2}(for pressed on the 600MPa pressure); the resistances of sintered martensitic stainless steel samples are obtained as 1032.7 (for pressed on the 400MPa) and 3816.8Ωcm^{-2}(for pressed on the 600MPa pressure). For 96h immersion time; polarization resistance of sintered austenitic stainless steel increases with increasing pressure while polarization resistance of sintered martensitic stainless steels decreases as pressure increases. Polarization Resistances of sintered austenitic stainless steels are acquired as 363.9 Ωcm^{-2} for pressed on the 400MPa pressure) and 370 Ωcm^{-2} (for pressed on the 600MPa pressure) and polarization resistances of other sintered stainless steels are recorded as 1462.3 (for pressed on the 400MPa) and 764.2 Ωcm^{-2} (for pressed on the 600MPa pressure). On the examining of charge transfer resistances (R_{ct}) of sintered 316L austenitic and 410 martensitic stainless steel samples from Table 4.5; for 30 min immersion time, as pressure increases; values of charge transfer resistances of sintered austenitic stainless steel decreases, values of charge transfer resistances of other stainless steel samples increases. Values of charge transfer resistances of austenitic stainless steel are obtained as

1602 (for pressed on the 400MPa pressure) and 1073 Ωcm^{-2} (for pressed on the 600MPa pressure); values of charge transfer resistances of martensitic stainless steel samples are recorded as 845 (for pressed on the 400MPa pressure) and 3511Ωcm^{-2} (for pressed on the 600MPa pressure). For 96h immersion time; when pressure increases, values of charge transfer resistances of sintered austenitic and martensitic stainless steel decreases. Values of charge transfer resistances of austenitic stainless steel are obtained as 220 (for pressed on the 400MPa pressure) and 210 Ωcm^{-2} (for pressed on the 600MPa pressure); Rct values of martensitic stainless steel samples are recorded as 1200 (for pressed on the 400MPa pressure) and 600 Ωcm^{-2} (for pressed on the 600MPa pressure). On the viewing all polarization resistances of sintered austenitic and martensitic stainless steel samples; it was observed that polarization resistances of martensitic stainless steel samples have higher than that of austenitic stainless steel samples. Because; on the surface of martensitic stainless steel samples faster oxide layer formation occurred and therefore passivation happened. (see in Table 8.) Compared to austenitic stainless steel, it was meant that martensitic stainless steel have higher hardness and density values and for this reason, progressing of corrosion products into the metal may be prevented. However, this case is always not occurred. This can be due to increasing of surface areas contacted with solution and increasing of corrosion resistance with fast- transforming of these surface areas to oxide layer form. No important increase on the passive oxide film amount on the surface of austenitic stainless steel was recorded. This oxide film layer formation is slower on the surface of austenitic stainless steel samples. Also, for 30 min of immersion time; when pressure increasing, polarization resistances of austenitic stainless steel decreased while polarization of martensitic stainless steel samples increased ; for 96hrs of immersion time when pressure increasing, polarization resistances of austenitic stainless steel increased whereas polarization of martensitic stainless steel samples decreased. From these values; this conclusion clearly seen that polarization resistances of sintered martensitic stainless steels are higher than

polarization resistances of sintered austenitic stainless steels. It is considered that oxide content in the structure of martensitic stainless steel increases, therefore Fe content in the structure of this stainless steel protected. The increasing of oxide amount based on the Fe and Cr on the microstructure of the martensitic stainless steels. It is also observed that no important increase on the amount of oxide on the surface of austenitic stainless steel samples. The main metal reacts very slowly with NaCl solution and has tendency to preserve its originary chemical composition. This case leads to decelerate formation of passive layer on the surface of austenitic stainless steel samples.

High polarization resistance is meant to low ion distribution therefore stainless steel having high polarization resistance possesses low corrosion resistance High charge transfer resistance are meant to high protective capability of passive film layer, high ion transfer rate and additionally high corrosion resistance. Stainless steels having high polarisation resistance with high charge transfer resistance posses low metal dissolving and more passivity behaviours. Stainless steel which has low porosity (3-7%) due to low sintering temperature show high metal dissolving (Pandya *et al.*, 2012). .

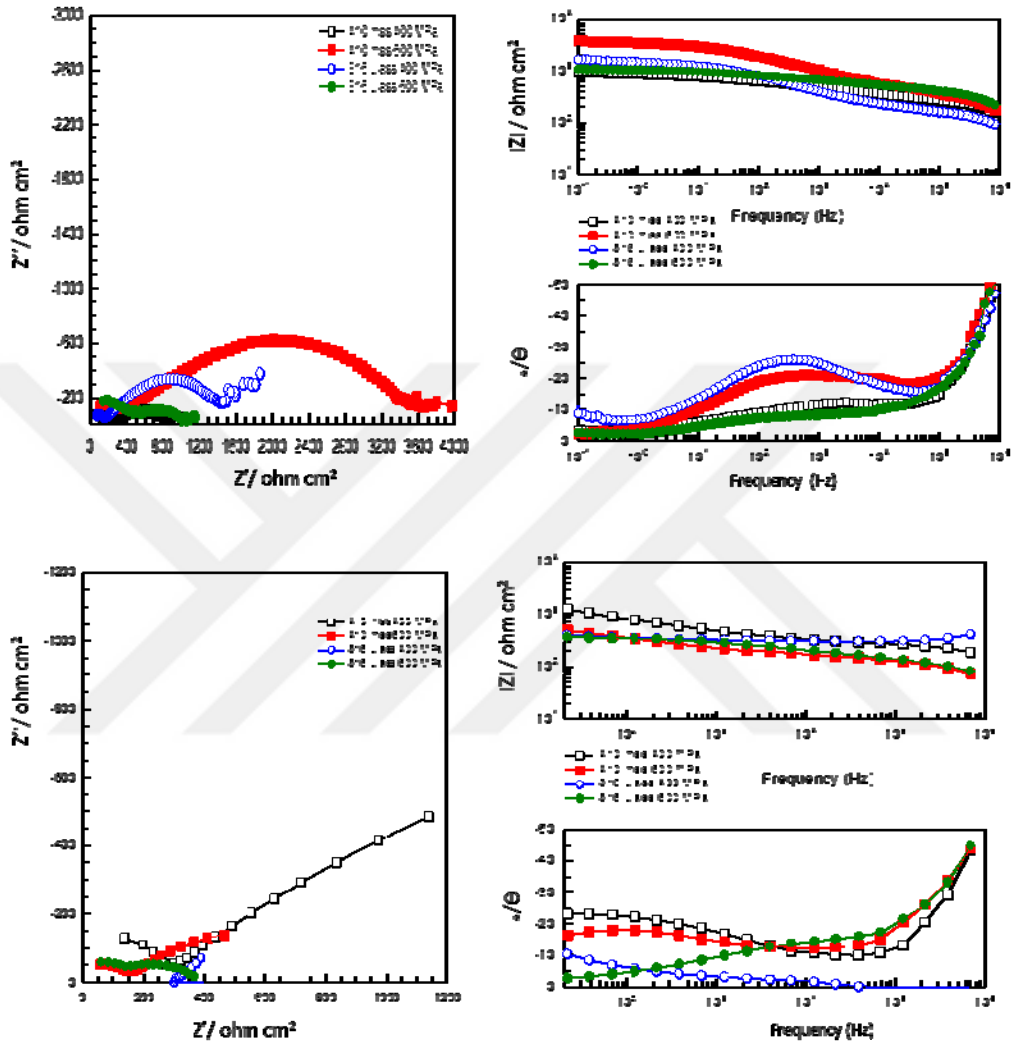


Figure 4.7. The EIS Measurement of 316L austenitic and 410 martensitic stainless steel prepared on the 400 and 600MPa pressures at 30 min (top figures) and 96h (bottom figures) in 3.5% NaCl solution; Nyquist curve (left sides), Bode curve (right sides))

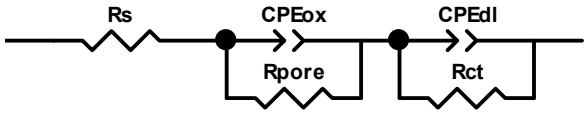


Figure 4.8. The schema of equivalent circuit of EIS measurements

Table 4.6: Fitted EIS measurements of 316L Austenitic and 410 Martensitic Stainless steel samples for 30min -96 h of immersion time

Time	**30 min**				**96 h**			
Electrodes	**316L**		**410**		**316L**		**410**	
Pressures (MPa)	**400**	**600**	**400**	**600**	**400**	**600**	**400**	**600**
R_a (Ω/cm^2)	12.09	22.00	37.68	27.38	42.50	18.00	25.41	24.37
CPE_{OX}	0.00116	0.0011	0.0016	0.2286	0.0003	0.9813	0.0025	0.2765
n	0.86	0.99	0.98	0.79	1.10	0.00	0.92	0.66
R_{pore}	142.3	238.2	186.7	305.8	143.9	160.0	262.4	164.2
CPE_{dl}	59.43	137.53	143.89	21.155	1245.9	42.178	113.16	248.57
n	0.45	0.22	0.29	0.45	0.39	0.35	0.39	0.41
R_{ct} (Ω/cm^2)	1602	1073	845	3511	220	210	1200	600
R_p (Ω/cm^2)	1744.3	1215.3	1031.7	3816.8	363.9	370	1462.3	764.2

This conclusion supported by EDS spectrums of non-corroded and corroded structures of sintered martensitic stainless steel on the Table 4.6 . From Table 4.6; the general argument is obtained. Polarisation resistances should be

inspected by Fe dissolving because of main alloying element of Fe and is treated in point of Fe dissolving (Pardo *et al*., 2008). Fe-passive dissolving via decreasement of activity of either Fe(I) or Fe(II) adsorbed intermediate species might be limited the occuration of adsorbed Cr(III)species (Pardo *et al*., 2008).

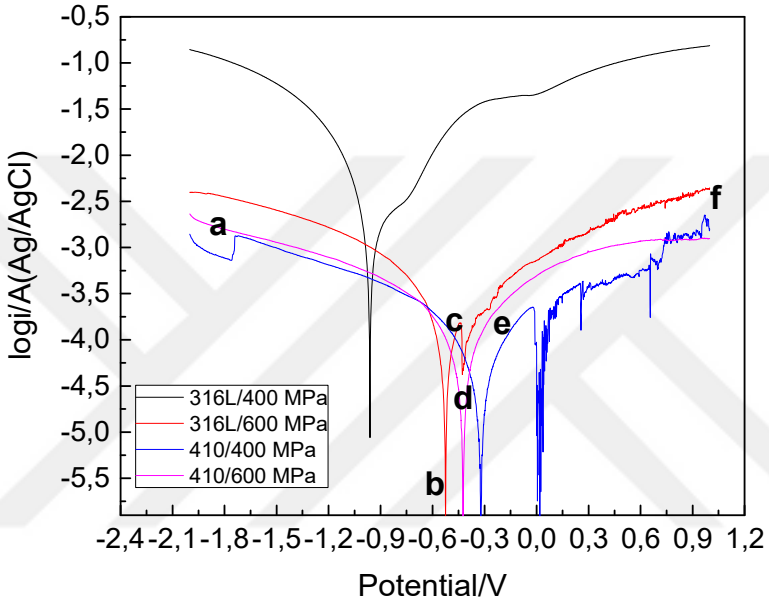


Figure 4.9. The Current – Potential curve of 316L Austenitic and 316L Martensitic Stainless steel Prepared on 400 and 600MPa pressures in 3.5% NaCl for 96 h of immersion time

In Figure 4.8., the current –potential curves of 316L austenitic and 410 martensitic stainless steel samples prepared on 400 and 600 MPa pressures taken in 3.5%NaCl solution for the end of 96h of immersion time. The current-potential curves consist of two primary branches as cathodic and anodic regions. In the cathodic region; as potential increases, the current density decreases. H_2 formation as the principal electrochemical process occurs at this region;

$$2H^+(aq) + 2e^- \rightarrow H_2(g) \quad (4.1)$$

$$1/2\, O_2 + H_2O + 2e^- \rightarrow 2OH^- \quad (4.2)$$

As can be understood from (4.1) and (4.2) redox reactions; O_2 reduction occurs at more positive values than H_2 reduction (1.23V).

On the current-potential curve; before current density sharply increased, at b point a passivity pletau occurs due to protective film layer cracking and growing of pits (Marcelin *et al*, 2013, Loto *et al.*, 2013) this b point is active region and anodic dissolving occurs at this region. (bc) region is anodic polarisation region and at this polarisation region, when the potential increases, the current density increases and also as the electrochemical reactions; dissolving of austenitic and martensitic stainless steels occurs (Wang *et al.*, 2014). (cd) region exceeding c point is referred active-passive transition region and as potential increases, current density decreases and protective film layer on the surface of austenitic and martensitic stainless steels forms (Wang et al., 2014). At more positive potential values; corrosion rate increases after active region ((b) point), and passivation potential reaches to maximum value at c point; this point is called passivation potential (E_{pp}) (Loto *et al.*, 2013). Except that sintered 316L austenitic stainless steel prepared on the 400MPa, at other stainless steel samples; active dissolving to passive dissolving transition from c point to d point occurs, protective film layers on the surface of stainless steels forms and this case lead to sharply decreasing of current density. d point is passive region and at this point; current density stabilizes and surfaces of stainless steels completely covers with protective film layer. Exceed d-point ; current density becomes to stabilize and surfaces of stainless steels samples will completely be coated with protective film layer, this region where occurred this case is referred passive region (de-region) (Wang *et al.*, 2014).Trans-passive region is also e point. At this region, as potential increases, current density increases, protective film layer on the surfaces of

stainless steels dissolves. This point is also called pitting potential (E_{pit}). Piting potential is potential at which pitting formation reaches to maximum level. At more positive potential values after e point; current density increases, more pitting forms and big pitting occur by accumulating these pitting. (ac) and (dc) regions are curves at which forming of redox reactions of main metal dissolving((Marcelin *et al*, 2013).

Anodic reaction in pit ocur in following reaction;

$$Fe \rightleftarrows Fe^{2+} + 2e^{-} \ (dissolutting\ of\ iron) \quad (4.3)$$

Pit that has positive charges attracts negative chlorine ions increases electrolytic acid ratio according to next reaction:

$$FeCl_2 + 2H_2O \rightleftarrows Fe(OH)_2 + 2HCl \quad (4.4)$$

In alkaline media; magnetic formation occur at -0.8V. According (4.5) and (4.6) redox reactions specify active-passive transition on the stainless steels. Magnetite which is a oxide mixture formed from Fe^{2+} and Fe^{3+} ions is a significant compound due to passive film layer (Wang *et al.*, 2014)

$$3Fe(OH)_2 + 2OH^{-} \rightarrow Fe_3O_4 + 4H_2O + 2e^{-} \quad (4.5)$$

$$3FeO + 2OH^{-} \rightarrow Fe_3O_4 + H_2O + 2e^{-} \quad (4.6)$$

In anodic potential region; as potential increases current density increases, pH decreases and Cr oxidation occur with dissolving of Cr, therefore protective film layer has structure of Cr-rich and this layer extends. Fe_3O_4 magnetite exposes (Zhang *et al.*, 2005). Accordingly, it can stated that stainless steels have high oxidation resistance and thicker protective film layers (Freire *et al.*, 2012).

$$Cr + 3H_2O \rightleftharpoons Cr(OH)_3 + 3H^- + 3e^- \quad (4.7)$$

In this thesis study; on the surfaces of austenitic stainless steel samples, passivation occurs later compared to that of martensitic stainless steel samples. With increasing of pressure; pores closed and current density on the anodic curve decreased. Surface of martensitic stainless steel into the NaCl solution firstly fastly disolutesi then, passive film occurs in accordance with above (1-5) reactions and therefore, it is observed that dissolution occurs at more positive values.

4.6 The Surface Characterisation of Austenitic and Martensitic Stainless Steels

The Figure 4.9. presents SEM images of 316L austenitic and 410 martensitic stainless steel prepared on 400 and 600 MPa pressures. SEM images of both of stainless steels waited in 3.5% NaCl solution for 96 hrs immersion time were also taken. Locally pitting corrosion were seen on the surface of samples waited in solution for 96 hrs. On formation of corrosion on the surfaces of stainless steels; porosity effect plays important role due to manufacturing method such as powder metallurgy [18]. Compared to corrosion of cast alloys corrosion of P/M- stainless steel in NaCl solution happens faster due to the penetration of chloride ions into the pores. Formation mechanism and strength of protective film layer on the surface of stainless steel samples have an important role. In order to form a dense and permanent protective film layer on the surface of stainless steel samples and prevent the progression of corrosion products into the base metal; Cr alloying element, which is found in main chemical composition of steel samples, combining with oxides has a significant effect on the local corrosion resistance of the steels. As the examining of SEM images of austenitic stainless steel samples before and after corrosion; effect of pressure on the corrosion resistance is clearly noticed (see in Figure 11). Surfaces of stainless steel samples prepared on the high pressure presents smoother surfaces than that of other austenitic stainless steel

samples. In the SEM images of surfaces of both of martensitic stainless steel samples before corrosion, flat surfaces are visible (see in Figure 4.9.). After corrosion; in the SEM images of steel samples, it is observed that surfaces of steel samples are protected with passive film. When investigating of SEM images of austenitic stainless steel samples together with martensitic stainless steel samples; surface of martensitic stainless steel samples have better appearances according to surface of austenitic stainless steel samples. This case can recommended with binder effect, which was used in bonding formation on the martensitic stainless steel samples and coarsening of grains and stabile oxide film layer formation on the surface of steel samples.

On the Table 4.7; the EDS spectrums of 316L austenitic and 410 martensitic stainless steel prepared on 400 and 600 MPa pressures before and after corrosion test. On the surfaces of austenitic stainless steel ; Fe content decreased, oxide layers on the surfaces of these stainless steels forms and therefore polarisation resistances of this stainless steel samples are increased when surfaces of these stainless steel exposes to corrosive. On the microstructures of martensitic stainless steels; it is observed that Fe contents of sintered martensitic stainless steels on the high pressure are higher than that other sintered martensitic stainless steel. on surface of this martensitic stainless steel ; Fe content leads to stable oxide layer. As seen on EDS spectrums in Table 4.6.; it is also appeared Fe and Mn amounts on the surfaces of martensitic and austenitic stainless steel samples are reduced. As known as, evaporation of Fe and Cr as metallic species are higher than evaporation of Mn (Samih *et al.*, 2014). The preferential selective evaporation of the Mn and Fe species lead to Cr-rich to medium (Samih *et al.*, 2014).

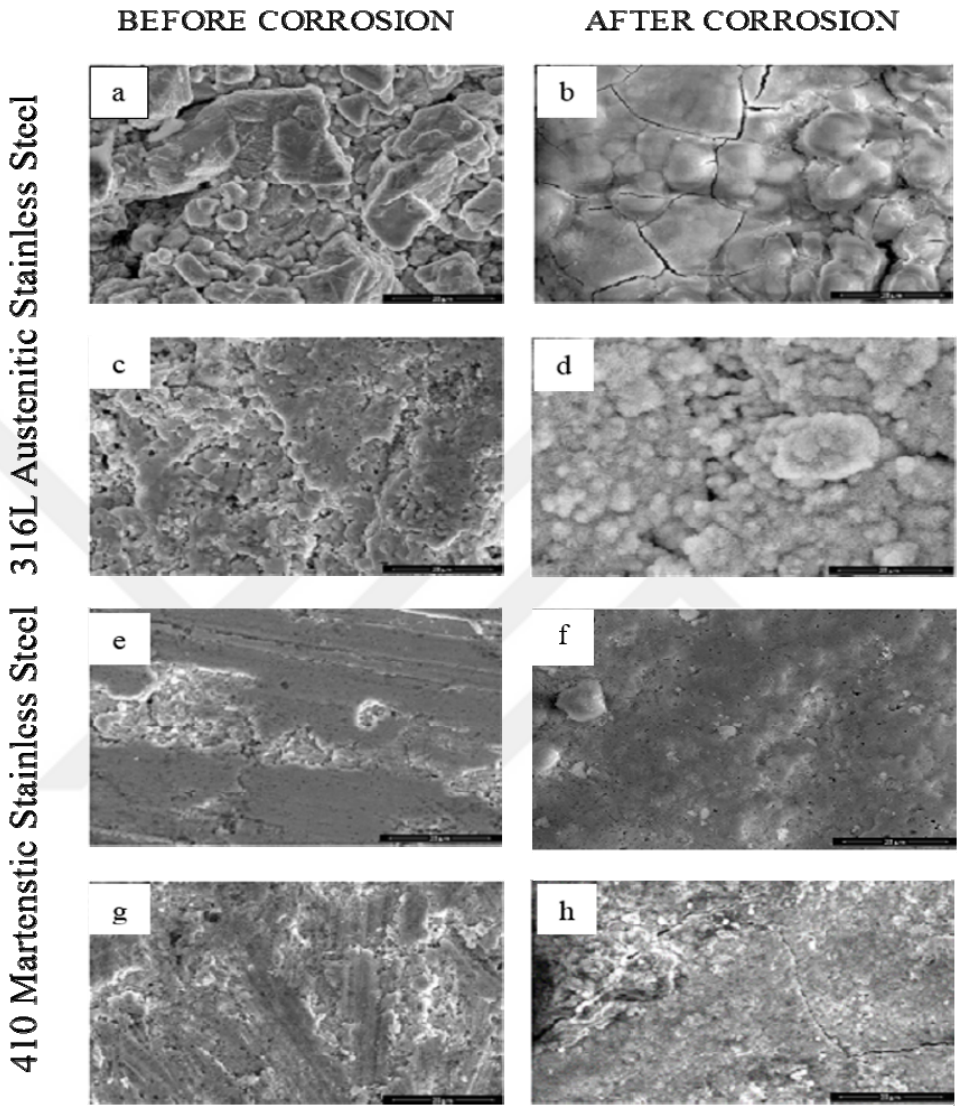


Figure 4.10. The SEM images of 316L austenitic prepared on 400 before (a) and after (b); austenitic stainless steel prepared on the 600 MPa before (c) and after (d) and 410 martensitic stainless steel prepared on the 400 MPa before (e) and after (f) ; martensitic stainless steel on the 600 MPa before (g) and after (h) corrosion test.

Table 4.7. The EDS spectrums of press-sintered 316L austenitic and 410 martensitic stainless steel prepared on the 400 and 600MPa pressures before and after corrosion test.

	Before Corrosion				**After Corrosion**			
	316L		**410**		**316L**		**410**	
wt%	**400 MPa**	**600 MPa**	**400 MPa**	**600 MPa**	**400 MPa**	**600 MPa**	**400 MPa**	**600 MPa**
Cr	6.43	27.27	14.65	15.46	0.75	16.79	0.40	0.71
Ni	0.57	-	-	-	-	-	-	-
Mo	0.15	1.03	-	-	0.15	1.33	-	-
Mn	0.47	0.08	0.31	0.60	0.18	0.0	035	0.21
Si	0.25	1.17	0.55	0.85	0.02	0.69	0.02	0.05
Fe	88.27	40.46	80.26	75.47	48.37	37.14	64.87	69.90
C	3.92	4.47	4.22	-	10.37	5.54	3.88	-
O	-	18.38	-	7.62	21.21	22.19	25.52	25.82
Cl	-	-	-	-	-	-	4.95	3.31

4.7 The Magnetic Measurements and Surface Characterization of Austenitic Stainless Steels

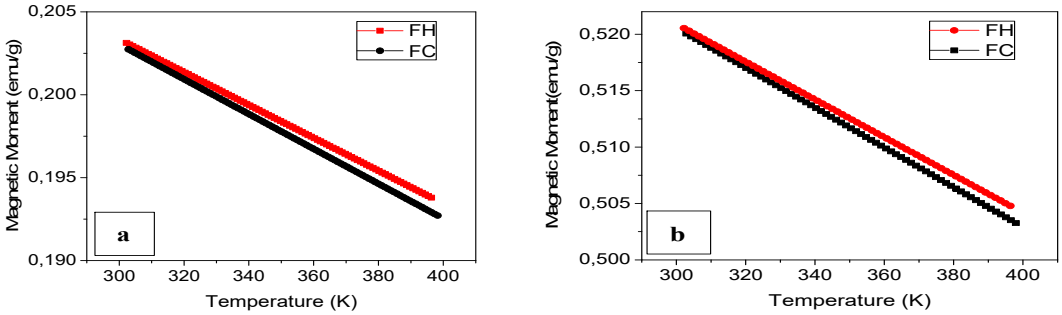


Figure 4.11. The magnetization as a function of temperature [M(T)] curves of press-sintered 316L austenitic stainless steel on the a) 400 MPa and b) 600MPa pressures

In Figure 4.10; for 316L austenitic stainless steel samples prepared on 400 and 600MPa pressures; the magnetic moments (emu/g) related to field heated (FH) and field-heated (FH) measured at 300-400K temperatures range under 0.5 T (50000Oe) magnetic field are given. For each austenitic stainless steel samples; it was observed that magnetic moment (emu/g) of these stainless steel samples increases as when temperature decreases and It is recommended that increasing in the saturation of ferromagnetic phases such as ferrite and martensite phases in the structure of these austenitic stainless steels leads to increase magnetic moment (Zhang *et al.*,2002). On the field-heated; it was observed that magnetic moments (emu/g) of both austenitic stainless steel prepared on the 400 and 600 MPa pressures decreases with increasing of temperature due to martensite phases's magnetic susceptibility and also, from ferromagnetic (α/α') to non-ferromagnetic γ-phase transition on the structure of both austenitic stainless steel samples (Zhang *et al.*,2002). For field-heated; on the sintered austenitic stainless steel on the 400MPa, magnetization values at the 300, 350 and 400K temperatures are obtained as 0.2031 (for 302.9K), 0.1983 (for 350K) and 0.1937 emu/g (for 396K), respectively; on the sintered austenitic stainless steel on the 600MPa, magnetization values at the 300, 350 and 400K temperatures are acquired as 0.5205 (for 302.2K), 0.5125 (for 350.2K) and 0.5047 emu/g (for 396.5K), respectively. On the field-cooled, it is considered that increasing of magnetic moment is increased because of leading of retained austenite to increasing of martensite phase ,when temperature decreases (Zhang *et al.*,2002). For field-cooled; on the sintered austenitic stainless steel on the 400MPa, magnetization values at the 300, 350 and 400K temperatures are obtained as 0.2027 (for 302,8K), 0.1977 (for 350K) and 0.1926 emu/g (for 398K), respectively; on the sintered austenitic stainless steel on the 600MPa, magnetization values at the 300, 350 and 400K temperatures are acquired as 0.5200 (for 302.85K), 0.5116 (for 351K) and 0.5032 emu/g (for 398K), respectively.

It was estimated that finishing temperatures of these stainless steel samples in terms of phase transformation; for austenitic stainless steel prepared on the low and high pressures, magnetic moment are obtained as 0.2021 emu/g at 327K and 0.5146 emu/g at 333K, respectively.

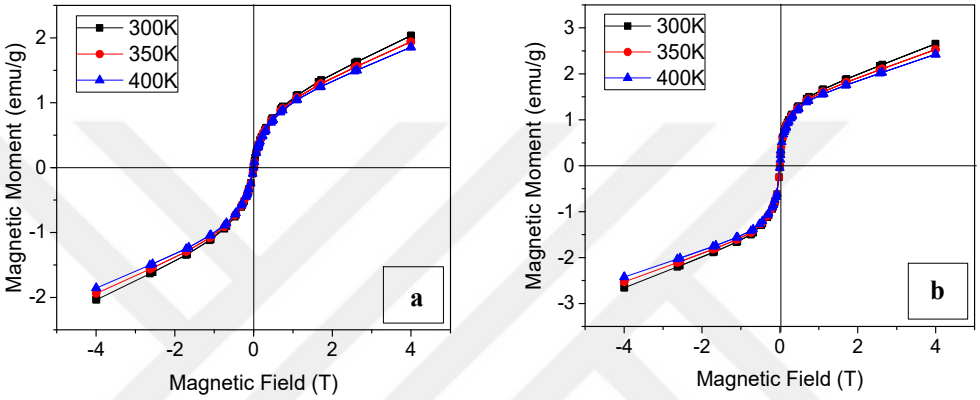


Figure 4.12. The magnetization as a function of magnetic Field M(H) curves of press-sintered 316L austenitic stainless steel on the a) 400 and b) 600 MPa pressures

The magnetic behaviours of 316L austenitic stainless steels are generally depended on microstructural variations of these stainless steels and these behaviours can explained be as magnetic hysteresis loop. This hysteresis loop is expressed with material properties which is presented by exterior magnetic field (Bas *et al.*, 2003) .For also examining of ferromagnetic behaviours of austenitic stainless steels prepared on the 400 and 600MPa pressures, in Figure 4.11; magnetic hysteresis loops curves are attained in ±4T magnetic field range and magnetic moment (emu/g) to applied field were measured at 300, 350 and 400K temperatures up to 4T magnetic field. The magnetic moment values (emu/g) of sintered austenitic stainless steel on the 400 and 600MPa pressures decreases when deformation temperature increased from 300 to 400K. Sintered austenitic stainless

steel on the 400 MPa pressure has ferromagnetic behaviour at the range of ±0.5T magnetic field except that these magnetic field range, at other magnetic strength fields this austenitic stainless steels presents paramagnetic behaviours. The magnetic moment (emu/g) is obtained as 0.103 emu/g at H=0. For other sintered austenitic stainless steels; magnetic field range that show ferromagnetic behaviour is at ±0.3T magnetic field. Except that these magnetic field range, at other magnetic strength fields this austenitic stainless steels presents paramagnetic behaviours. At H=0, magnetic moment of this austenitic stainless steel sample is given as 0,595 emu/g. At H=0; from magnetic moment values of these austenitic stainless steels; it is clearly seen that magnetic moment of sintered austenitic stainless steels on the high pressure higher than that of other austenitic stainless steel and it is meant that sintered austenitic stainless steel on the high pressure has more ferromagnetic behaviour according to other austenitic stainless steels. At 300, 350 and 400K temperature; as seen in Figure 4.11 (a) and (b; hysteresis curves of these austenitic stainless steels have small areas of coercive, remanences and also saturation magnetisation. It can be stated that small areas of coercive, remanence and saturation magnetisation are resulted from coarsening of precipitated BCC-(α or α') Fe phase and possessing small fraction of δ-ferrite (Mumtaz *et al.*, 2004. Magnetic saturation observed on the paramagnetic austenite matrix (Wan *et al.*, 2011). The saturation magnetization values of sintered austenitic stainless steel on the low pressure are obtained as 2.0376 (for 300K), 1.9370 (for 350K) and 1.8545 emu/g (for 400K) respectively; for sintered austenitic stainless steel on the high pressure, saturation magnetic moment values are recorded as 2.6580 (for 300K), 2.5274 (for 350K) and 2.4234 emu/g (for 400K), respectively. From values of saturation magnetization of these austenitic stainless steels, it is seen that saturation magnetization values decreases with increasing temperature and high saturation magnetization is obtained on the sintered austenitic stainless steel on the high pressure (2.6580 emu/g, 300K). High saturation magnetization value of this stainless steel can stated by transition from FCC –austenite almost exactly to

BCC-martensite in the structure of this stainless steel and this transition is related to ferromagnetic behaviour of this stainless steel (Ma *et al*., 2016; Sort *et al*., 2006; Multigner *et al*., 2009; Oztürk *et al*., 2009).

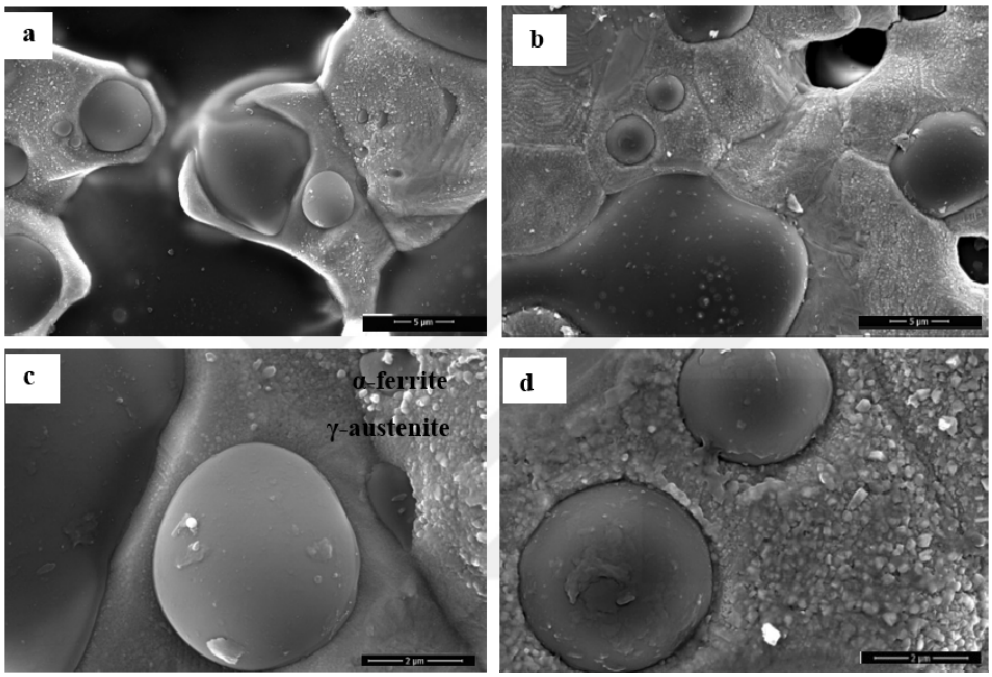


Figure 4.13. The SEM images of 316L austenitic stainless steel prepared on the 400 MPa (a and c) and 600MPa (b and d) pressures (a and b, 5,000x; c and d, 20,000x)

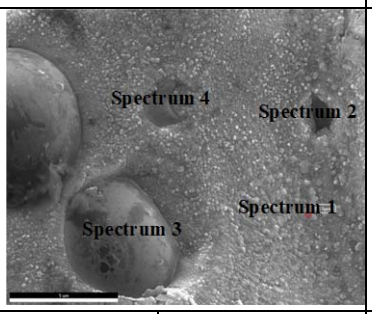
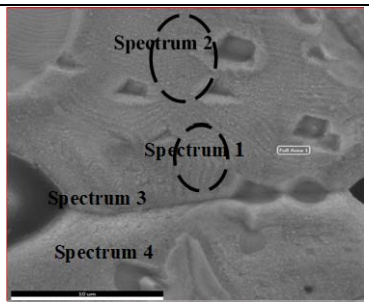
		316L /400 MPa		316L/ 600 MPa	
					
	Element	**Weight %**	**Atomic%**	**Weight %**	**Atomic%**
Spectrum 1	**Cr**	16.89	17.97	16.53	15.25
	Fe	67.44	66.82	68.87	59.14
	Ni	12.01	11.32	12.24	10.00
	Mo	2.40	1.38	1.67	0.83
	Si	1.26	2.50	0.68	1.17
Spectrum 2	**Cr**	16.01	15.46	15.52	14.19
	Fe	64.02	57.52	69.85	58.97
	Ni	11.04	9.43	12.20	9.87
	Mo	2.18	1.14	1.66	0.82
	Si	6.74	1.44	0.76	1.29
Spectrum 3	**Cr**	13.85	4.86	10.28	2.90
	Fe	43.47	14.19	38.80	10.18
	Ni	7.64	2.37	4.34	1.08
	Si	33.24	21.58	46.57	24.30
	Mn	1.77	0.59	-	-
Spectrum 4	**Cr**	16.53	14.44	16.49	14.61
	Fe	68.32	55.56	69.06	59.92
	Ni	11.96	9.26	12.02	9.42
	Mo	2.41	1.14	1.69	0.81
	Si	0.78	1.36	0.73	1.20

Figure 4.14. The separated regions with EDS spectrums of press-sintered austenitic stainless steel (316L) prepared on the 400 and 600MPa pressure

In Figure 4.12 and 4.13, the SEM images and EDS spectrums of sintered 316L austenitic stainless steels on the 400 and 600MPa pressure are observed. For 5000X magnified SEM images; on the surface of sintered austenitic stainless steel

on the 600MPa pressure; grain bonding and grain boundaries occur and at least porosity is available comparing to other sintered austenitic stainless steel. On the surface of austenitic stainless steel on the low pressure ; locally grain boundaries observed and some regions grain bonding is still not complete.

From Figure 4.12-13., It was considered that on the analysing SEM images and EDS spectrums for the surfaces of both austenitic stainless steel samples prepared on the 400 and 600MPa pressures showed and the uniform circular δ-ferrite islands betwwen γ- austenite phase and σ-phase precipitations in the δ-ferrite matrix; According to article of Hsieh *et al.*; sigma phase precipitates,as triple point precipitation,form at the triple point of the δ-ferrite grain boundary and also this phase, as corner precipitation; forms directly in corner δ-ferrite particles owing to high δ-ferrite amount. Again, according to this article; sigma phase precipitates as Cr content of δ-ferrites uses up. As laminate precipitation; sigma and secondary austenite ($\sigma+\gamma_2$) precipitates in δ-ferrite matrix occur. This reaction forms in the occuring of eutectoid decomposition ($\delta \rightarrow \sigma+\gamma_2$). sigma phase consumes the Cr, Mo and Si of the δ-ferrites as finishing the eutectoid decomposition (Hsieh *et al.*, 2012).

From Figure 4.13.; on the EDS spectrum and profile lines of 316L austenitic stainless steel prepared on the 400 and 600MPa pressures; the austenite precipitation depended to increase in Cr and Mo and deplete in Ni within δ-ferrite (Hsieh *et al.*, 2012). For sample prepared at the 400MPa pressure; Cr and Mo elements(wt%) are recorded as 16.53/13.85 % and 2.41 /2.18 % respectively; Ni element (wt%) possesses 7.64/11.98 %; for other stainless steel; Cr and Mo elements(wt%) are recorded as 16.49/10.28 % and 1.69 /1.66 % respectively; Ni element (wt%) gave 4.34/11.24 %. Amounts Cr and Mo elements of both these stainless steels prepared on the 400 and 600MPa pressures obtained almost some values for each other, but values of Ni elements of both stainless steels changes from each other.

Also, on the all EDS spectrum and profile lines; in the austenite phase, higher concentrations of nickel, molybdenum and silisium were showed in spite of appearing of higher concentrations of chromium in the ferrite phase. But, molybdenum and silisium alloying elements stabilize the ferrite phase. This situation is stated with only seeing in austenitic powder and starting elements diffusing to ferrite phase (García *et al.,* 2009).

In the thesis work; the austenitic stainless steel powder used and applied on the experimental studies was powder type manufactured by water atomization (WA). This WA-typed austenitic stainless steel powder has affected with oxide environment owing to consisting of high values of Mn contents. This manganese causes to high permeability to oxygen and surface oxide formations (Heldberg *et al.,*2013). On the surfaces of X2CrNiMo17-12-2 austenitic stainless steel prepared on the 400 and 600 MPa pressures; oxides such as Fe_2O_3, Cr_2O_3, spinels (XCr_2O_4 (X:Fe or Mn)) and chromates were appeared. This result also supported in the XRD patterns of these materials. It is also considered that the base mechanism consists of formation of a Cr_2O_3 and spinel protective film such as $FeCr_3O_4$ (Heldberg *et al.*, 2013).

From Figure 4.12-13., it is also interestingly leapt out; surface of austenitic stainless steel prepared on the high pressure has perlitic-like lamellaes which is placed on the locally on the surface of sample. It was recommended that, the applied high compressive pressure causes to lattice distortion in spite of subjecting of γ-austenite led to stoppage of martensite phase bands in slip directions (García *et al.*, 2009). As a known from literature; the crystal structure of austenite phase has fa-centered cubic crystal structure characterized with 12 slip systems as 3 directions on 4 slip planes. With plastic deformation via mechanical experiments and production method; slpi parallel movement to the nearest packed plane{111}and direction<110> that is shortest distance cut off two atoms (Zhang *et al.,*2015). Martensitic transformation from austenite phase occur via plastic deformation with twinning and slip. Martensitic phase in the austenite matrix

phase disturbes as particle or islands and formed martensite phase nucleates and grows at the slip bands (Zhang *et al.*, 2015). The base-chemical compositions of austenite and martensite phases are same (Zhang *et al.*, 2015). These phases observed on the dotted lines in Figure 4.13.

On the Table 4.7; it was also seen that approximately same amounts of Ni, Cr and Fe dispersed, but C and P are not seen. Because; their amounts have small quantites to the other alloying elements (seen in Table 4.1).

4.8 The Magnetic Measurements and Surface Characterization of Martensitic Stainless Steels

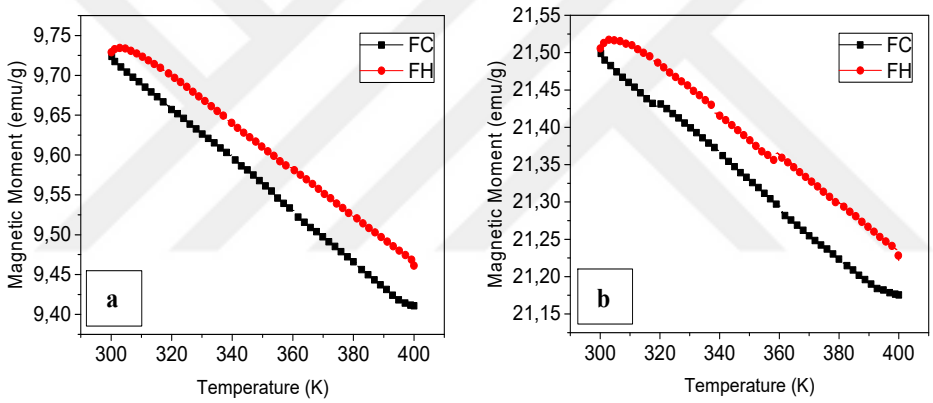


Figure 4.15. The magnetization as a function of Temperature [M(T)] curves of 410 martensitic stainless steel samples press-sintered on the a) 400 MPa and b) 600MPa pressures

In Figure 4.14; for 410 martensitic stainless steel prepared on the 400 and 600MPa pressures the magnetic moments (emu/g) related to field heated (FH) and field-cooled (FC) measured at temperature range of 300-400K temperature under 0.5 T magnetic field are observed. On the field-heating; For each sintered martensitic stainless steel samples; Magnetic moment (emu/g) decreases as when temperature increases due to austenite phase having paramagnetic behaviour and

on the field-cooling magnetization increases with temperature decreases because of more retained (reversed) austenite (Bojack *et al*., 2014 and Song *et al*., 2010). This reversed austenite induced by the traversal martensite to austenite phase transition. α-martensite to γ austenite phase transformation happens. This inducing reversed austenite will decrease to low magnetization. (Song *et al*., 2010). On Figure 4.14 b ; plateau regions clearly observed; again According to article of Song et al. İt was recommended that seeing of plateau region meant that increasing of austenite amount with decreasing temperature (Song *et al*., 2010). According to article of Christien et al; because of the fomation α martensite – γ austenite transition at high temperatures on both heating and cooling cycles and of both of phases having paramgnetic behaviours at that temperatures, this transition is not seen. Throuhout the α martensite – γ austenite transformation ; a separation of alloying elements such as Cr, Ni etc., between the two phases is hoped (Christien *et al.,* 2013). Again, at that according to article of Christien et al, when the specimen is heated to high temperature , the α martensite – γ austenite transformation is fully not completed and cooled from high temperature , steel includes of two phases consisting of various compositions. The chemical composition of martensite phase varies from the steel's begining composition (Christien *et al.,* 2013)

For field-heated; on the sintered martensitic stainless steel prepared on the 400MPa, magnetization values at the 300, 350 and 400K temperatures are obtained as 9.728 (for 300.15K), 9.609 (for 350K) and 9.461 emu/g (for 399.97K), respectively; on the sintered austenitic stainless steel on the 600MPa, magnetization values at the 300, 350 and 400K temperatures are acquired as 21.503 (for 300.14K), 21.380(for 350.2K) and 21.227 emu/g (for 399.89K), respectively. For field-cooled; on the sintered martensitic stainless steel on the 400MPa, magnetization values at the 300, 350 and 400K temperatures are obtained as 9.724 (for 300.20K), 9.565 (for 350K) and 9.411 emu/g (for 400.01K), respectively; on the sintered austenitic stainless steel on the 600MPa, magnetization values at the 300, 350 and 400K temperatures are acquired as 21.49

(for 300.24K), 21.380(for 351K) and 21.176 emu/g (for 399.89K), respectively. The Curie transformation temperatures of austenitic and martensitic stainless steel samples are not clear, because operating temperature of the devices is setup at low temperature.

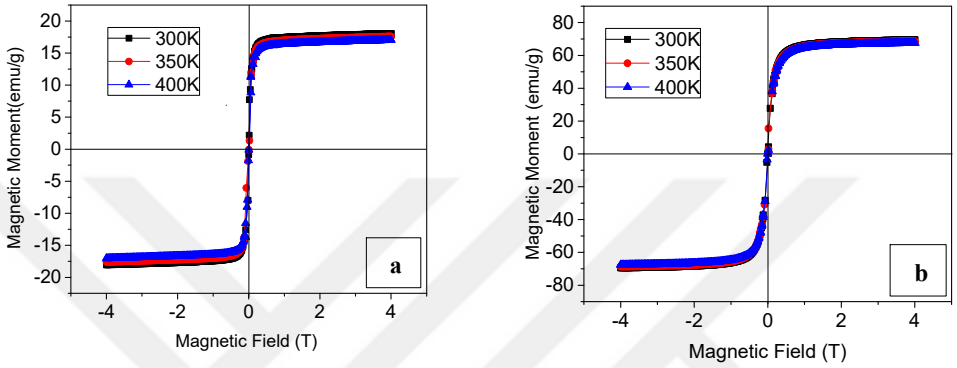


Figure 4.16. The Magnetization as a function of Magnetic Field [M(H)] curves of 410 martensitic stainless steel samples prepared on the a) 400MPa and b) 600MPa pressures

For examining of ferromagnetic behaviours of sintered martensitic stainless steels prepared on the 400 and 600MPa pressures; magnetic hysteresis loops curves are attained in ±4T magnetic field range and magnetic moment (emu/g) to applied field were measured at 300, 350 and 400K temperatures up to 4T magnetic field seen in Figure 4.15. The magnetic moment values (emu/g) of sintered martensitic stainless steel on the 400 and 600MPa pressures decreases when deformation temperature increased from 300 to 400K. Sintered martensitic stainless steel on the 400 MPa pressure has ferromagnetic behaviour at the range of ±0.046T magnetic field except that these magnetic field range, at other magnetic strength fields this martensitic stainless steels presents paramagnetic behaviours. The magnetic moment (emu/g) is obtained as 9.302 emu/g at H=0. For other sintered martensitic stainless steels; magnetic field range that show ferromagnetic behaviour is at ±0.019T magnetic field. Except that these magnetic field range, at other magnetic

strength fields this martensitic stainless steels presents paramagnetic behaviours. At H=0, magnetic moment of this martensitic stainless steel sample is given as 15.512 emu/g. At H=0; from magnetic moment values of these martensitic stainless steels; it is clearly seen that magnetic moment of sintered martensitic stainless steels on the high pressure higher than that of other martensitic stainless steel and it is meant that sintered martensitic stainless steel on the high pressure has more ferromagnetic behaviour according to other martensitic stainless steels. At 300, 350 and 400K temperature; as seen in Figure 4.11 (a) and (b; hysteresis curves of these austenitic stainless steels have small areas of coercive, remanences and also saturation magnetisation. The saturation magnetization values of sintered martensitic stainless steel on the low pressure are obtained as 18.047 (for 300K), 18.044 (for 350K) and 17.026 emu/g (for 400K) respectively; for sintered martensitic stainless steel on the high pressure, saturation magnetic moment values are recorded as 70.001(for 300K), 69.449 (for 350K) and 67.407 emu/g (for 400K), respectively. From values of saturation magnetization of these martensitic stainless steels; it is seen that saturation magnetization values decreases with increasing temperature and high saturation magnetization is obtained on the sintered martensitic stainless steel on the high pressure (70.001 emu/g, 300K).From magnetic hysteresis curves; it is recommended that according to article of Bojack *et al.,* both martensite and austenite are not decomposed and austenite decompositiion is time based process. Because , again according to Bojack *et al.,* article, austenite decomposition was depended on the holding time at this temperature and only happens after occuration of martensite throuhout cooling process,austenite decompostion may be owing to the stored energy from transition stresses (Bojack *et al.*, 2014)

On the Figure 4.16; The SEM images of 410 martensitic stainless steel prepared on 400 and 600MPa pressures seen. With increasing of pressure; surface of martensitic stainless steel sample improves, smoothes. As pressure increases, grain binding and porosity closes and therefore more strengthening structures occurs. On the Figure 4.16, b and d it was also observed the occuuring of finely

dispurted retained austenite along martensite lath bonundaries according to Song et al., (Song *et al*., 2010) .

Physical and chemical properties of martensitic stainless steel varies via heat treatment process. As known as, these stainless steel consits of undissolved fine, spherodized carbide precipitates, martensite , δ-ferrite , reversed/retained austenite related to heat treatment, carbon and austenite stabilizing elements (Isfahany et al., 2011, Song *et al*., 2010). Because of this complex metallurgical microstructure of this material, heat treatment of these stainless steel must carefully be controlled. In the martensitic stainless steel involving more than 0.2% C, carbon solutes in the matrix. Because of this situation, grain coarsening, decarburization and austenite repository must be prevented. (Isfahany *et al., 2*011). Physical properties of these stainless steel base on the strenghthening microstructure via precipitates and reversed or retained austenite phase (Song *et al*., 2010

The EDS spectras of 410 martensitic stainless steel samples prepared on the 400 and 600 MPa pressures are given in Figure 4.17. From EDS spectras of these stainless steel materials, it was observed that Cr element increased, Manganese sometimes increased, locally stabilized and carbon and iron amount decreased. Manganese in composition of these materials has an effect on the austenite formation from martensite phase. According to the article of Bojack et al., it presents Fe to be consisted owing to substituent diffusion effect of this element. The difusion of Mn and Fe may be a driving force on the austenite forming from martensite phase. Low heating rates selected because of austenite formation and diffusional transformation (Bojack *et al.,* 2014). Carbon influence in austenite phase is low because of carbide bonding. Occurring of carbides can not directly affect the stability of austenite via adulterate C from austenite (Bojack *et al.,* 2014).

Small hysteresis loops of both austenitic and martensitic stainless steels prepared on the 400 and 600MPa pressure are also depended on the lower hysteresis losses. These losses relates to the defect level into the material structure

limited magnetic domain movements with impurities, porosity, dislocations *etc.*[Bas *et al.,* 2003]. Owing to limiting of magnetic domain motion , porosity existence into the structure of stainless steels play a role on the increasing of hysteresis losses .[Bas *et al.,* 2003].

On the powder metallurgy method which is used on the preparing of austenitic and martensitic stainless steel samples , high density technologies apply due to decrease porosity existence in the microstructure of these stainless steel samples (Bas *et al.,* 2003). These technologies consist of shaping on the high pressure and sintering at high temperature and high purity atmosphere (Bas *et al.,* 2003). In the thesis study; austenitic and martensitic stainless steel samples were shaped under the high pressures and sintered at high temperature (~1200°C) under inert gas atmosphere. Prepared stainless steel samples possesses high density and correspondingly low percentage of porosity ((as seen in Table 4.2). Therefore; physical properties such as saturation magnetization behaviour improves.

Also, according to Oxley *et al*.'s study; stainless steel consisting of higher carbon amount have high coercive forces and lower maximum permeabilities owing to higher chromium carbide precipitates' amounts, these chromium carbide precipitates restricts movement of domain wall. This movement causes to severer magnetical behaviours (Oxley *et al.*, 2009). Throughout heat treatment of stainless steels, with rising of dissolved carbon in the ferrite phase magnetic domain wall restrictes and internal strains and resistance of grain boundary decrease. Slow cooling rate such as 5°C/min selected in this study play important role on the increasing of grain size and correspondingly corsening chromium carbides and hence, limiting domain wall movement (Oxley *et al.*, 2009)

From Figure 4.15-16. with increasing pressure, the saturation magnetism of martensitic stainlesss steel increased due to low C content of ferromagnetic matrix because of coarse carbide precipitates. From EDS spectrums, it was clearly seen that with increasing pressure, carbon decreased and Cr amount increased. Therefore, Throughout heat treatment, as carbon and chromium occur large

precipitates of carbides, their concentration in the ferromagnetic matrix is decreased thus magnetization values of steels increased due to anisotropy and crystalline defects throughout martensitic transition according to article of Tavares *et al.,* . (Tavares *et al.*,2000*)*

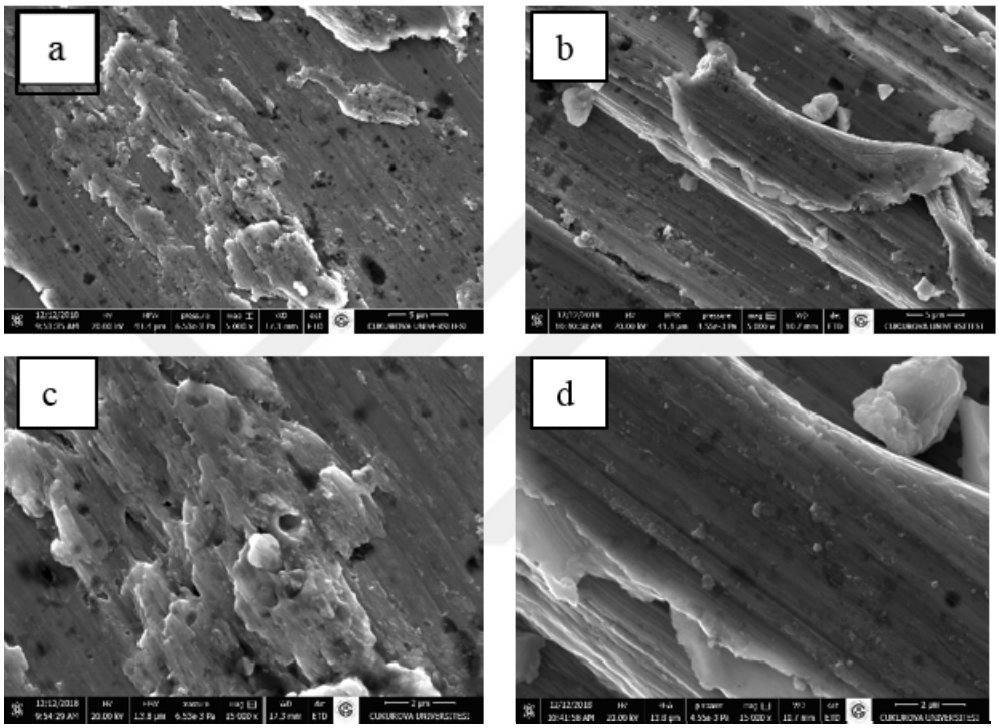


Figure 4.17. The SEM images of 410 martensitic stainless steel prepared on 400 (a and c) and 600MPa pressures (b and d)

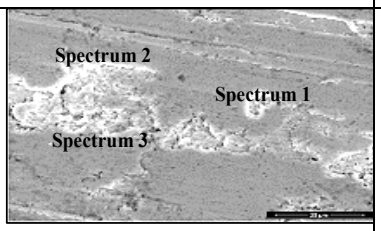
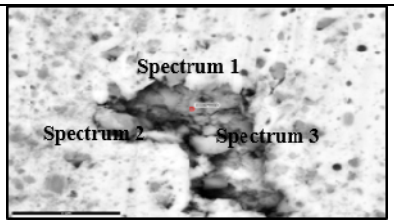
		410 /400 MPa		410 /600 MPa	
					
	Element	**Weight %**	**Atomic%**	**Weight %**	**Atomic%**
Spectrum 1	**C**	2.65	11.15	2.13	8.76
	Si	0.27	0.49	0.68	1.18
	Cr	8.84	8.58	63.42	60.20
	Mn	0.50	0.46	1.55	1.39
	Fe	87.74	79.32	32.20	28.46
Spectrum 2	**C**	3.34	13.72	3.31	13.09
	Si	0.28	0.49	0.47	0.78
	Cr	10.56	10.01	70.17	63.99
	Mn	1.25	1.13	1.20	1.04
	Fe	84.56	74.65	24.84	21.09
Spectrum 3	**C**	3.55	14.45	3.57	14.45
	Si	0.27	0.48	0.76	1.31
	Cr	12.73	11.97	19.43	18.10
	Mn	0.45	0.40	0.45	0.39
	Fe	83.00	72.70	75.78	65.73

Figure 4.18. The EDS spectrums of 410 martensitic stainless steel prepared on 400 and 600MPa pressures

4.9 The Thermophysical Properties Measurements of Austenitic and Martensitic Stainless Steels

In this thesis study; on examining of the physical properties sintered 316L austenitic and 410 martensitic stainless steel samples; specific heat capacity and enthalpy measurements of these steels occurred.

As known as specific heat capacity is defined as required heat amount in order to increase 1 g/kg of material to 1°C/1K of temperature of this material and enthalpy is referred also stored internal energy of the system. Spesicic heat

capactiy and enthalpy of these materials are briefly showed with c and h symbols, respectively and also units of specific heat capacity and enthaply of system are J/g°C and J/g. Morîntale *et al*., 2013; Fang *et al*., 2015; Wielgosz *et al*., 2014).

Specific heat capacity and enthalpy calculates with following equations;

For specific heat capacity (J/g°C);

$$c_p = c_0 + c_1 T^1 + c_2 T^2 + \frac{c_3}{T^2} \quad (4.8)$$

$$c_p(T) = \sum_{i=1}^{N} x_i c_p^i \ (T) \quad (4.9)$$

For enthalpy;

$$\Delta H(T) = \int c_p(T) dT \quad (4.10)$$

In equations (4.8), (4.9) and (4.10) ; due to specific heat capacity and enthalpy are based on temperature changing. General temperature relation is defined as polinominal developed by Kelly and equation (4.8) can be referred as Kelley rule (Wielgosz *et al*., 2014; Kelley, 1949). In equation (4.8); c_0, c_1, c_2 and c_3 are referred as characteristics for a phase in the material possessing the allotropics forms. Equation (4.9) is also defined as Neumann-Kopp rule. On this equation; N, x_i and c_p^i are defined as the number of alloying elements, the weight percent and specific heat capacity of i_{th} element, respectively (Wielgosz *et al*., 2014). Equation (4.10) is obtained integrating of specific heat capacity formula in the range of initial (T_0) and measured/final temperature (T).

On the Figure 4.18., specific heat capacity (Cp) and enthalpy (ΔH) versus temperature curves of austenitic and martensitic stainless steel samples produced on the 400 and 600 MPa pressures are observed. As increasing temperature; specific heat capacity and enthalpy values of samples increased but not linear increase due to increasing of atomic vibration's amplitude of composition of

samples with rising of temperature (Karthikeyan *et al.*, 2010). It was also seen that on specific heat capacity values the austenitic stainless steel prepared on the 600 MPa pressure; decrease recorded after approximately 300°C. and some behaviour of martensitic stainless steel prepared on the 400 MPa pressure show frustrating at temperature range of 430- 530°C, after 530°C , specific heat capacity values of this sample decreased with increasing temperature.

Generally; on the materials prepared by powder metallurgy method; physical properties of these materials improves with increasing pressure. Sometimes, exceptional situations can happen just like in austenitic stainless steel materials used in this thesis study. While, it was expected that specific heat capacity and enthalpy values of these materials increases with increasing pressure, these values of these samples decreases. Maximum specific heat capacity and enthalpy values of these austenitic stainless steel samples prepared on the 400MPa pressure 1.96J/g°C and 2268.2 J/g at 579°C temperature, respectively.

On the Figure 4.18; for martensitic stainless steel produced on the low pressure; specific heat capacity values of this martensitic stainless steel sample shows frustrating but for other martensitic stainless steel sample; increasing parabolic changing occurred. However; on the examining of enthalpy values of martensitic stainless steel samples; it was naturally observed that when increasing of temperature; enthalpy values of these samples increased. Both specific heat capacity and enthalpy v.s curves are also showed that pressure increased; both thermophysical magnitudes of these samples increased. Pressure increased; porosity decreases, grain bonding occurs, structures gain strength and therefore thermophysical magnitudes such as specific heat capacity improves. Maximum specific heat capacity and enthalpy values of this martensitic stainless steel sample prepared on the high pressure are 1.85J/g °C and 536.05 J/g at 579°C temperature, respectively.

316L 410

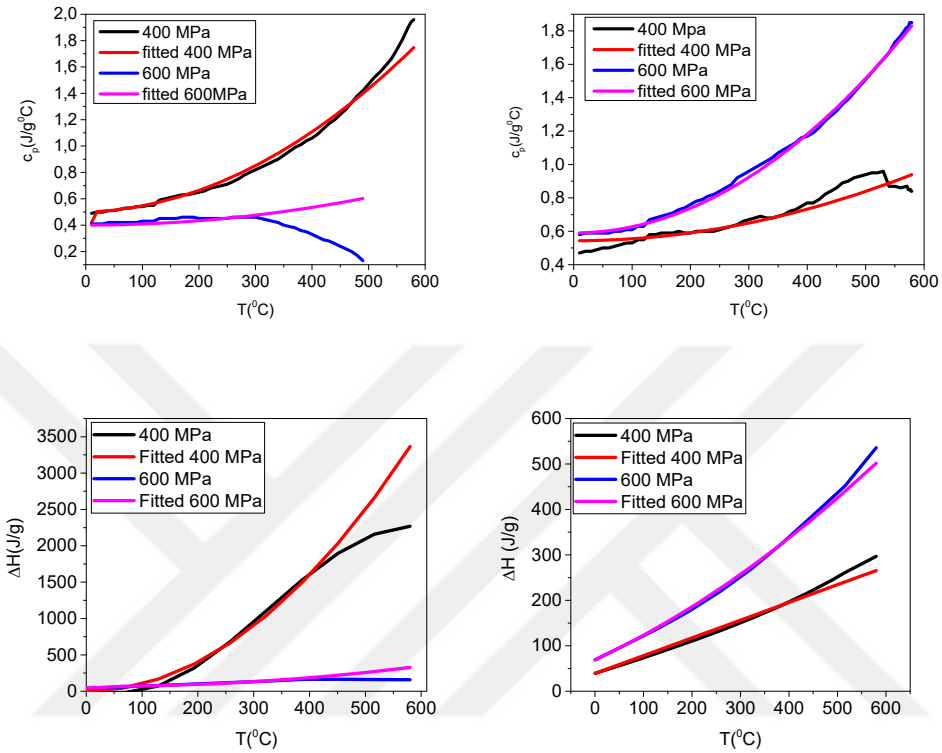


Figure 4.19. The specific heat capacity v.s temperature (above) and entalpy v.s. temperature (below) of 316L austenitic and 410 martensitic stainless steel samples prepared on 400 and 600 MPa pressures.

These thermophysical amplitudes' (specific heat capacity and enthalpy) values fitted with nonlinear regression method using Microsoft- Excel program. Following fitted curves and values with errors (%). were given in Table 4.8-11

Table 4.8. The specific heat capacity v.s. temperature values of 316L austenitic stainless steel samples prepared on the 400 and 600 MPa Pressures

T (°C)	**c_p (J/°Cg) 400 MPa**	**Fitted c_p(J/°Cg) 400MPa**	**Error (%)**	**c_p (J/°Cg) 600 MPa**	**Fitted c_p(J/°Cg) 600 MPa**	**Error (%)**
10	0,49	0,42	-14,2857	0,41	0,400092	-2,41659
20	0,5	0,503801	0,760225	0,41	0,400352	-2,35317
30	0,5	0,506750	1,350067	0,41	0,40078	-2,24878
40	0,51	0,510400	0,078459	0,42	0,401376	-4,43429
50	0,51	0,514750	0,931387	0,42	0,40214	-4,25238
60	0,52	0,519800	-0,03845	0,42	0,403072	-4,03048
70	0,53	0,525550	-0,83962	0,42	0,404172	-3,76857
80	0,53	0,532000	0,377362	0,42	0,40544	-3,46667
90	0,54	0,539150	-0,15741	0,42	0,406876	-3,12476
100	0,54	0,547000	1,296298	0,43	0,40848	-5,00465
110	0,55	0,555550	1,009092	0,43	0,410252	-4,59256
120	0,55	0,564800	2,69091	0,43	0,412192	-4,1414
130	0,59	0,574750	-2,58475	0,45	0,4143	-7,93333
140	0,6	0,585400	-2,43333	0,45	0,416576	-7,42756
150	0,61	0,596750	-2,17213	0,45	0,41902	-6,88444
160	0,62	0,608800	-1,80645	0,45	0,421632	-6,304
170	0,63	0,621550	-1,34127	0,46	0,424412	-7,73652
180	0,63	0,635000	0,793651	0,46	0,42736	-7,09565

Continued

190	0,64	0,649150	1,429688	0,46	0,430476	-6,41826
200	0,65	0,664000	2,153846	0,45	0,43376	-3,60889
210	0,66	0,679550	2,962121	0,45	0,437212	-2,84178
220	0,68	0,695800	2,32353	0,45	0,440832	-2,03733
230	0,69	0,712750	3,297102	0,45	0,44462	-1,19556
240	0,7	0,730400	4,342857	0,45	0,448576	-0,31644
250	0,71	0,748750	5,457747	0,45	0,4527	0,6
260	0,73	0,767800	5,178082	0,46	0,456992	-0,65391
270	0,75	0,78755	5,006667	0,46	0,461452	0,315652
280	0,78	0,808	3,589744	0,46	0,46608	1,321739
290	0,8	0,82915	3,64375	0,46	0,470876	2,364348
300	0,82	0,851	3,780488	0,46	0,47584	3,443478
310	0,84	0,87355	3,994048	0,45	0,480972	6,882667
320	0,86	0,8968	4,27907	0,44	0,486272	10,51636
330	0,88	0,92075	4,630682	0,43	0,49174	14,35814
340	0,9	0,9454	5,044444	0,42	0,497376	18,42286
350	0,93	0,97075	4,38172	0,4	0,50318	25,795
360	0,96	0,9968	3,833333	0,39	0,509152	30,55179
370	0,99	1,02355	3,388889	0,38	0,515292	35,60316
380	1,01	1,051	4,059406	0,36	0,5216	44,88889
390	1,04	1,07915	3,764423	0,35	0,528076	50,87886
400	1,06	1,108	4,528302	0,33	0,53472	62,03636
410	1,09	1,13755	4,362385	0,31	0,541532	74,68774
420	1,13	1,1678	3,345133	0,29	0,548512	89,14207
430	1,17	1,19875	2,457265	0,28	0,55566	98,45
440	1,2	1,2304	2,533333	0,26	0,562976	116,5292
450	1,24	1,26275	1,834677	0,24	0,57046	137,6917

Continued

460	1,28	1,2958	1,234375	0,22	0,578112	162,7782
470	1,33	1,32955	-0,03383	0,2	0,585932	192,966
480	1,38	1,364	-1,15942	0,17	0,59392	249,3647
490	1,42	1,39915	-1,46831	0,13	0,602076	363,1354
500	1,47	1,435	-2,38095			
510	1,52	1,47155	-3,1875			
520	1,56	1,5088	-3,28205			
530	1,61	1,54675	-3,92857			
540	1,66	1,5854	-4,49398			
550	1,73	1,62475	-6,08382			
560	1,81	1,6648	-8,0221			
570	1,9	1,70555	-10,2342			
575	1,94	1,726187	-11,0213			
580	1,96	1,747	-10,8673			

Table 4.9. The enthalpy v.s. temperature values of 316L austenitic stainless steel samples prepared on the 400 and 600 MPa Pressures

T (°C)	**ΔH (J /g) 400 MPa**	**Fitted ΔH(J/g) 400 MPa**	**Error (%)**	**ΔH (J /g) 600 MPa**	**Fitted ΔH(J /g) 600 MPa**	**Error (%)**
0,1	-0,83	-0,00358	99,5677	39,17	42,5000	-8,50147
64,45	-29,14	41,53452	242,5344	59,24	67,9408	-14,6874
128,9	72,24	166,14861	-129,995	79,26	76,9017	2,97534
193,35	317,86	373,83875	-17,6111	99,16	92,1290	7,09052
257,8	681,18	664,60498	2,43328	118,88	113,8689	4,21517
322,25	1105,17	1038,44728	6,0373	137,83	142,3679	-3,29241
386,7	1529,15	1495,36567	2,2093	162,78	177,8721	-9,27148
451,15	1897,55	2035,36015	-7,2625	164,48	220,6278	-34,1366

Continued

515,69	2159,43	2659,35890	-23,151	161,31	270,9570	-67,9729
580,05	2268,2	3364,57743	-48,3369	158,15	328,8792	-107,954

Table 4.10. The specific heat capacity v.s. temperature values of 410 martensitic stainless steel (410) samples prepared on 400 and 600 MPa pressures.

T (°C)	**c_p(J/°Cg) 400 MPa**	**Fitted c_p(J/°Cg) 400MPa**	**Error (%)**	**c_p(J/°Cg) 600 MPa**	**Fitted c_p(J/°Cg) 600MPa**	**Error (%)**
10	0,47	0,543566	15,65236	0,58	0,590371	1,788086
20	0,48	0,543920	13,31687	0,59	0,591482	0,251153
30	0,48	0,544512	13,44003	0,59	0,593333	0,564864
40	0,49	0,545339	11,2938	0,59	0,595924	1,004
50	0,5	0,546403	9,280667	0,59	0,599255	1,568559
60	0,5	0,547703	9,540667	0,59	0,603325	2,258542
70	0,51	0,549239	7,694042	0,6	0,608136	1,35605
80	0,52	0,551012	5,963878	0,6	0,613687	2,2812
90	0,53	0,553020	4,343583	0,61	0,619978	1,635754
100	0,53	0,555266	4,767187	0,61	0,627009	2,788361
110	0,55	0,557747	1,40863	0,63	0,63478	0,758714
120	0,55	0,560465	1,902748	0,63	0,643291	2,109651
130	0,58	0,563419	-2,85879	0,67	0,652542	-2,60572
140	0,58	0,566609	-2,30875	0,68	0,662533	-2,56874
150	0,59	0,570035	-3,38378	0,69	0,673264	-2,42558
160	0,59	0,573698	-2,76297	0,7	0,684734	-2,1808
170	0,59	0,577597	-2,10212	0,71	0,696945	-1,83869
180	0,6	0,581732	-3,04454	0,73	0,709896	-2,75395
190	0,59	0,586104	-0,66028	0,74	0,723587	-2,21796

Continued

200	0,59	0,590712	0,120712	0,76	0,738018	-2,89237
210	0,6	0,595556	-0,74061	0,78	0,753189	-3,43732
220	0,6	0,600636	0,10612	0,79	0,7691	-2,64559
230	0,6	0,605953	0,992232	0,81	0,785751	-2,99374
240	0,6	0,611506	1,917724	0,82	0,803142	-2,0559
250	0,61	0,617295	1,195994	0,84	0,821273	-2,22946
260	0,62	0,623321	0,535655	0,86	0,840143	-2,30891
270	0,63	0,62958	-0,06622	0,88	0,859754	-2,30065
280	0,64	0,636080	-0,61236	0,92	0,880105	-4,33639
290	0,66	0,642815	-2,60376	0,94	0,901196	-4,12807
300	0,67	0,649785	-3,01705	0,96	0,923027	-3,85135
310	0,68	0,656992	-3,38343	0,98	0,945598	-3,51042
320	0,69	0,664435	-3,70496	1	0,968909	-3,10912
330	0,68	0,672115	-1,15953	1,02	0,99296	-2,65101
340	0,68	0,680030	0,004547	1,04	1,017751	-2,13937
350	0,69	0,68818	-0,26335	1,07	1,043282	-2,49706
360	0,7	0,696571	-0,48984	1,09	1,069552	-1,87593
370	0,72	0,705195	-2,05616	1,11	1,096563	-1,21051
380	0,73	0,714056	-2,18405	1,13	1,124314	-0,50317
390	0,75	0,723153	-3,57953	1,16	1,152805	-0,62025
400	0,77	0,732486	-4,87184	1,17	1,182036	1,028718
410	0,77	0,742056	-3,62903	1,19	1,212007	1,849319
420	0,79	0,751862	-4,82755	1,22	1,242718	1,862115
430	0,82	0,761904	-7,08481	1,26	1,274169	1,1245
440	0,84	0,772182	-8,07346	1,29	1,30636	1,268186
450	0,86	0,782697	-8,98864	1,32	1,339291	1,461402
460	0,89	0,793448	-10,8485	1,36	1,372961	0,953044

Continued

470	0,9	0,804435	-10,6182	1,39	1,407372	1,249806
480	0,92	0,815659	-11,3414	1,43	1,442523	0,875748
490	0,93	0,827119	-11,0624	1,47	1,478414	0,572388
500	0,94	0,838815	-10,7643	1,51	1,515045	0,334106
510	0,95	0,850747	-10,4476	1,55	1,552416	0,155865
520	0,95	0,862916	-9,16669	1,59	1,590527	0,033132
530	0,96	0,875321	-8,8207	1,63	1,629378	-0,03818
540	0,87	0,887962	2,064656	1,67	1,668969	-0,06176
550	0,87	0,900839	3,544824	1,73	1,7093	-1,19656
560	0,86	0,913953	6,273687	1,77	1,75037	-1,10902
570	0,87	0,927303	6,586635	1,82	1,792181	-1,5285
571	0,87	0,928651	6,741577	1,82	1,796403	-1,29653
573	0,85	0,931354	9,571153	1,82	1,804869	-0,83138
575	0,85	0,934067	9,890275	1,85	1,813364	-1,98031
576	0,85	0,935427	10,05025	1,85	1,817623	-1,75011
577	0,85	0,936789	10,21051	1,85	1,821889	-1,5195
578	0,84	0,938153	11,68498	1,85	1,826163	-1,2885
579	0,84	0,939520	11,84771	1,85	1,830444	-1,05709

Table 4.11. The enthalpy v.s. temperature values of 410 martensitic stainless Steel (410) Samples prepared on 400 and 600 MPa pressures.

T (°C)	ΔH(J /g) 400 MPa	Fitted ΔH(J/g) 400 MPa	Error (%)	ΔH(J /g) 600 MPa	Fitted ΔH(J /g) 600 MPa	Error (%)
0,1	39,41	39,429	-0,0482	69,17	69,0500	0,1734
64,43	60,83	6,45E+01	-6,0631	102,81	102,9792	-0,1646
128,86	83,95	8,96E+01	-6,7868	137,7	140,4871	-2,0240
193,29	108,23	1,15E+02	-6,0500	175,78	181,5236	-3,2675
257,72	133,22	1,40E+02	-5,0215	219,44	226,0888	-3,0299
322,15	160,17	1,65E+02	-3,0421	269,18	274,1827	-1,8585
386,58	189,65	1,90E+02	-0,2777	325,93	325,8054	0,0382
451,01	222,92	2,15E+02	3,4127	388,51	380,9569	1,9440
515,44	260,84	2,40E+02	7,8173	451,51	439,6373	2,6295
579,87	296,86	2,66E+02	10,5343	536,05	501,8467	6,3806

Austenitic and martensitic stainless steel samples do not transition into martensite; the balanced calculation shows an maximum limit for the heat capacity. at high temperatures, allotriomorphic ferrite occurs;therefore; austenite amount that exposed to martensitic transformation is decreased, therefore in enthaply values; smaller variations occurs and faster cooling rate of 20°C/min base on the those alloys that occur completely martensitic phase at low temperature (Hasan *et al.*, 2011).

Variations in thermophysical behaviours such as specific heat capacity (c_P, J/kg°C), enthalpy (ΔH, J/kg) can be gradual and continuous to observe the effects of phase transitions. besides the existence of eutectic, peritectic and other phase transformations that form throughout solidification, macro and micro segregations can scarcely found out (Wielgosz *et al.,* 2014) On Figure 4.17.; from specific heat capacity values of stainless steel prepared on the 400MPa pressure; frustrating

was observed at temperature ranges of (100-150°C), 300-350°C) and (450-500°C). It can be recommended the rising from minor precipitation throughout heat treatment cycle on the manufacturing process. (Witthan *et al.*,2008)

As temperature increased, the measured enthalpy rised with fitting to an appropriable emprical equation to estimate the temperature relating to specific heat capacity values of steels (Raju *et al.,* 2010). Enthalpy values of prepared martensitic stainless steel on the 600MPa pressures separates on higher values than that of other stainless steel. It can considered that phase transformation clearly occurred.

On the Figures 4.16- 4.17 ; it was also observed that Si and Cr amounts increased while C amount decreased with increasing pressure. This case supported to increase specific heat capacity and enthalpy values of these martensitic stainless steels (Tables 4.9-4.10.). Silisium alloying element in the microstructure of the stainless steel have an significant role as stabilizing ferrite structure and improves strength of stainless steel according to Isfahany *et al*.,.(Isfahany *et al,* 2011*)* According to the Mola and Cooman; waiting at annealing temperatures (for 600 and 900 °C in this thesis study); for holding at initial temperature, large expansion that pursues at longer times is owing to the austenite decomposition to ferrite and carbide phases. In terms of forming of stable Cr-carbide, this reaction is preferred via important carbon loss. At 600 °C temperature; this austenite decomposition became fast, correspondingly, in the austenite phase carbon and chromium loss leads to rise in the M_s temperature of residual austenite. Waiting at 900°C temperature for 30 minutes; it happens in a completely austenite matrix by sepulchred $M_{23}C_6$ –type carbides. (Mola and Cooman, 2013)

For each 316L austenitic and 410 martensitic stainless steel samples prepared on the 400 and 600 MPa pressures; fit coefficients and nonlinear –squares regression values of specific heat capacity and enthalpy magnitudes were given in Table 4.12-13.

Table 4.12. The fit coefficients and nonlinear–squares regression values of specific heat capacity behaviour of 316L austenitic and 410 martensitic stainless steel samples prepared on the 400 and 600 MPa pressures.

	316L/400 MPa	**316L/600 MPa**	**410/400 MPa**	**410/600 MPa**
$\mathbf{c_0}$	0,5	0,4	0,543447451	0,59
$\mathbf{c_1}$	0,00012	0,0000008	0,000000049	0,00000009
$\mathbf{c_2}$	0,0000035	0,00000084	1,18137E-06	0,0000037
$\mathbf{c_3}$	0,009	0,0000003	9,9E-11	0,000000023
$\mathbf{R^2}$	0,9494	0,9401	0,9446	0,9446

Table 4.13. The fit coefficients and nonlinear –squares regression values of enthalpy behaviour of 316L austenitic and 410 martensitic stainless steel samples prepared on the 400 and 600 MPa pressures.

	316L/400MPa	**316L/600MPa**	**410/400MPa**	**410/600MPa**
$\mathbf{c_0}$	0	0,0002	3,90E-01	5,00E-01
$\mathbf{c_1}$	0,02	0,00139	0,00000025	0,00085
$\mathbf{c_2}$	1,40E-11	0,00000046	9,90E-11	8,90E-11
$\mathbf{c_3}$	0,000000075	0,009	0	0
$\mathbf{c_4}$	0,0035	-65	-3,94E+01	-69
$\mathbf{R^2}$	0,9248	0,9448	1,0000	0,9915

According to Table 4.12; a better fit provided on the austenitic stainless steel prepared on the 600 MPa pressure according to other austenitic stainless steel samples (R^2=0.9448) and also it was also observed that a better fit provided on the martensitic stainless steel prepared on the 400 MPa pressure according to other martensitic stainless steel and martensitic stainless steel samples (R^2=1.000) On the Table 4.13. a better fit provided on the martensitic stainless steel sample and also showed on the Figure 4.17.

5. CONCLUSION

In the thesis work; mechanical, electrochemical, magnetization, thermophysical properties and surface characterization of austenitic and martensitic stainless steel manufactured using powder metallurgy method were examined. Characterized austenitic and martensitic stainless steel powders pressed under low (400 MPa) and high (600 MPa) pressures and compacted stainless steel samples sintered according to specified heat treatment cycle and sintering process performed under inert gas (Ar) atmosphere.

Hardness, density and Charpy-V impact strength measurements as mechanical properties, corrosion resistance experiment as electrochemical, M-H and M-T as magnetization and specific heat capacity and enthalpy measurements as thermophysical properties of stainless steel samples were performed. Structural features of samples were supported by SEM images, EDS spectrums and XRD patterns.

Following experimental results are given;

1. Both of austenitic and martensitic stainless steel powders have irregular shaped particles which are water atomized powder particle type.

2.Particle size distributions of these stainless steel present positively skewed particle size distribution because of having have finer particles. Martensitic stainless steel powder has finer particles comparing to austenitic stainless steel powder.

3.With increasing pressure; bulk density, apparent solid density values of both of austenitic and martensitic stainless steel samples increased, apparent porosity and water adsorption of both of stainless steel samples decreased. Whereas density values of austenitic stainless steel samples have higher values than that of other stainless steel samples. On the porosity values of samples maximum decreasimg recorded on the martensitic stainless steel samples.

4. As pressure increasing of pressure; hardness and CharpyV- notch impact strengths of both stainless steel samples increased. Maximum hardness and impact strengths recorded on the martensitic stainless steel prepared on the high pressure, because of increasing of austenite phase in the martensite matrix structure, decreasing of carbide precipitation and homogeneous dispersion of these precipitations on the structure of stainless steel sample, besides grain bonding, closed porosity with increasing pressure.

5.For electrochemical process of both stainless steel samples; corrosion resistance measurements of these samples performed. The best corrosion resistance obtained on the martensitic stainless steel prepared on the 400 MPa pressure. This situation related to martensitic stainless steel having finer particle size according to other stainless steel powder.

6.There are more studies about magnetization of austenitic stainless steels but a few studies about relationships between physical properties and magnetization of austenitic stainless steels. Also, there are at least studies about magnetization of martensitic stainless steels. With this thesis study; it was aimed and studied to fill the gaps in the literature studies on these properties of these stainless steels. Martensitic stainless steel have more ferromagnetic behaviours and higher magnetic moments (emu/g) values compared to magnetization curves of austenitic stainless steels. This situation can recomended that carbide precipitations and phase transformations have influences on the magnetic features of these martensitic stainless steels.

7-There are at least studies about thermophysical behaviours of both of austenitic and martensitic stainless steels. With this thesis study; it was aimed and studied to fill these gaps in the literature studies on the these properties of these stainless steels. With increasing temperature; specific heat capacity and enthapy values of both of austenitic and martensitic stainless steel samples increased. When pressure increased, these thermophysical properties of austenitic stainless steel samples decreased while these properties of other stainless stainless steel sample increased.

Maximum specific heat capacity and enthalpy values of austenitic stainless steel sample prepared on the 400MPa pressure are 1.96 J/g°C and 2268.2 J/g at 579 °C temperature, respectively and maximum specific heat capacity and enthalpy values are recorded on the martensitic stainless steel sample prepared on the 600MPa presuure.

From these all experimental results; it observed that mechanical (except that density), corrosion resistance, magnetic and thermophysical properties of martensitic stainless steel samples have higher values than that of austenitic stainless steels. It can recommented that these results related to finer raw powders of these stainless steel samples. Powder having finer particle, bulk product has more strenghthening structure and show better physical, mechanical, magnetic properties. etc., these results supported with literature studies.

For future studies; it can be planned that physical, mechanic, magnetic, corrosion resistance,thermophysical and also thermoelectric studies of these stainless steels doped with alloying elements such as Mn, Si etc. by variying ratios will be examined.And also these properties of these stainless steels will be examined on the higher sintering temperatures with controlled slower and higher heating and cooling rates. Corrosion resistances of these stainless steels will be studied under different conditions except that NaCl solid solution.

REFERENCES

A Basic Guide to Particle Characterization, 2015 Malvern Instruments Limited.

A Guidebook to Particle Size Analysis, Horiba Scientific.

Akhavan Tabatabae B., Ashrafizadeh F., Hassanlı A.M., Influence of Retained Austenite on the Mechanical Properties of Low Carbon Martensitic Stainless Steel Castings, ISIJ International, Vol. 51 No. 3, (2011), 471–475.

Anjos A.D., Scheuer C.J., S.F. Brunatto S.F., Cardoso R.P., Low-temperature Plasma Nitrocarburizing of the AISI 420 Martensitic Stainless Steel: Microstructure and Process Kinetics, Surface and Coatings Technology 275 (2015), 51–57.

Arrayago I., Real E.,, L. Gardner L., Description of Stress–Strain Curves for Stainless Steel Alloys, Materials and Design 87 (2015), 540–552.

ASM Alloy Digest Sourcebook: Stainless Steels,2000.

Azevedo C.R.F., Maia R.R., Ariza E.A., Tschiptschin A.P., Failure Analysis of a Martensitic Stainless Steel (CA-15M) Roll Manufactured by Centrifugal Casting. Part I: Material and Fractographic Characterization Engineering Failure Analysis 36 (2014), 343–352.

Bas J.A., Coleroj A., Dougan M.J., 2003, Sintered Soft Magnetic Materials. Properties and Applications, Journal of Magnetic and Magnetic Materials (254-255) (2003),391-398.

Bojack A., Zhao L., Morris P.F., J. Sietsma J., In Situ Thermo-magnetic Investigation of the Austenitic Phase During Tempering of a 13Cr6Ni2Mo Supermartensitic Stainless Steel, Metallurgical and Materials Transactions A,—Volume 45A, (2014), 5956-5967.

Borgioli F., Galvanetto E., Bacci T., Pradelli G., Influence of the Treatment Atmosphere on the Characteristics of Glowdischarge Treated Sintered Stainless Steels, Surface And Coatings Technology 149 (2002) 192–197.

Brachet J., Correlation Between Thermoelectric Power (TEP) and Martensite Start Temperature (Ms) Measurements of 9Cr-W-V-(Ta) Martensitic Steels. Journal de Physique IV,05 (1995), (C8),C8-339-C8-344.

Brink B. K.,Ståhl K.,Christiansen T.L., Frandsen C., Hansen M.F., Somers M.A.J., Composition-Dependent Variation of Magnetic Properties and Interstitial Ordering in Homogeneous Expanded Austenite, Acta Materialia 106 (2016),32-39.

Butković S., Oruč M., Šarić E., Mehmedović M., Effect of Sınterıng Parameters on the Density, Microstructure And Mechanical Properties of the Niobium-Modified Heat-Resistant Stainless Steel GX40CrNiSi25-20 Produced by MIM Technology, Materiali in tehnologije / Materials and technology 46 (2012) 2, 185–190.

Butković S., Sinterability And Tensile Properties of Nickel Free Austenitic Stainless Steel X15CrMnMoN 17 11 3,Tehnički vjesnik 20, 2(2013), 269-274 269, (Technical Gazette 20, 2(2013), 269-274.

Caballero F.G.,, Capdevila C., de Andrés C.G., Thermoelectric Power Studies on a Martensitic Stainless Steel, Scripta Materialia 50 (2004),1061–1066.

Cabral-Miramontes J. A., Barceinas-Sánchez J. D. O., Poblano-Salas C. A., Pedraza-Basulto G. K., Nieves-Mendoza D., Zambrano-Robledo P. C., Almeraya-Calderón F., Chacón-Nava J. G., Corrosion Behavior of AISI 409Nb Stainless Steel Manufactured by Powder Metallurgy Exposed in H_2SO_4 and NaCl Solutions, International Journal of Electrochemical Science, 8 (2013) 564 – 577.

Cain V., 2006 High Temperature Creep Behaviour Niobium Bearing Ferritic Stainless Steels, master thesis Cape Peninsula University of Technology.

Cajner F., Kovačić S., Rafael H., Vugrinčić A., Šimunović V., Gržeta B., Influence of Nitriding on Corrosion Resistance of Martensitic X17CrNi16-2 Stainless Steel, Mat.-wiss. u. Werkstofftech. 2015, 46, No. 1.

Carreon H., Barriuso S., Barrera G., González-Carrasco J.L., F.G. Caballero F.G., Assessment of Blasting Induced Effects on Medical 316 LVM Stainless Steel by Contacting and Non-Contacting Thermoelectric Power Techniques, Surface and Coatings Technology 206 (2012),2941–2946.

Carrouge D., Bhadeshia H.K.D.H.,Woollin P. Effect of δ-ferrite on Impact Properties of supermartensitic stainless Steel Heat Affected Zones, Science and Technology of Welding and Joining, Vol. 9 No. 5, 2004; 377-389.

Ceccon T., Belloli P., Ramina P., , The Magnetic Properties of a Precipitation Hardening and a Soft Martensitic Stainless Steel, Acciaierie Valbruna "Soft Martensitic S. S." (2005), 1-6.

Choi J.y. ,T. Fukuda T., Kakeshita T.,Effect of Magnetic Field on Isothermal Martensitic Transformation in a Sensitized SUS304 Austenitic Stainless Steel, Journal of Alloys and Compounds 577S (2013), S605–S608.

Christien F., Telling M.T.F., Knight, K.S., A Comparison of Dilatometry and In-Situ Neutron Diffraction in Tracking Bulk Phase Transformations in a Martensitic Stainless Steel, Materials Characterization 82(2013) 50-57.

Covert R.A., Tuthill A.H., Stainless Steel: An Intrduction to Their Metallurgy and Corrosion Resistance. Dairy, Food and Environmental Sanitation vol.20 No.7(, 2000) pp 506-517.

Cunat P.C., Alloying Elements in Stainless Steel and Other Chromium-Containing Alloys, Euro Inox 2004, The International Chromium Development Association.
www.euroinox.org

Das A., Magnetic Properties of Cyclically Deformed Austenite, Journal of Magnetism and Magnetic Materials 361, (2014), 232–242.

Davis J.R. (Ed.): ASM Speciality Handbook: Stainless Steels, ASM International, Materials Park, OH (1994).

Dyankova S. , Doneva M. , Todorov Y. , Terziyska M. Determination of Particle Size Distribution and Analysis of a Natural Food Supplement on Pectin Base, IOSR Journal Of Pharmacy Volume 6, Issue 5 (May 2016), PP. 01-08.

Espitia L.A., Dong H., Li X.-Y., Pinedo C.E., Tschiptschin A.P. Cavitation Erosion Resistance and Wear Mechanisms of Active Screen Low Temperature Plasma Nitride AISI410 Martensitic Stainless Steel, Wear 332-333(2015)1070–1079.

Fang H.,Wong M.B., Bai Y.,Use of Kinetic Model for Thermal Properties of Steel at High Temperatures, Australian Journal of Civil Engineering, 13:1, 2015, 40-47.

Ferreira L.M., Brunatto S.F., Cardoso R.P., Martensitic Stainless Steels Low-temperature Nitriding: Dependence of Substrate Composition, Materials Research. 2015; 18(3): 622-627.

Freire L., Catarino M.A., Godinho M.I., Ferreira M.J., Ferreira M.G.S., Simões A.M.P., Montemor M.F., Electrochemical and Analytical Investigation of Passive Films Formed on Stainless Steels in Alkaline Media, Cement and Concrete Composites, 34(9), 2012, pp.1075-1081.

Forghani F., Nili-Ahmadabadi M., Microstructural Characteristics and Second-phase Particles in Yttrium-bearing Fe-10Ni-7Mn Martensitic Steels, Journal of Rare Earths, Vol. 32, No. 4, 2014, 326-333.

Fortan M., Dejans A., Debruyne D., Rossi B., The Strength of Stainless Steel Fillet Welds Using GMAW, Stainless Steel in Structures –Fifth International Experts Seminar London, UK, 18-19 September 2017

Fossati A., Borgioli F., Galvanetto E., T. Bacci T., Corrosion resistance properties of Glow-Discharge Nitrided AISI 316L Austenitic Stainless Steel in NaCl Solutions, Corrosion Science 48 (2006), 1513–1527.

García C., Martín F., Blanco Y., Abnormal Magnetic Behaviour of Powder Metallurgy Austenitic Stainless Steels Sintered in Nitrogen, J. Mag. and Magn. Mater. 321 (2009) 3171-3177.

García C., Martin A.F., Blanco Y., De Tiedra M.P., Aparicio M.L., Influence of Sintering under Nitrogen Atmosphere on Microstructures of Powder Metallurgy Duplex Stainless Steels, Metall and Mat Trans A (2009) 40: 292-301 .

García de Andrés C., Caruana G., Alvarez L.F., Control of M23C6 Carbides in 0.45C–13Cr Martensitic Stainless Steel by means of Three Representative Heat Treatment Parameters, Materials Science and Engineering A241 (1998) 211–215.

German R.M., Powder Metallurgy and Particulate Materials Processing Toz Metalurjisi ve Parçacıklı Malzeme İşlemleri Türkçeye Çeviren Sarıtaş s., Türker M., Durlu N. Türk Toz Metalurjisi Derneği Yayınları:05, 2007.

German R.M., Sintering Theory and Practice , Sinterleme teorisi ve Uygulamaları çeviren Gülsoy H.Ö., nobel Akademik Yayıncıık xxii+554 sayfa , 2014

Ghosh S.K., Mallick P.,Chattopadhyay P.P., 2012, Effect of Cold Deformation on Phase Evolution and Mechanical Properties in an Austenitic Stainless Steel for Structural and Safety Applications, Journal of Iron and Steel Research, International,19(4): 63-68.

Hasan H.S., Peet M.J., Jalil J.M., Bhadeshia H.K.D.H., Heat transfer Coefficients During Quenching of Steels , Heat Mass Transfer 2011, 47:315-321.

Hedberg Y., Norell M., Hedberg J., Szakálos P., Linhardt P., Wallinder O., Surface characterisation of fine inert gas and water atomised stainless steel 316L powders: formation of thermodynamically unstable surface oxide phases Powder Metallurgy, (2013) 158-163.

Hedström P., 2007, Deformation and Martensitic Phase Transformation in Stainless Steels, Doctoral Thesis, Luleå University of Technology.

Hoffelner W., Materials for Nuclear Plants from Safe Design to Residual Life AssesmenT, Chapter 2 Materials, Springer-Verlag London Limited 2013, 65-134.

Hsieh C.-C., Wu W., Overview of Intermetallic Sigma (σ) Phase Precipitation in Stainless Steels, Int. Sch. ISRM Metall (2012), Article ID: 732471 1-16.

Hsu C-H., Teng H.-Y., Chen Y. J., (2004) "Relationship Between Ultrasonic Characteristics and Mechanic Properties of Tempered Martensitic Stainless Steel ", Journal of Materials Engineering and Performance 13: 593-599.

Huang K.-T., Chang S.-H., Hsieh P.-C., Microstructure, Mechanical Properties and Corrosion Behavior of NbC Modified AISI 440C Stainless Steel by Vacuum Sintering and Heat Treatments, Journal of Alloys and Compounds 712, (2017),760-767.

Huttunen-Saarivirta E., Kilpi L., Hakala T.J., Carpen L. Ronkainen H., Tribocorrosion Study of Martensitic and Austenitic Stainless Steels in 0.01M NaCl Solution, Tribology International 95 (2016), pp.358–371,

Isfahany A.N., Saghafian H., Borhani G., "The Effect of Heat Treatment on Mechanical Properties and Corrosion Behaviour of AISI420 Martensitic Stainless Steel ", Journal of Alloys and Compounds 509 (2011), pp. 3931–3936.

Javanbakht M., Hadianfard M.J., Salahinejad E., Microstructure and Mechanical Properties of a New Group of Nanocrystalline Medical-Grade Stainless Steels Prepared by Powder Metallurgy, Journal of Alloys and Compounds 624 (2015),17–21.

Javanbakht M., Salahinejad E.,, Hadianfard M.J., 2016, The Effect of Sintering Temperature on the Structure and Mechanical Properties of Medical-grade Powder Metallurgy Stainless Steels Powder Technology 289 (2016), 37–43.

Kan Y., Zhang S.G., Zhang L.G., Cheng M., Song H.G., Lu H.G, Healing Behavior of Micropores in Powder Metallurgy 316L Stainless Steel during Hot Forging and Heat Treatment, Journal of Iron and Steel Research, International, (2014), 21(9): 862-868.

Karthikeyan B., Ramanathan S., Ramakrishnan V., A calorimetric study of 7075 Al/SiC_p composites, Materials and Design 31 (2010),S92–S95.

Kelley K.K., X. High-Temperature Heat-Content, Heat-Capacity, and Entropy Data for Inorganic Compounds, Bureau of Mines Bull. 476 (1949), 192.

Kishor B., Chaudhari G.P., Nath S.K., Cavitation Erosion of Thermomechanically Processed 13/4 Martensitic Stainless Steel Wear319(2014)150–159.

Kundalkar D., Mavalankar M., Tewari A., Effect of Gas Nitriding on the Thermal Fatigue Behaviour of Martensitic Chromium Hot-Work Tool Steel, Materials Science and Engineering A 651(2016)391–398.

Kyogoku H., Komatsu S., Shinzawa M.,Matsuoka T, Fatigue and Impact Strengths of Austenitic Stainless Steel by Powder Injection Molding, J. Jpn. Soc. Powder Powder Metallurgy Vol. 50, No.11, (2003) 903-907.

Laborne A.R., Gavoille P., Malaplate J., Pokor C., Tanguy B., 2015, Correlation of Radiation-Induced Changes in Microstructure / Microchemistry, Density and Thermo-electric Power of type 304L and 316 Stainless Steels Irradiated in the Phénix Reactor, Journal of Nuclear Materials 460 (2015), 72–81.

Lai JK.L., Shek C.H. Saho Y.Z. Pakhomov A.B. 2004, Magnetic Properties oF Thermal Aged 316 Stainless steel and ıts Precipitated Phases, Materials Science and Engineering A379 (2004), 308-312

Lasseigne A.N., Olson D.L.,Kleebe H.-J., Boellinghaus T., Microstructural Assessment of Nitrogen-Strengthened Austenitic Stainless-Steel Welds Using Thermoelectric Power Metallurgical and Materials Transactions A Volume 36A, (2005), 3031-3039.

Lee Y.-K., Shin H.-C., Leem D.-S., Choi J-Y., Jin W., Choi C.-S., Reverse Transformation Mechanism of Martensite to Austenite and Amount of Retained Austenite After Reverse Transformation in Fe–3Si–1 3Cr–7Ni (wt-%) Martensitic Stainless Steel, Materials Science and Technology March 2003 Vol. 19 393-398.

Lee K.-H., Suh J.-Y., Hong S.-M., Huh J.-Y.,Jung W.-S., Microstructural Evolution and Creep-Rupture Life Estimation of High-Cr Martensitic Heat-Resistant Steels, Materials Characterization 106 (2015) 266–272.

Lee K.-H., Hong S.-M., Shim J.-H., Suh J.-Y., Huh J.-Y.,Jung W.-S., Effect of Nb Addition on Z-Phase Formation and Creep Strength in High-Cr Martensitic Heat-Resistant Steels, Materials Characterization 102 (2015) 79–84.

Lee S.H., Kakati N., Maiti J., Jee S.H., Kalita D.J., Yoon Y.S., Corrosion and Electrical Properties of CrN- and TiN-Coated 316L Stainless Steel used as Bipolar Plates for Polymer Electrolyte Membrane Fuel Cells, Thin Solid Films 529(2013), 374–379.

Leffler B., Stainless- stainless steels and their properties, http://www.outokumpu.com/files/group/hr/documents/stainless20.pdf

Łepicka M., Grądzka-Dahlke M., Effect of Heat Treatment and Plasma Nitriding on Corrosion Resistance of 440B Martensitic Stainless Steel, Acta Mechanica et Automatica, vol.7 no.3 (2013), 155-159

Li C.X., Bell T. Corrosion Properties of Plasma Nitrided AISI 410 Martensitic Stainless Steel in 3.5% NaCl and 1% HCl Aqueous Solutions, Corrosion Science 48 (2006) 2036–2049.

Li S., Yuan X., Jiang W., Sun H., Li J., Zhao K., Yang M., Effects of Heat Treatment Influencing Factors on Microstructure and Mechanical Properties of a Low-Carbon Martensitic Stainless Bearing Steel, Materials Science & Engineering A 605(2014) 229–235.

Lin Y. , Lin C.-C., Tsai T.-H., Lai H.-J.(2010) Microstructure and Mechanical Properties of 0.63C-12.7Cr Martensitic Stainless Steel during Various Tempering Treatments, Materials and Manufacturing Processes, 25:4 (2010), 246-248.

Lo K.H., Shek C.H.., J.K.L. Lai J.K.L. Recent developments in stainless steels, Materials Science and Engineering R 65 (2009) 39–104.

Loto R.T., Pitting Corrosion Evaluation of Austenitic Stainless Steel type 304 İN Acidic Chloride Media, J. Mater. Environ. Sci., 4(4) (2013),448-459.

Ma B., Li C., Han Y., Wang J., γ→α′ Martensitic Transformation and Magnetic Property of Cold Rolled Fe–20Mn–4Al–0.3C Steel, J. Mag. and Magn. Mater. 419(2016), 249-254.

Ma X.P., Wang L.J., Qin B., Liu C.M., Subramanian S.V., Effect of N on Microstructure and Mechanical Properties of 16Cr5Ni1Mo Martensitic Stainless Steel, Materials And Design 34 (2012) 74–81.

Marcelin S., Pébère N., Régnier S.,Electrochemical Characterisation of a Martensitic Stainless Steel in a Neutral Chloride Solution, Electrochemica Acta 87 (2013),32-40.

Martelli V., Bianchini G., Ventura G. 2004, Measurement of the Thermal Expansion Coefficient of AISI 420 Stainless Steel Between 20 and 293 K, Cryogenics 62 (2014) 94–96.

Martín F., García C., Blanco Y.,Rodriguez-Mendez M.L., Influence of Sinter-Cooling Rate on the Mechanical Properties of Powder Metallurgy Austenitic, Ferritic, and Duplex Stainless Steels Sintered in Vacuum, Mater. Sci. and Eng. A 642 (2015) 360-365.

Mola J.,Cooman B.C. De, Quenching and Partitioning (Q&P) Processing of Martensitic Stainless Steels, Metalurgical and Materials Transactions A, volume 44A, (2013), 946-967.

Mondal B.N. Bhattacharyay R., Nath D.N., Chattopadyay P.P., Magnaetic Response of Cu (25wt%)-316 grade Stainless Steel Processed by Ball Milling, Journal of Non-Crystalline Solids, 358 (2012), 810-813.

Mondal B., Chabri S., Sardar G., Bhowmik N., Sinha A., Chattopadyay P.P., Magnetic and Mechanical Properties of Cu (75%)-316Lgrade Stainless Steels Sybthesized by Ball Milling and Annealing, Journal of Magnetism and Magnetic Maaterials, 381 (2015), 14-20.

Morîntale E., Harabor A., Constantinescu C., Rotaru P., Use of Heat Flows From DSC Curve for Calculaion of Specific Heat of the Solid Materials, Physics AUC. Vol. 23, (2015), 89-94.

Multigner M., Frutos E., González-Carrasco J.L., Jiménez J.A., Marín P., Ibáñez J., Influence of the Sandblasting on the Subsurface Microstructure of 316LVM stainless steel: Implications on the Magnetic And Mechanical Properties, Mater. Sci. and Eng. C 29 (2009) 1357-1360.

Mumtaz K., Takahashi S., Echigoya J., Kamada Y., Zhang L.F., Kikuchi H.K., Ara K.,Sato M., Magnetic Measurements of Reverse Martensitic to Austenitic Transformation in a Rolled Austenitic Stainless Steel, J.Mater. Sci. 39 (6) (2004), 1997-2010.

Mumtaz K., Takahashi S., Echigoya J., Zhang L.F., Kamada Y., Sato M., Detection of Martensite Transformation in High Temperature Compressively Deformed Austenitic Stainless Steel by Magnetic NDE Technique, J.Mater.Sci. 38 (2003) 3037-3050.

Mumtaz K., Takahashi S., Echigoya J., Kamada Y., Zhang L.F., Kikuchi H.K., Ara K., Sato M., Magnetic Measurements of Martensitic Transformation in Austenitic Stainless Steel After Room Temperature Rolling, J.Mater. Sci. 39 (2004) 85-97.

Olaseinde O.A. Comparative Study of the Effect of Temperature on the Corrosion Behaviour of 2205 Duplex Stainless Steel and 316 Austenitic Stainless Steel in Acidic Chloride Environment, Advances in Materials Physics and Chemistry, 5 (2015), 185-190.

Oxley P., Goodell J., Molt R., Magnetic Properties Of Stainless Steels at Room and Cryogenic Temperatures, Journal of Magnetism and Magnetic Materials 321 (2009) 2107–2114.

Özcan E., 2012 Corrosıon Behavıors of Staınless Steels in Molten Zinc Aluminum Alloy, Master Thesis Middle East Technical University.

Öztürk O., Okur S., Riviere J.P., Structural and Magnetic Characterization of Plasma Ion Nitrided Layer on 316L Stainless Steel Alloy, Nucl. Ins. and Meth. in Phy. Res. B 267 (2009) 1540–1545.

Pahlavan S.,Moazen S., Taji I., Saffar K., Hamrah M., Moayed M.H. and Mollazadeh Beidokhti S., Pitting Corrosion of Martensitic Stainless Steel in Halide Bearing Solutions, Corrosion Science 112, (2016), pp.233–240,

Pandya S., Ramakrishna K.S., Annamalai A.R., Upadhyaya A., Effect of Sintering Temperature on the Mechanical and Electrochemical Properties of Austenitic Stainless Steel, Materials Science and Engineering A 556 (2012) 271–277,

Pardo A., Merino M.C., Coy A.E., Viejo F., Arrabal R.,Matykin E., Effect of Mo and Mn Additions on the Corrosion Behaviour of AISI 304 and 316 Stainless Steels in H_2SO_4, Corrosion Science 50(3) (2008), 780-794,

Pinedo C.E.,Monteiro W.A., On the Kinetics of Plasma Nitriding a Martensitic Stainless Steel Type AISI 420,Surface and Coatings Technology 179 (2004) 119–123

Rahaman M.N., 2000, Ceramic Processing and Sintering, , Marcel Dekker Inc,

Raju S., Ganesh B.J., rai A.K., Saroja S., Mohandas E., Vijayalakshi M., Raj B., Drop Calorimetry Studies on 9Cr-1W-0.23V-0.06Ta-0.09c Reduced Activation Steel , International Journal of Thermophysics (2010) 31:399-415.

Rogante M., Mikula P., Vrana M., 2009, Through-the-Thickness Residual Stress Analysis by Neutron Diffraction in Inoxidizable Martensitic Steel Samples with and without Tungsten Carbide Coating, Surface and Coatings Technology 204 (2009) 650–656.

Roland Berger R. 2013, A Game Changer for the Manufacturing Industry? Additive Manufacturing – Roland Berger, Strategic Consultants, Munich, November 2013.

Rudianto, H., Jang, G., Yang, S., Kim, Y., Dlouhy, I., “Effect of SiC Particles on Sinterability of Al-Zn- Mg-Cu P/M Alloy”, Archives of Metallurgy and Materials, Vol. 60No. 2 (2015), 1383-1385.

Rudianto, H., Jang, G.J., Yang, S.S., Kim, Y.J., Dlouhy, I. “Evaluation of Sintering Behavior of Premix Al-Zn- Mg-Cu Alloy Powder”, Advances in Materials Science and Engineering, Vol. 2015., 2015, Article ID 987687, 8 pages.

Sabetghadam H., Zarei Hanzaki A.Z., Araee A., Hadian A.; Microstructural Evaluation of 410 SS/Cu Diffusion-Bonded Joint, Journal of Material Science Technology, 26(2) (2010), 163-169.

Samih Y., Marcos G., Stein N., Allain N., Fleury E., Dong C., T. Grosdidier T., Microstructure Modifications and Associated Hardness and Corrosion Improvements in the AISI 420 Martensitic Stainless Steel Treated by High Current Pulsed Electron Beam (HCPEB), Surface & Coatings Technology, 259 (2014),737–745.

Shashanka. R, Chaira D., Phase Transformation and Microstructure Study of Nano-Structured Austenitic and Ferritic Stainless Steel Powders Prepared by Planetary Milling, Powder Technology 259, (2014), 125–136.

Slotwinski J.A., Garboczi E.J., Stutzman P.E., Ferraris C.F., S. S. Watson S.S., Peltz M.A., Characterization of Metal Powders Used for Additive Manufacturing, J Res Natl Inst Stand Technology (2014), 119: 460–493.

Song Y., Li X. , Rong L., Li Y. Anomalous Phase Transformation from Martensite to Austenite in Fe-13%Cr-4%Ni-Mo Martensitic Stainless Steel, J.Mater. Sci. Techn., 26(9) (2010), 823-826.

Sort J., Concustell A., Menéndez E., Suriñach S., Baró M.D., Farran J., Nogués J., Selective Generation of Local Ferromagnetism in Austenitic Stainless Steel Using Nanoindentation, Appl. Phy. Lett. 89(3) (2006) ID 032509 1-3.

Souza Filho I.R, Sandim M.J.R., Cohen R., Nagamine L.C.C.M., Hoffmann J., Bolmaro R.E., Sandim H.R.Z., , Effects of Strain-Induced Martensite and its Reversion on the Magnetic Properties of AISI 201 Austenitic Stainless Steel, Journal of Magnetism and Magnetic Materials 419 (2016),156–165.

Stagno E.. Pinasco M.R., Palombarini G., Ienco M.G., Bocchini G.F., Behaviour of Sintered 410 Low Carbon Steels Towards Ion Nitriding,Journal of Alloys and Compounds 247(1997), 172-179.

Subramanian R., Tripathy H., Rai A.K., Hajra R.N., Saibaba S.,Jayakumar T., Kumar E.R., Thermal Expansion Characteristics of Fe–9Cr–0.12C–0.56Mn–0.24V–1.38W–0.06Ta (wt.%) Reduced Activation Ferritic–Martensitic Steel, Journal of Nuclear Materials 459 (2015), 150–158.

Tavares S.S.M.,, Fruchart D., Miraglia S.,, Laborie D., Magnetic Properties of an AISI 420 Martensitic Stainless Steel, Journal of Alloys and Compounds 312 (2000), 307–314.

Tavares S.S.M., da Silva M.R., Neto J.M., Miraglia S., Fruchart D., Ferromagnetic Properties of Cold AISI304L Steel, Journal of Magnetism and Magnetic Materials 242-245,(2002), 1391-1394.

Tosangthum N., Coovattanachai O., Krataltong R., Morakotjinda M., Daaraphan A., Vetayanugul B., Tongsri R., Densitiy and Strength Improvement of Sintered 316L Stainless Steel, Chiang Mai Journal of Science, (2006), 33(1): 53-66.

Tsuchiyama T., Tobata J., Tao T., Nakada N., Takaki S., Quenching and Partitioning Treatment of a Low-Carbon Martensitic Stainless Steel, Materials Science and Engineering A 532 (2012) 585– 592.

Vignal V., Ringeval S., Thiébaut S., Tabalaiev K.,Dessolin C.,Heintz O.,Herbst F., Chassagnon R., Influence of The Microstructure on the Corrosion Behaviour of Low-Carbon Martensitic Stainless Steel After Tempering Treatment, Corrosion Science, 85 (2014), 42-51.

Wan P., Ren Y., Zhang B.,Yang K., Analysis of Magnetism in High Nitrogen Austenitic Stainless Steel and Its Elimination by High Temperature Gas Nitriding, J. Mater. Sci. Technol. 27(12) (2011) 1139-1142.

Wang L., Sun J., Kang B.,Li S., Ji S., Wen Z., Wang X., Electrochemical Behaviour and Surface Conductivity of Niobium Carbide-Modified Austenitic Stainless Steel Bipolar Plate, Journal of Power Sources, 246 (2014), pp.775-782.

Watanabe, T.. Sagara A.,2 Hishinuma Y. Takayama S., Tanaka T. , Sano S., 2015, Magnetism Induced by Electrochemical Nitriding on an Austenitic Stainless Steel, AIP Advances 5 (2015), 047138.

Weidmann E., Guesnier A., Taylor B., Application Notes ,Metallographic Preparation of Stainless Steel, www.struers.com

Weng F., Gao S., Jiang J., Wang J., Gua,P. A Novel Strategy to Fabricate Thin 316L Stainless Steel Rods by Continuous Directed Energy Deposition In Z Direction, Additive Manufacturing 27(2019) 474-481.

Wielgosz E., Kargul T., Falkus J., Comparison of Experimental and Numerically Calcuated Thermal Properties of Steels, International Conference on Metallurgy and Materials, May 21 st-23rd 2014,Brno, Czech Republic, Metal 2014, 6 pages.

Wiessner M., Gamsjäger E., van der Zwaag S., Angerer P., 2017, Effect of Reverted Austenite on Tensile and Impact Strength in a Martensitic Stainless Steel−An In-situ X-ray Diffraction Study, Materials Science & Engineering A 682 (2017), 117–125.

Witthan B., Reschab H., Tanzer R. Shützenhöfer W., Pootlacher G., Thermophysical Properties of Chromium-Nickel-Molybdenum Steel in the Solid and Liquid phases , International Journal of Thermophysics (2008) 29:434-444.

Wu K., Liu G.Q., Wang L.,Xu B.F, Research on New Rapid and Deep Plasma Nitriding Techniques of AISI 420 Martensitic Stainless Steel, Vacuum 84 (2010) 870–875.

Xi Y.-t., Liu D.-x., Han D.,Improvement of Corrosion and Wear Resistances of AISI 420 Martensitic Stainless Steel Using Plasma Nitriding at low Temperature, Surface and Coatings Technology 202 (2008) 2577–2583.

Yang S.T., Hwang W.-S., Shyr T.-W., Cheng I-L., Evolution of Magnetic Phase at Low Aging Temperature in a Heavily Cold-drawn Stainless Steel Fiber, Journal of Magnetism and Magnetic Materials 324 (2012), 2388–2391.

Yao B.,, Zhou Z., Duan L., Zhiyu Xiao Z., Compressibility of 304 Stainless Steel Powder Metallurgy Materials Reinforced with 304 Short Stainless Steel Fibers, Materials, 9 (161) (2016), 1-11.

Yasuhisa, O.; Yu, T.; Mano, M.; Okada, T. Design of Ship Hull Structures: A Practical Guide for Engineers; Springer: Berlin/Heidelberg, Germany; London, UK, 2009; pp. 319–333.

Yazıcı M., Yıldız F., Yetim A.F., Çelik A., 316l İmplant Malzemesinin Aşınma Ve Manyetik Özellikleri Üzerine Plazma Nitrürleme Sıcaklığının Etkisi, Suleyman Demirel University Journal of Engineering Sciences and Design 2(3), (2014), 319-326.

Yetim A.F., Yazıcı M., Wear Resistance and Non-Magnetic Layer Formation on 316L Implant Material with Plasma Nitriding, Journal of Bionic Engineering 11 (2014), 620–629.

Yıldızlı K., Investigation on The Microstructure and Toughness Properties of Austenitic and Duplex Stainless Steels Weldments under Cryogenic Conditions, Materials and Design 77 (2015) 83–94.

Yi Y., Xu W., Xia F., Gang T., Chen L., Effects of Alloying Elements M (M = Fe, Mo) on Phase Stability of $Cr_{23}C_6$ Carbides from First-principles, 2nd International Conference on Advances in Materials, Mechatronics and Civil Engineering. Proceedings; 2017 January 19-20, Guangzhou, China: ICAMMCE; p.74-80.

Yoon S., Kang S., Choi Y., Choi H., Lee S.-J., 2016, Effect of Relative Density on Microstructure and Mechanical Properties of Fe-12Mn-0.2C Alloy Fabricated by Powder Metallurgy, Powder Technology 298 (2016),106–111.

Zhang S.Y., Compagnon E., Godin B., Korsunsky A.M., Investigation of Martensite Transformation in 316L Stainless Steel, Materials Today: Proceedings 2S (2015)S251 – S260.

Zhang H., Zhao Y.L., Jiang Z.D., Effects of Temperature on the Corrosion Behavior of 13Cr Martensitic Stainless Steel During Exposure to CO_2 and Cl^-Environment,Materials Letters, 59(27), 3370-3374, 2005.

Zhang W., Technical Problem Identification for the Failures of the Liberty Ships, Challenges 2016, 7, 20 1-8

Zhao L., Tegus O., Brück E., van Dijk N.H., Kruijver S.O., Sietsma J., van der Zwaag S., Magnetic Determination of the Thermal Stability of Retained Austenite in TRIP Steel, Proc. Int. Conf. On TRIP-Aided High Str. Ferr.All., Gent, Belgium, (2002), 71-74.

5. Welding of High-Alloy Steels, Corrosion, ISF AACHEN,

WEB,URL1 http://solidpic.pw/austenitico-ferritico.html

WEB, URL2 http://mercury.kau.ac.kr/welding/

WEB, URL3 https://www.thecoffeebrewers.com/de.html

WEB,URL3https://www.pickpm.com/design-resource-center/powder-metallurgy-consolidation-processes/

CIRRICULUM VITAE

Ayşe Nur Acar graduated from Kılıçarslan High School in 2003,, and enrolled in Ceramic Engineering Department of Dumlupınar University. In 2009, she graduated with a Bachelor of Science degree in Ceramic Engineering. She began to undergraduate program of Mechanical Engineering with double major in the 2007 and completed the double major program in the 2011. She graduated from her MSc education at the Mechanical Engineering department in the Çukurova University in 2014 with MSc thesis about thermoelectric studies of aluminum compounds and She began doctora of philosophy at the same department on the same year. She studied her PhD thesis about physical and mechanical properties of stainless steels. During her thesis study; she published an article in the SCI journal and presented proccedings in various international scientific meetings and, she has planned 3 article in preparing, which will be printed international journals, from her thesis study. She works materials such as steels, metals etc., manufacturing methods such as powder metallurgy and materials characterization methods. She has worked as a research assistant since August 2011.